University of Zurich[UZH]

Determination of soil disturbances in Geopark Estrela (Portugal)

GEO 511 Master's Thesis

Author
Wasja Dollenmeier
16-713-125

Supervised by
Dr. Gerald Raab

Faculty representative
Prof. Dr. Markus Egli

28.02.2021
Department of Geography, University of Zurich

Abstract

The erosion risk in the Mediterranean climate is considered high, especially on slope sites. Soil erosion is caused by intense precipitation in the autumn and winter months because the parched soils are unstable at the end of the hot summertime. The examined area is in the UNESCO Geopark Estrela in East Central Portugal, which reaches altitudes of almost 2000 m a.s.l. Some parts of the plateau were glaciated during the last ice age. This work aims to compare a formerly glaciated area with a non-glaciated place. For this purpose, physical and chemical soil characteristics are determined. The last ~60 years' erosion rates are estimated with $^{239+240}$Pu, which is done for the first time in this area. The soil aggregates in the formerly glaciated area are expected to be less developed because of the younger soil age. Therefore, higher soil erosion rates and more soil disturbances are expected compared to the non-glaciated area. Three sites are chosen at both locations; a reference site and two slope sites each, whereas most of the pits reach a depth of 25 cm. One pit at the formerly glaciated area has been dated with ^{10}Be.

Contrary to the hypothesis, the estimated erosion rates are higher at the non-glaciated site (1000-2000 $tkm^{-2}yr^{-2}$) than at the former glaciated site (around 0 $tkm^{-2}yr^{-2}$). Erosion rates depend not only on the glacier history but also on slope angles, vegetation, and soil production rates. We found a strong correlation between the erosion rates and the slope angle and vegetation density. Besides, the soil production rates are higher at younger soils than at more developed soils. In the formerly glaciated area, the long and mid-term soil disturbances were higher than the short-term soil disturbances. Maybe, the soil experienced more vertically mixing through cryoturbation in the past than nowadays. Global warming leads to fewer frost events, which could explain these changes. A further soil disturbance are forest fires, which increase the carbon content in the soil. It must be expected that forest fires and extreme rainfall events increase in the future, which in turn causes higher erosion rates.

Table of content

List of figures

List of tables

ABBREVIATIONS

a	Latin: annum = year
Be	Beryllium
B.P.	Before present. Present is defined as the year 1950.
EAG	Estrela Aspiring Geopark
GPS	Global positioning system
LGM	Last glacial maximum
m a.s.l.	meter above see level
Pu	Plutonium
TEA	Tor exhumation approach
XRF	X-ray fluorescence

1 Introduction

1.1 Objectivities

This study investigates soil characteristics and disturbances at two locations in the Estrela Aspiring Geopark (EAG) in Portugal, which reaches elevations up to almost 2000 m a.s.l. Although the EAG is in a Mediterranean climate, some parts were glaciated during the Last Glacial Maximum (LGM). Signs of glaciation appear in the terrain, and the moraines allow the estimation of the maximum glaciation. One of the two locations is within the formerly glaciated area; the other location is beyond the maximum glaciation during the LGM (earlier glaciations are not excluded per se). We selected three sites in each location, one on flat ground as a reference site and two on a sloping site, to assess the slope angle's influence. Erosion rates are estimated using fallout radionuclides, more specifically, plutonium isotopes. It is possible to estimate the erosion rates over the last ~60 a with this application. So far, practically no data exists on soil erosion in this area, and it is the first time that $^{239+240}$Pu analysis is applied there. Also, some general soil properties are examined to see if the two sites are comparable. The determining erosion rates are compared with the erosion rates of the last millennia in the overarching project. As a result, changes in erosion rates can be identified. This knowledge forms the basis for the debate on humans' influence on soil erosion in this region. Soil erosion rates in the Geopark have not been described in detail so far, which is why this project can bridge these blanks.

1.2 Background

This master thesis contributes to a comparative study by Gerald Raab on previously glaciated and non-glaciated tors in the EAG. Tors are boulders, which are still connected to the bedrock. The tors exhumation approach (TEA) allows a detailed reconstruction of the soil erosion variations of the last 100'000 to 160'000 a. Current erosion rates are then compared with these values, allowing the detection of possible erosion changes. Two types of sampling are taking place in Portugal; on the one hand, in situ cosmogenic radionuclide measurements (10-beryllium-isotope, ^{10}Be) are performed vertically at the tors. On the other hand, soil samples for the later fallout radionuclide (Plutonium isotopes, $^{239+240}$Pu) are taken to model soil degradation rates of the last 56 a (Raab, et al., 2018). This thesis is about soil analysis, with a focus on soil erosion rate estimations.

In the Mediterranean area, erosion due to precipitation is high; after the hot summer months, the soil has dried out, making the soil unstable and susceptible to damage (Imeson, 1990). Also, the European Environment Agency (2009) classifies most parts of Portugal as a vulnerable area (see Figure 1). In the higher regions of the EAG, rainfall is intense, so that the investigation area is hypersensitive to this type of erosion (Vieira, et al., 2017). Various studies (including Nunes, et al., 2010 or Bochet, et al., 1998) indicate that flora reduces erosion. The vegetation covers the soil, while the roots make the soil material more stable. Soil formation- and erosion rates are not constant over time. Abrupt natural events or human impacts can change these rates in a short time. On the one hand, anthropogenic influences, such as intensive agriculture or deforestation, leads to higher erosion rates (Egli & Poulenard, 2016). On the other hand, environmental disasters as forest fires destroy the ecosystem, resulting in increased erosion rates. As Nunes et al. (2010) describe in their paper, with the disappearance of plants, the soil becomes less stable, making the soil even more vulnerable to erosion. Because of the high risk of wildfires and soil loss through agriculture, Portugal is classified as a particularly vulnerable land to desertification (Nunes, et al., 2010).

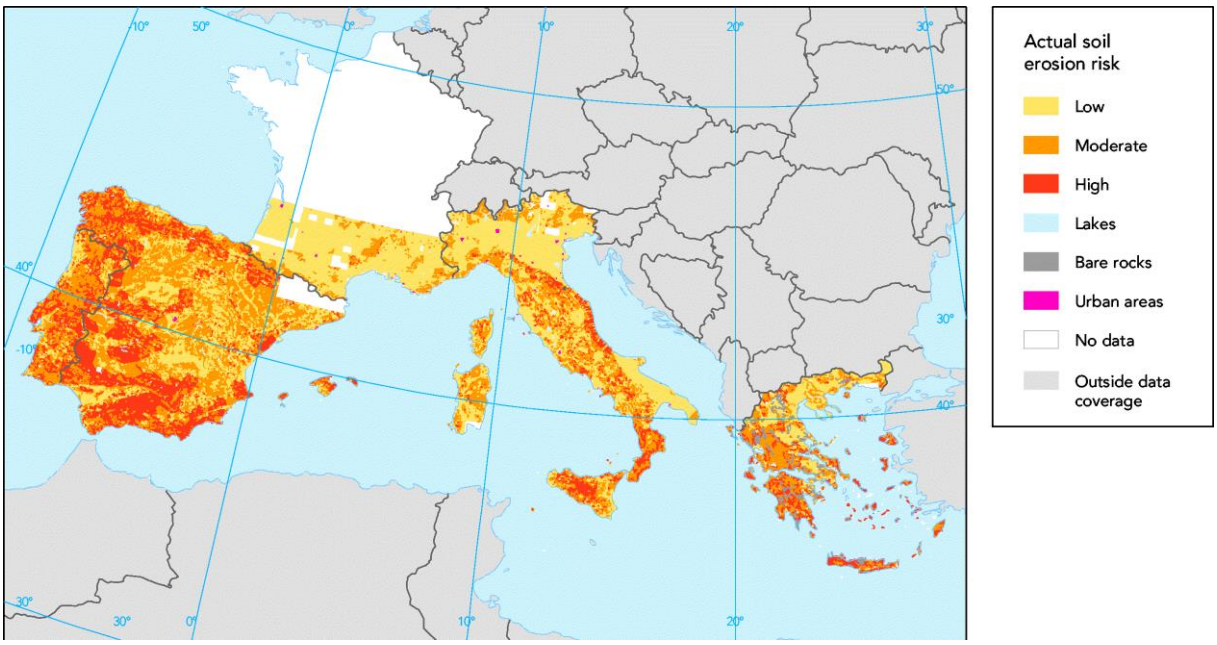

Figure 1; Actual soil erosion risk in Southern Europe (EEA, 2009.)

1.3 Soil formation and weathering

Soils are complex structures and develop through biological, climatic, geological, and topographical influences. The evolution of soils is called soil formation or pedogenesis (Stahr, et al., 2016). Depending on the environmental conditions, soil formation is progressive or

regressive. In progressive soil formation, the soil depth increases. Parent rock in the bottom transforms into primary minerals through chemical weathering. This process is accelerated by reducing the grain size through physical weathering. In addition, microorganisms help decompose organic matter (humification) in the upper soil layers (Graham, et al., 2010). In regressive soil formation, the soil profile loses thickness because it is moved away, so-called erosion. Soil erosion is essentially caused by rainwater run-off or by wind, i.e., by climatic conditions (Dixon & von Blanckenburg, 2012).

In contrast to physical weathering, which leads to a particle size reduction, chemical weathering changes the elemental composition. The most significant influence is exerted by the addition of water and carbon dioxide (CO_2), which can wash out (leach) elements out of the soil (Stahr, et al., 2016). Not all elements are equally affected by the leaching; there is a classification between mobile and immobile elements. Mobile elements have a low field strength due to their sizeable atomic radius and so dissolve more quickly. Otherwise, immobile elements have a smaller radius and a high field strength, which is why they are not readily leached (Kabata-Pendias, 2011). Weathering indexes determine the ratio between the immobile and mobile elements, which allows the estimation of different degrees of weathering in the soils (Price & Velbel, 2003).

1.4 Fallout radionuclides to estimate the erosion rates

The fallout radionuclides analysis aims to determine recent years' erosion rate (Mabit, et al., 2013). In the literature are calculations described for 137-cesium isotope (^{137}Cs), 239 or 240-plutonium isotope (Xu, et al., 2015; Alewell, et al., 2014; Ketterer, et al., 2004). Nuclear weapon tests and power plant accidents such as Chernobyl have massively increased the concentration of fallout radionuclides in the atmosphere during the 1950s and 1960s (Alewell, et al., 2014). The atmospheric fallout radionuclide concentration is worldwide fairly uniformly (especially in the northern hemisphere) distributed. Therefore, the soil particles absorbed approximately the same amount of the fallout radionuclides (Xu, et al., 2015). In undisturbed soils, the highest concentration is within the upper soil layers and decreases in depth. Soil erosion removes the upper soil layers, whereby the concentration of fallout radionuclides is lower than at soils, which are not (or less) affected by soil erosion. The comparison of the fallout concentration between flat sites and slope sites allows a soil erosion estimation. In this thesis, the erosion estimation is conducted with $^{239+240}Pu$. ^{137}Cs is used less and less, among other reasons, because of the decreasing concentration in the soil due to the shorter half-life time compared to $^{239+240}Pu$ (Ketterer, et al., 2004; Xu, et al., 2015).

1.5 Research Questions and Hypothesis

This work aims to determine erosion values in formerly glaciated and non-glaciated areas in the Geopark Estrela. By using $^{239+240}$Pu analysis, a soil erosion estimation of the last ~60 a is possible. Therefore, the rates at the two locations can be compared. In addition, the analysis of some general soil properties allows conclusions on soil disturbances like forest fires or cryoturbation, which will be discussed in this work.

Research Questions

(1) How do short-term soil erosion rates differ in a formerly glaciated area compared to non-glaciated sites over the last ~60 years?

(2) To what extent are the investigated soils affected by long-, mid-, and short-term soil disturbances, and how do the soil disturbances differ between the two sites?

Hypothesis

(1) Many factors influence soil erosion, e.g., the precipitation, the slope angle, or the vegetation. Therefore, it is challenging to determine if changing erosion rates are caused by glacial history. Overall, higher soil erosion rates are expected in the formerly glaciated areas compared to the non-glaciated area. The soil structures are less developed in the formerly glaciated area because of the younger soil age. As a result, the soil is more susceptible to erosion.

(2) The long-term soil disturbances are only available for the formerly glaciated area and are expected to be high because of cryoturbation. The mid-term soil disturbances are expected to be higher because of anthropogenetic influences, especially in the non-glaciated area, which is easier to reach for humans. The short-term soil disturbances are expected to be lower because of the higher protection of the Geopark. Nevertheless, the number of forest fires increases, which could cause more soil disturbances.

2 Investigation area

The research site is in north-central Portugal, in the Estrela Aspiring Geopark (EAG). The EAG extends over 2000 km^2, whose center is the plateau with the Torre mountain (1993 m a.s.l.), which is the highest elevation on the Portuguese mainland (Vieira, et al., 2017). The nature park is a popular tourist area for cycling, hiking, and climbing. In the winter months, there is even enough snow to ski. Agriculturally, the area is mainly used for grazing. There are several reservoirs within the park, and three rivers flow out of the rainy region. There are few roads through the park, but it is possible to reach the highest point, the Torre, by car. The closest of our sites is Manteigas, a small town with just under 3500 inhabitants. On the southern edge of the nature park is the town of Covilhã, with 50'000 inhabitants, and it even has a university.

Dr. Gerald Raab selected this location for several reasons. Firstly there are easy-to-sample tors in formerly glaciated and non-glaciated areas close together. Furthermore, the area is comparable to the previous research site in Italy (Sila) because both regions have a similar Mediterranean climate and are located at a similar altitude (Raab, et al., 2018). In the following sections, typical parameters of the area are described in more detail.

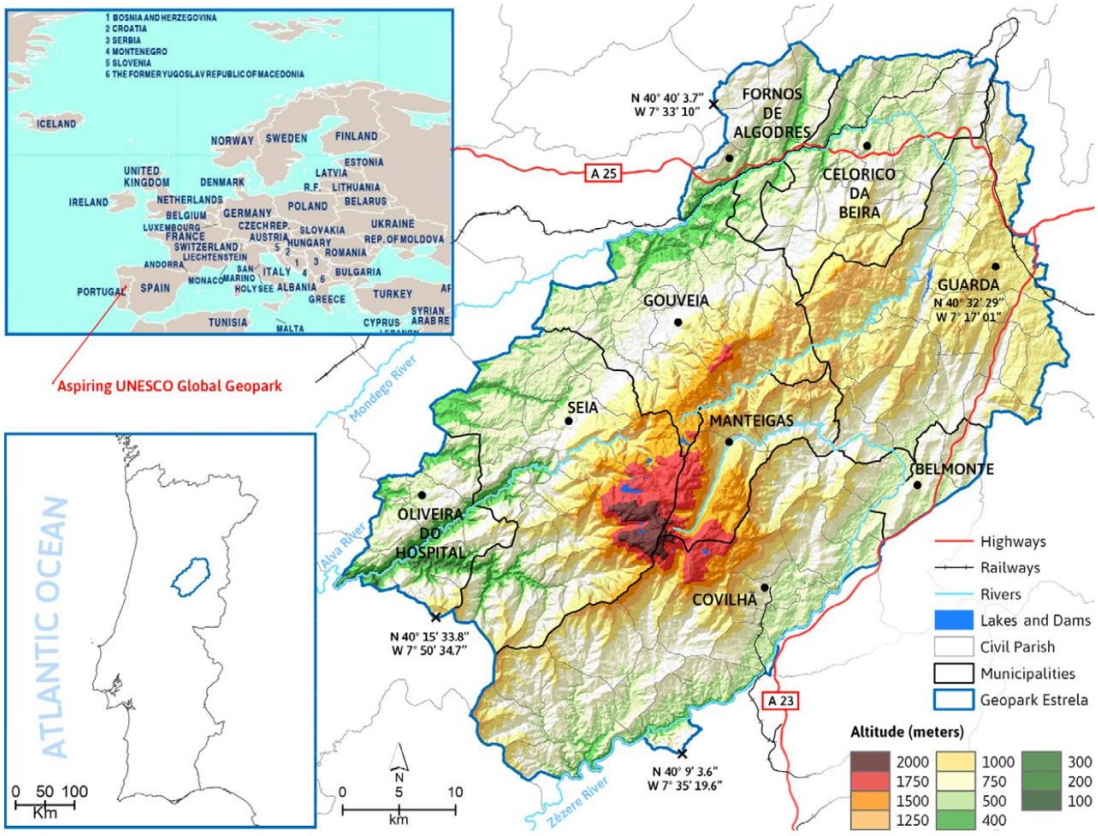

Figure 2; Location of the Geopark Serra de Estrela (Vieira, et al., 2017, p. 3)

2.1 Climate

The climatic conditions in the investigated area can be described the best with the Mediterranean climate regime with some influence of the temperate climate zone. Arid summers are followed by wet and colder winter months. The temperature, as well as the precipitation, varies widely according to altitude. The average annual temperature is 9.2°C at lower altitudes (AEMet & IM, 2011) and decreases to 3-4°C at the plateau's top (Mora, et al., 2001). During the summer, the temperature reaches values around 20°C (in Penhas Douradas, compare Figure 3), resulting in a high risk of wildfires (Vieira, et al., 2017). There is more rainfall from October to May, which can fall as snowfall in the higher regions. It even has ski lifts, which attract tourists during the winter season. At lower altitudes, the snow rarely stays on the ground for long, but on the plateaus, the snow cover can remain for up to 90 days (ICNB, 2007). The winds usually blow from western or north-western directions (Vieira, et al., 2017).

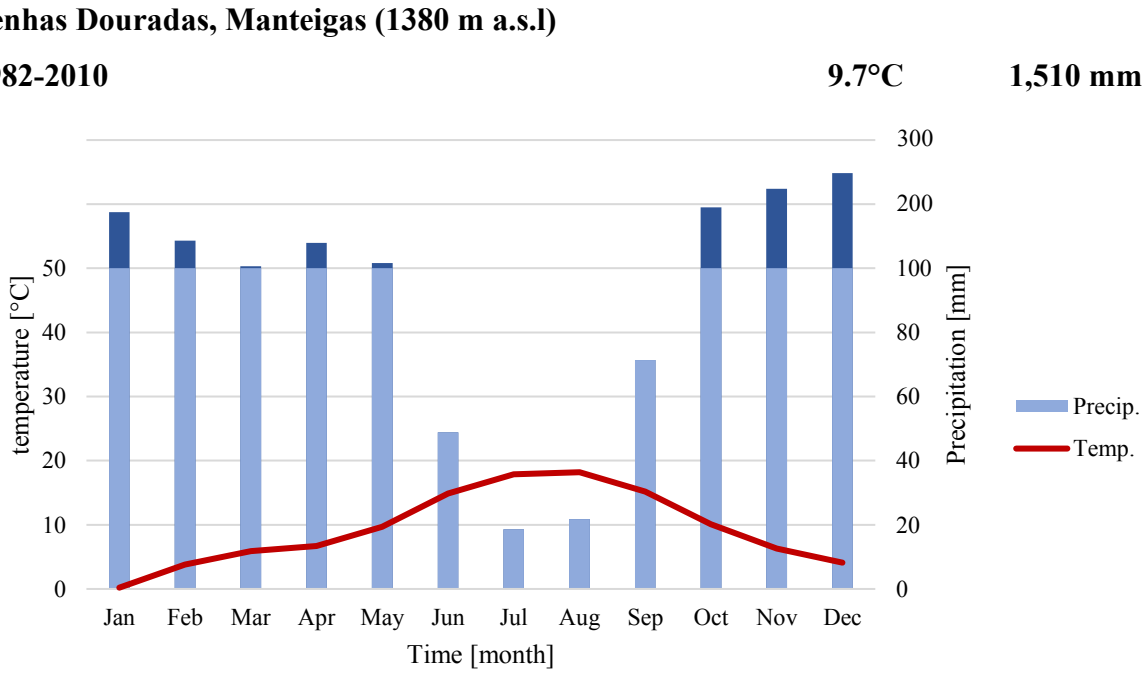

Figure 3; Mean monthly temperature and precipitation in Penhas Douradas (1380 m a. s. l) according to IPMA (2021)

2.2 Vegetation

Natural conditions such as altitude, exposure, or water availability influence the vegetation. The lower areas (up to a height of 900 m a.s.l.) are naturally covered by permanent green deciduous woods, dominated by holm oak (Quercus robur) (Connor, et al., 2012). At the intermediate altitudes, the Pyrenean oak dominates, and in the higher areas, there are pine forests or shrublands. Only frost-resistant grasses survive in the highest regions (Vieira, et al., 2017). The

vegetation has been changed by anthropogenic use. Up to an altitude of 900 m a.s.l., many cultivated plants such as olive trees, fruit trees, vegetables, or vines are common. Pine forests (Pinus pinaster) are also cultivated for forestry (Connor, et al., 2012). Besides the anthropogenic influences, wildfires influence the vegetation. Large areas of forest regularly fall victim to fire. Forest fires are not a new issue in this region because some soil layers contain macroscopic charcoal from the Holocene (Braun-Blanquet, et al., 1952). Overall, the soil is highly vulnerable to erosion due to the low vegetation density.

2.3 The last glacial maximum

There were four great ice ages in the Quaternary, the last one begun approximately 120 ka B.P., and temperatures began to rise again about 11.7 ka B.P. The glacier maximum was reached by all glaciers in the northern hemisphere fairly synchronously, nearly 19 to 23 ka B.P. This cold period is known as the Würm glaciation in the Alpine region (Grotzinger & Jordan, 2016). Gonçalo Vieira et al. (2017) describe the morphological structure in the EAG and conclude that a glacial overlap occurred. Thus, an ice field covered the plateau during this time, which is unusual at these latitudes. It can be assumed that the ice field responded very strongly to temperature differences, causing the glaciers to change rapidly. Figure 4 shows the glacier overlap during the Last Maximum. The largest glacier was likely located in the Zêzere Valley, where the city of Manteigas is located today (Vieira, et al., 2017)

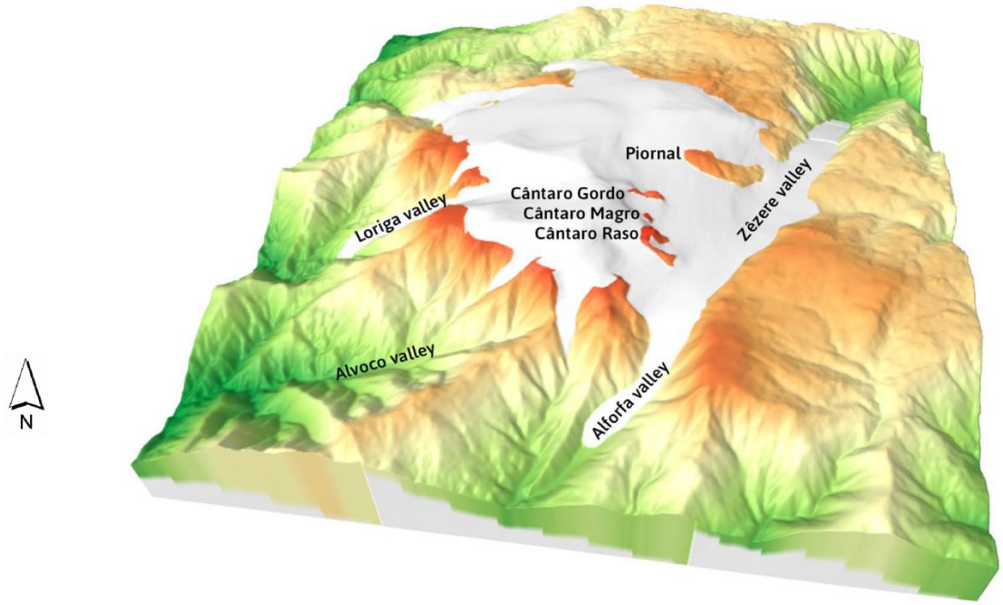

Figure 4; Modelled glacier surface of the Estrela plateau ice-field during the Last Maximum of the Glaciation of the Serra da Estrela. View from the south (Vieira, et al., 2017)

2.4 Geology and morphological shape

The Serra da Estrela is geologically dominated by an approximately 300 million-year-old Hesperian granite (Ribeiro, et al., 1979). The plateau's formation has its origin in the Hercynian orogeny during the Neoproterozoic (Díez Balda, et al., 1990). The granite intruded through the surrounding Precambrian-Cambrian schist/greywacke sedimentary complex (Connor, et al., 2012). The tectonic movements deformed the metasediments, accompanied by granitic batholith intrusion in the late orogenic stages (Migoń & Vieira, 2014).

In a long period during the Mesozoic and Cenozoic, the Variscan rocks eroded and leveled the range into a plain (Vieira, et al., 2017). In the Miocene, the Variscan faults reactivated, leading to the Alpine uplift, which led to the Serra da Estrela's uplift up to some 1,500 m and formed a plateau mountain. This process changed the fold axes' orientation in SSW-NNE, SW-NE, and NW-SE direction (Ribeiro, et al., 1990).

Gonçalo Vieira et al. (2017) describe the morphological structure with all the signs of glacial overlapping. An icefield covered the plateau during the Pleistocene, which is unusual in this latitude. Due to this geographical position and the altitude, the ice field reacted very strongly to temperature differences, which caused the glaciers to change rapidly. Based on moraines and other landscape forms, Vieira, et al. (2017) managed to model the glacier overlay during the Last Maximum (see Figure 4). Probably the largest glacier was in the Zêzere valley, where today the city of Manteigas is located.

Today, various granite forms are in this area; coarse-grained porphyric biotite-muscovite granite predominates within the batholith. In the central part of the massif, medium to fine-grained muscovite granite occurs (Sant'Ovaia, et al., 2010). The soil types are not described in detail but often are lithosols on the granitic plateaus, and at lower altitudes, more developed cambisols can be detected above the schist bedrock (Connor, et al., 2012).

2.5 Location of the research sites

The non-glaciated area (area was not glaciated during the LGM) is defined as Location 1, and there are two pits each at a reference site (Reference 1) and on two slopes (Slope 1 and Slope 3). The site is located at an altitude of almost 1500m.a.s.l. Location 2 is 150m higher, at approximately 1650m.a.s.l. and is located in a formerly glaciated area. There is where the sites Reference 2, Slope 3, and Slope 4 are located.

Investigation area

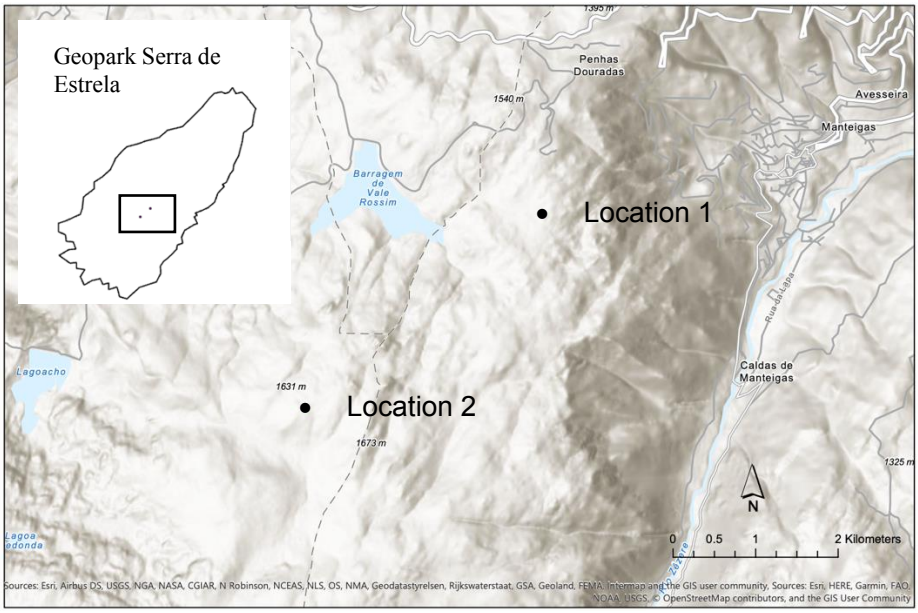

Figure 5; Location of the non-glaciated (Location 1) and former glaciated (Location 2) sites (Map was designed with ArcGis)

Table 1 summarize the exact information about the sites, whereby the land use and the geological substrate is at all sites the same. The sites are located in a national park, and the only land use is grazing by sheep, goats, and cows. The milk products are used to make cheese, which is a trademark of the region.

Table 1; General characteristics of the study sites in the Geopark Estrela (Portugal)

Site	Coordinates WGS 84 (N/W)	Elevation m a.s.l.	Geologic substrates along the profile	Vegetation	Slope	Exposure °N	Soil type WRB	Land use
Location 1 (non-glaciated)								
R1	40°23'51.0" / 7°33'60.0"	1495	Seia Granite (Granites and porphyritic granodiorites)	Shrubs, grass	2°	-	Cambisol	national park (pasture)
S1	40°23'51.1" / 7°34'00.1"	1492	Seia Granite (Granites and porphyritic granodiorites)	Grass	10°	300	Cambisol	national park (pasture)
S2	40°23'51.8" / 7°33'59.5"	1494	Seia Granite (Granites and porphyritic granodiorites)	No vegetation	20°	325	Cambisol	national park (pasture)
Location 2 (glaciated)								
R2	40°22'53.6" / 7°35'33.4"	1651	Seia Granite (Granites and porphyritic granodiorites)	frost-resistant Grass	0°	-	Cambisol	national park (pasture)
S3	40°22'53.1" / 7°35'32.3"	1655	Seia Granite (Granites and porphyritic granodiorites)	frost-resistant Grass	5°	90	Cambisol	national park (pasture)
S4	40°22'52.6" / 7°35'31.9"	1645	Seia Granite (Granites and porphyritic granodiorites)	frost-resistant Grass	5°	90	Cambisol	national park (pasture)

2.5.1 Non-glaciated area

The sampled area is generally flat. Only occasionally, tors emerge from the ground. The uncultivated site has shrub-like vegetation. The soil belongs to the class of brown earth (Cambisol). The reference pits were drilled on a flat location with a slope of 2°, and some shrubs cover the ground. The danger of erosion is lower at this location due to the vegetation. Slope 1 is covered by light grass vegetation, whereas Slope 2 has almost no vegetation. The sampling was on 25. July 2020, a hot summer day, according to which the soil was parched.

Figure 6; Slope 2, Pit 2

2.5.2 Formerly glaciated area

The sampling in the formerly glaciated area is on a plateau at approximately 1650 m.a.s.l. At this altitude, the soil freezes in winter, which causes a mixing of the upper soil layers (about 10cm). This process is visible through the gravel on the surface (see Figure 7). The pits at this site are deeper to be able to investigate properties in the depth profile. Only frost-resistant vegetation can grow. Therefore, the location is covered with grass-like plants. The pits of the reference sites are in a shallow area. The slope's incline in this area is low. The sampling was on July 26, 2020, also a hot summer day.

Figure 7; Gravel on the surface, near to Reference 2

3 Materials and methods

3.1 Sampling strategy and preparation

Both selected locations in the formerly glaciated and the non-glaciated area are examined with six pits each. Two pits are placed at a flat reference site, and four pits are located at two slightly sloping sites. Most pits reach a depth of 25 cm, except R2-P1 and S4-P1 reach 35 cm. In each pit, two profiles were taken, resulting in 12 profiles per site. One sample is collected every five centimeters, which gives five or six samples per profile. That makes a total of 123 samples within 24 profiles, plus two soil samples for ^{14}C analysis. These ^{14}C samples are not described further in this thesis. The pits were dug manually with shovels, pickles, and spades so that the cylinders could be used to take the soil samples at the desired depths. In order to maintain an overview, all pits were recorded photographically (compare Figure 8).

Figure 8; Pit 1 at Slope 2 with tools to dig the pit

In the laboratory at the University of Zurich, all samples were dried in the oven at 70° C for 36 hours (samples were already dry, therefore, not for 48 hours). After, the samples were sieved to < 2 mm (fine earth) and then homogenized. The bulk density (proportion of soil skeleton and fine earth) of the soil could be calculated using the samples' known volume. Approximately 15 g of the fine earth was milled to < 63 µm with the carbide mill (Retsch® MM400, Germany). The milled samples were used for further investigations.

3.2 Physical and chemical analyses

3.2.1 Grain Size

The grain size analyzer determines the amount of clay, silt, and sand. In the first step, the organic matter is removed from the fine soil by H_2O_2. Subsequently, the determination of grain size up to 32 µm was done by wet sieving. Smaller particles are measured with a SediGraph 5100, which can analyze the particle size in a liquid. According to Stokes' law, spheres' frictional force differs according to the radius in a liquid (Flottweg, 2020). According to this law, the particles are deposited selectively, allowing the grain size to be measured by X-ray (Wartel, et al., 1995). Esmaeil Taghizadeh (Lab technician, UZH) carried out the particle size analysis from the two reference sites. Several samples had an insufficient amount of material, so the grain size analysis could not be performed on all samples. Through the grain size composition of the investigated soils, it is possible to describe the soil type in more detail, and the different sites can be compared. Besides, an estimation of the aggregate stability is possible, which allows conclusions on the weatherability.

3.2.2 Loss on ignition (LOI)

The organic fraction of soil was determined by burning the soil sample. A high temperature (550° C) and oxygen destroyed the soil's organic fraction. 2 g of fine earth was weighted into a crucible and then heated in an oven for six hours until the organic fraction was burned. After the burning, the crucibles were reweighted to calculate the weight loss. The used fine earth samples must be thoroughly dried before burning because otherwise, the results would be falsified through the water content (Pansu & Gautheyron, 2006).
Previous experience of LOI measurements indicated that very carbon-rich samples tended to burn heavily. Therefore, too much combustion took place. A slower, gradual temperature ramp was used, allowing combustion to proceed in a more regulated way. The burned soil samples were used for the plutonium extraction. Therefore the LOI was measured as part of the plutonium analysis. Additionally, the LOI serves to describe the observed soil better. A high LOI value indicates a large amount of organic material in the sample.

3.2.3 pH-measurements

The hydrogen ion concentration in short pH describes the acidity of the soil solution. The acid content depends on the H^+ and OH^- activity, whereas in most cases, only the H^+ activity is measured. The measurement can be performed in an electrolytic solution ($CaCl_2$) or an aqueous solution. The saline solution's determination is more precise, with lower values (0.3-0.8) than in the aqueous solution. In this study, the measurement was done with fine-earth samples (unmilled) using 0.01Mol $CaCl_2$ solution with a standard soil to solution ratio of 1: 2.5. For most samples, 10 g soil and 25 ml solution was used, except for one sample (SdE 31 from Slope 1) that contained an insufficient amount of soil, and for this reason, 5 g soil and 12.5 ml solution has been used. After stirring the solution regularly for one hour, the pH was detected with a combined glass electrode (Pansu & Gautheyron, 2006). The calibration was performed according to the standard (Egli, et al., 2020). All samples were measured twice. The pH-values can be used to describe the soil type in more detail, and the different sites can be compared.

3.2.4 X-Ray Fluorescence (XRF)

The purpose of the XRF method is to determine the total elemental content of solids or liquids. The analysis is performed by the stimulation of single atoms by X-rays, whereby electrons are pushed from inner to outer orbits. The inner orbits are replaced by electrons of higher energy levels, which releases fluorescent radiation. Since all elements have different nuclear charges, there is almost no overlap between the individual elements' fluorescence X-rays. Accordingly, the radiation detector can measure the fluorescence radiation and provide information about the contained elements and their frequency (Alfeld, et al., 2016). Atoms with a too-small mass are not measurable, so elements smaller than potassium cannot be determined by XRF (Beckhoff, et al., 2006).

For the measurement, 5 g milled soil was weighted into sample cups and analyzed with an energy dispersive X-ray fluorescence spectrometer (SPECTRO X-LAB 2000, SPECTRO Analytical Instruments, Germany). A calibration with MCA was performed regularly to guarantee the accuracy of the measurements. Additionally, the standard (NCS DC 73326) was routinely included in the analysis, whereas the values were always within the valid range. The total elementary composition is used for the calculation of weathering indexes.

3.2.4.1 Calculation of weathering indexes

Depending on the varying radii and the resulting different field strength of the individual elements, they have induvial residence times in the soil. Typically, elements with higher radii – as Na, Mg, K – are mobile because of their lower field strength. In contrast, smaller elements – as Ti, Zr - remains longer in the soil. They are called immobile elements. The elementary composition evolves, which allows the calculation of chemical weathering indexes (CWIs) (Kabata-Pendias, 2011). Undisturbed soils are more weathered in the upper soil layers than in the lower layers (Stahr, et al., 2016). By comparing the different weathering indexes, relative age estimation is possible. Many authors have described mobile to immobile elements' ratio, and there are different formulas to calculate weathering indexes. In this work, the formulas listed in Table 2 were applied. If the ratio is calculated by mobile to immobile elements, lower indexes mean more advanced weathering and vice versa.

Table 2; Applied weathering indexes

Index name	Author	Meaning	Formula	
(Ca + K) / Ti	Harrington & Whitney, 1987	W ↑ I ↓	$\frac{Ca+K}{Ti}$	*Eq 1*
WIP (Weathering index of Parker)	Parker, 1970	W ↑ I ↓	$100 * \left[\frac{2\,Na_2O}{0.35} + \frac{MgO}{0.9} + \frac{2\,K_2O}{0.25} + \frac{CaO}{0.7}\right]$	*Eq 2*
B-Index	Kronberg & Nesbitt, 1981	W ↑ I ↓	$\frac{CaO + K_2O + Na_2O}{Al_2O_3 + CaO + K_2O + Na_2O}$	*Eq 3*
CIA (Chemical index of alteration)	Nesbitt & Young, 1982	W ↑ I ↑	$100 * \left[\frac{Al_2O_3}{Al_2O_3 + CaO + K_2O + Na_2O}\right]$	*Eq 4*
SA (Silico -aluminum ratio)	Ruxton, 1968	W ↑ I ↓	$\frac{SiO_2}{Al_2O_3}$	*Eq 5*
VR (Vogt ratio)	Vogt, 1927	W ↑ I ↑	$\frac{Al_2O_3 + K_2O}{MgO + CaO + Na_2O}$	*Eq 6*
PIA (Plagioclase index of alteration)	Fedo et al. (1995)	W ↑ I ↑	$100 * \left[\frac{Al_2O_3 - K_2O}{Al_2O_3 + CaO + K_2O + Na_2O}\right]$	*Eq 7*
CPA (Chemical proxy of alteration)	Buggle et al. (2011)	W ↑ I ↑	$100 * \left[\frac{Al_2O_3}{Al_2O_3 + Na_2O}\right]$	*Eq 8*
CIW (Chemical index of weathering)	Harnois (1988)	W ↑ I ↑	$100 * \left[\frac{Al_2O_3}{Al_2O_3 + CaO + Na_2O}\right]$	*Eq 9*

3.2.5 Picarro-measurements

The Picarro analyzer is used to determine the total carbon content and $\delta^{13}C$ values. For this purpose, around 12 mg milled soil is weighed into tin-capsules (Ser. No. tin cups: 7929). In the incinerator is a flame, which burns the samples. The analyzer is only able to measure the CO_2 if no other elements are in the steam. Therefore, other elements must be filtered out. After, a Cavity Ring-Down Spectroscopy analyzer (G2131-i) measures the CO_2 concentration. The

laser wavelength changes when the sample is present, which allows us to terminate C-isotopes' content. So, laser's wavelength and the wavelength of the ^{13}C and ^{12}C isotopes must be known. The laser measures continuously (approx. 1 x per second), resulting in a concentration curve over time. The area under the curve contains the total amount of carbon in the sample, which can be determined by the surface integral. The ratio of ^{13}C and ^{12}C isotopes is constant during one measurement. This ratio allows the calculation of the $\delta^{13}C$ value, which is the ratio between the ^{12}C and ^{13}C. An advantage of measuring with a laser is the possibility to register a high carbon concentration, whereas, with a C/N-analyzer, the upper limit of the measurable range is reached faster (more details in chapter 3.2.6). A chernozem standard is also measured to achieve accurate results and to correct the potential drift. In the laboratory at UZH, this standard is measured before and after six samples. The procedure was carried out in collaboration with Marcus Schiedung (PhD student, UZH) and Severin-Luca Bellè (PhD student, UZH). The relationship between the $\delta^{13}C$ values and the total amount of carbon indicates the soil disturbances and the aggregate stability.

3.2.6 C/N-measurements

Similar to the Picarro analyzer, the C/N analyzer is used to investigate the carbon content. Besides, the C/N analyzer measures the nitrogen content, allowing the calculation of the C/N ratio. In contrast to the Picarro analyzer, the measurement is not performed with a laser but with a thermal conductivity detector (TCD). The measurable range of this detector is less wide than that of the Picarro analyzer. Hence it is important not to weigh too much amount of soil. Depending on the sample's carbon content, which is known from the Picarro analyzer, the weighed amount varies. The necessary amount of milled soil samples were weighed into tin capsules (Ser. No. tin cups: 7929 and 7184). For the measurement, the carbon compounds must be oxidized to CO_2, and nitrogen compounds have to be separated. Therefore, the samples were combusted at about 1000° C in a column filled with tungsten and copper. The measurement was performed with a Thermo Fisher Scientific Flash HT Plus elemental analyzer with SmartEA option, equipped with a thermal conductivity detector, and coupled to a ConFlo lV to Delta V Plus isotope ratio mass spectrometer. For accuracy, all samples had been analyzed twice, and additionally, chernozem standards were measured (Giani, et al., 2015). The measurements were performed by Aline Hobi (Lab technician, UZH). The C/N ratio was used to describe the soil characteristics.

3.2.7 Atomic Absorption Spectrometry (AAS)

Atomic absorption spectrometry (AAS) is a method to determine the concentration of selected atoms. This work aims to determine the concentration of iron, magnesium, and aluminum. The AAS technique works only if the samples are in the gas phase, so the samples are burned in a flame. Afterward, the concentration of the individual elements can be determined by a light beam. Every element has different absorption properties, so the wavelength of the emitted light beam changes depending on the contained elements. The detector measures the wavelength of the light beam after atoms have absorbed specific radiation. The resulting concentrations are then calibrated with standards (Bashour & Sayegh, 2007). The results can be used to characterize the soil and determine the soil type. The oxalate and dithionite extraction was made only for the reference sites and was performed by Esmaeil Taghizadeh (Lab technician, UZH).

3.2.7.1 Oxalate extraction

The samples are treated with an oxalate extract, which dissolves amorphous and poorly crystallized Fe, Mn, and Al phases. The reaction during the extraction is light sensitive, so the samples are protected from light irradiation with an aluminum foil. The samples are shaken for two hours until the pH value is around three and then filtered. The measurement of the Fe, Mn, and Al concentrations is performed with the AAS (Egli, et al., 2020).

3.2.7.2 Dithionite extraction

Dithionite extraction dissolves organically bonded Fe, Mn, and Al as well as crystallized oxides and hydroxides. For this purpose, the sample is heated in a dithionite citrate bicarbonate buffered solution followed by adding sodium dithionite (strong reducing agent). Subsequently, the extract's elements can be measured with the AAS (Egli, et al., 2020).

3.3 Fallout radionuclides

3.3.1 $^{239+240}$Plutonium extraction and measurements

The extraction and the measurements from the Plutonium were done according to Ketterer et al. (2004). In the laboratory of Zurich, only the preparation was done; the milled samples were weighed (5 g) in 40 mL Pyrex "VOA" bottles, burned, and before sending, the vials were well packed. Additional to the samples, duplicates, rock powder (as negative standards), standards (IAEA-447), and blank samples were prepared. The samples were sent to Dr. Michael Ketterer (northern Arizona university, USA). In a first step, the samples were leached by adding a Pu-242 spike solution and HNO3 and placed in a 75° C oven for 18 hours with occasional shaking. After additional leaching with water addition, the Pu is contained in the solution and ready for filtration. Afterward, 0.10 g of $FeSO_4$* 7 H_2O and 0.4 g of $NaNO_2$ were added, and the solution was heated, whereby the Pu convert to the Pu (IV) oxidation state. In the next step, the matrix elements U and Th are removed. This is done by adding TEVA resin and a complex application of columns. In the end, the eluted Pu was collected. The Pu-activity was measured with the Thermo X2 quadrupole ICPMS system located at Northern Arizona University. The soil erosion rates were estimated by comparing the $^{239+240}$Pu activity from the reference and the slope sites.

3.3.2 Erosion estimation by using the inventory method (IM)

With the $^{239+240}$Pu activity, it is possible to calculate the erosion rate. Lal et al. (2013) have developed the inventory method (IM), which is done by the following formula:

$$L = \frac{1}{\alpha P} \times \ln\left(1 - \frac{l_{ref} - l_{inv}}{l_{ref}}\right) \qquad \textit{Eq 10}$$

Where L = loss of soil (cm), α = a coefficient of the least-squares exponential fit of the profile depth to activity after Alewell et al. (2014), P = particle size correction factor, I_{ref} = reference inventory as mean of all reference sites [Bqm^{-2}], I_{inv} = measured total inventory at the sampling point [Bqm^{-2}] (Lal, et al., 2013). The particle size correction should be done because small particles are removed faster due to erosion, whereby the grain size distribution is disturbed. Depending on the source, a correction of 1.0 to 1.2 (Walling & He, 1999) or 1.5 (Lal et al., 2013) is proposed.

3.3.3 Erosion estimation by using the profile distribution model (PDM)

Walling and He (1999) and Zhang, Higgitt, and Walling (1990) have developed the profile distribution model (PDM). The amount of the isotope inventory above the depth is calculated with the following formula:

$$A'(x) = A_{ref}\left(1 - e^{\frac{M_x}{h_0}}\right) \qquad \textit{Eq 11}$$

Where A'(x) = the amount of the isotope inventory above the depth [Bqm^{-2}], A_{ref} = the reference inventory as mean of all reference sites [Bqm^{-2}], M_x = the mass [kg^{-2}] between the top and actual depth (x) and h_0 = the profile shape factor [kgm^{-2}], which describes the rate of exponential decrease in inventory with depth. This factor could be determined with the solver function in excel, which factor is used to estimate the erosion rate per year:

$$E_{soil} = \frac{10}{t - t_0} \times \ln\left(1 - \frac{l_{ref} - l_{inv}}{l_{ref}}\right) \times h_0 \times 100 \qquad \textit{Eq 12}$$

Where E_{soil} = Erosion rate [$tha^{-1}yr^{-1}$], t = sampling year, t_0 = 1963 (maximum level of the testing of thermonuclear weapons), I_{ref} = the reference inventory as mean of all reference sites [Bqm^{-2}], I_{inv} = measured total inventory at the sampling point [Bqm^{-2}], h_0 = the profile shape factor [kgm^{-2}] and the multiplication with 100 is to change the unit from [kgm^{-2}] to [tha^{-1}].

3.4 Beryllium analysis

The beryllium-10 isotope belongs to the cosmogenic nuclides, which originates in situ, which means on the surface (Chmeleff, et al., 2010) or meteorically, in the atmosphere (Graly, et al., 2010). The meteoric ^{10}Be reacts already in the atmosphere and falls to the surface with the precipitation (McHargue & Damon, 1991). Thus, the ^{10}Be concentration is higher in the upper soil layers, but due to wash-out, the ^{10}Be can accumulates in deeper soil layers (Graly, et al., 2010). The half-life of ^{10}Be is 1.39 x 10^6 y (Korschinek, et al., 2010), allowing age dating. Assuming that the cosmogenic radiation is constant (Wagner, 1998) and with the half-life time, the erosion rate can be calculated.

3.4.1 Beryllium Extraction and measurement

The meteoric ^{10}Be is only present in tiny amounts in the soil. Therefore, a careful extraction is necessary. The extraction steps were performed according to the standard scheme of von Blanckenburg, et al. (1996), simplified to von Blanckenburg, et al. (2004). This analysis was only done for the first pit from Reference 2. Because the ^{10}Be concentration changes in the depth profile, this analysis must be performed on a sample that reaches a certain depth, and the selected pit is more in-depth than most others.

First, 2 g fine earth was heated for three hours at 550°C to remove organic matter. The samples were leached two times overnight by adding HCl and continuous shaking. In this solution are contained Be, Al, Fe, Mn, Ca, and other metals. The complex metals are removed by adding EDTA, by bringing the pH to a value around 8.6, whereby the complex metals are dissolved in the solution in contrast to beryllium, which can be separated by using the centrifuge. NaOH is added to the gel to allow $Be(OH)_2$ and $Al(OH)_2$ to redissolve at a pH of 14. Some foreign metals are still in the solution, which can be removed by adding HCl until the pH is around 2 and EDTA. Then, the pH is modified to 8 by using NH_4OH, and the separation can be done by using the centrifuge again. The gel is dissolved with 0.4 M Oxalic acid to separate the $Al(OH)_2$ from the $Be(OH)_2$, whereby the samples are ready for the cation exchange columns. The collected solution was heated to 80°C to reduce the amount of liquid, followed by adding NH_4OH to precipitate the $Be(OH)_2$. The Gel is dried overnight at 70°C afterward heated to 190°C for 4-5 hours. The gel is calcined in the oven at 850°C for two hours to obtain BeO. The extracted beryllium was measured at the ETH Zurich with Accelerator mass spectrometry (AMS) (Christl, et al., 2013).

3.4.2 Beryllium calculation

Maejima, et al. (2004) defined a formula to estimate the soil age, by using the ^{10}Be concentration in the soil:

$$t = -\frac{1}{\lambda}\ln\left(1 - \lambda\frac{N}{q}\right) \qquad \textit{Eq 13}$$

Where t = the soil age, λ = decay constant of ^{10}Be ($4.997 * 10\text{-}7\ yr^{-1}$), N = inventory of ^{10}Be in time t, q = annual deposition rate of ^{10}Be. The inventory of ^{10}Be can be calculated by using the amount of ^{10}Be atoms per g, the soil density and the percentage of rock fragments in the observed depth.

The annual deposition rate (q) of ^{10}Be for the past thousands of years is mostly unknown. Various methods for estimating soil erosion rates can be found in the literature. In this work, the following methods are used:

1. Annual deposition rate (q) according to Monaghan et al. (1986):
   The assumption is that every millimeter of rain contains 1-1.5 x 10^4 atoms cm^{-3} ^{10}Be, resulting in q = precipitation * 1210 [atoms cm^{-2} yr^{-1}]

2. Annual deposition rate (q) according to Willenbring & von Blanckenburg (2010):
   For this estimation, the long-term solar modulation factor and long-term geomagnetic field are used and recalculated for each latitude. This results in a world map with the individual deposition rate. For Portugal is the annual deposition rate around 1'400'000 [atoms cm^{-2} yr^{-1}].

3. Annual deposition rate (q) according to Graly, et al., 2011:
   Based on the measured ^{10}Be concentration from different locations, a formula for low and mid-latitudes was defined:

$$q = P * \frac{1.44}{1 + Exp\frac{30.7 - L}{4.33}} + 0.63 \qquad \textit{Eq 14}$$

   Where P = precipitation and L = latitude

For the mentioned calculations, the current precipitation values cannot be used. It has to be calculated with the average precipitation since the beginning of the soil formation. Because of the missing data, this average can only be roughly estimated. There is a climate station (Penhas Douradas in Manteigas at 1380 m.a.s.l.) near the sample sites, where the actual precipitation rates are recorded since 1982. But because of the higher altitude of the site, the real values could be higher. The estimated precipitation of today is around 1800 mm yr^{-1} (Vieira, et al., 2017). In the last 20 ka, the precipitation was most certainly lower than nowadays, so the average precipitation is most likely between 1400 and 1800mm yr^{-1}.

4 Results

4.1 Soil Profile

The main focus of this master thesis is the plutonium analysis. $^{239+240}$Pu activity concentration decreases in the depth profile, which is why the pits were mainly dug to a depth of 25 cm. In the non-glaciated and the formerly glaciated area, six pits each were made. The soils were dry during the fieldwork, which made digging lightly. The horizon sequence of all observed soil profiles is similar and consists of an Ah, Bv, and a C horizon (was not always reached). The boundary between the Ah horizon and the Bv is approximately between 10 and 15 cm. The soil type can be classified as a Cambisol (according to WRB), which is a relatively young developed soil. The Munsell color is described as brown-soil (10 YR). Up to the vegetation density, the rooting differs. The densest vegetation is at Reference 1, resulting in many roots (compare Figure 9). In contrast, the vegetation at Reference 2 is less dense, which leads to fewer roots in the soil profile (see Figure 10). At Location 2 are signs of frost events, which could cause mixing of the soil. Therefore, one pit at the reference site and one pit on a sloping site were dug deeper (up to 35 cm) at Location 2.

Figure 9; Soil profile at Location 1 (Reference 1, Pit 2)

Figure 10; Soil profile at Location 2 (Reference 2, Pit 1)

4.2 Physical characteristics

The investigated physical soil characteristics are summarized in Table 3 for the two references site. The data of all observed sites are listed in the appendix (Table 12 and Table 13). The percentage of soil skeleton is in general higher at Location 1 with varying values around 50%. The soil skeleton range at Location 2 is more extended than at Location 1; in the upper soil, depths are the lowest values nearby 20% and rise to 70% with increasing depth. The variation in the Munsell color is low. The Hue of the analyzed soil samples is described as brown-soil (10 YR). The values are 3 or 4, and the chroma values are all described with the number 2.

Table 3;Physical characteristics of the observed references sites

Sample	Depth [cm]	Soil skeleton (> 2 mm) [wt%]	Sand [%]	Silt [%]	Clay [%]	Bulk density [g/cm3]	Munsell color [dry]
Location 1 (non-glaciated)							
R1-P1-P1							
SdE-1	0–5	56.64%				0.58	10YR 3/2
SdE-2	5–10	75.55%				0.73	10YR 4/2
SdE-3	10–15	51.21%	40.8	28.8	29.2	0.71	10YR 4/2
SdE-4	15–20	53.90%				0.65	10YR 4/2
SdE-5	20–25	57.49%				0.60	10YR 4/2
R1-P1-P2							
SdE-6	0–5	43.05%				0.59	10YR 4/2
SdE-7	5–10	60.76%				0.75	10YR 4/2
SdE-8	10–15	53.62%	29.2	36.4	33.2	0.79	10YR 3/2
SdE-9	15–20	57.32%				0.80	10YR 4/2
SdE-10	20–25	54.50%				0.90	10YR 4/2
R1-P2-P1							
SdE-11	0–5	56.98%				0.59	10YR 4/2
SdE-12	5–10	32.01%	32	31.2	36.8	0.59	10YR 3/2
SdE-13	10–15	47.61%	29.2	32.8	36.4	0.68	10YR 3/2
SdE-14	15–20	49.15%				0.66	10YR 3/2
SdE-15	20–25	37.87%	33.2	27.6	39.2	0.60	10YR 3/2
R1-P2-P2							
SdE-16	0–5	47.25%				0.56	10YR 4/2
SdE-17	5–10	52.03%				0.74	10YR 3/2
SdE-18	10–15	48.95%	24.8	36	39.2	0.85	10YR 3/2
SdE-19	15–20	50.18%	38.8	26	35.2	0.74	10YR 3/2
SdE-20	20–25	51.30%	38.4	34.8	25.6	0.82	10YR 3/2
Location 2 (glaciated)							
R2-P1-P1							
SdE-61	0–5	17.27%	42	22.8	34.8	0.53	10YR 3/2
SdE-62	5–10	29.58%	19.2	39.6	40.8	0.64	10YR 3/2
SdE-63	10–15	23.15%	28.4	27.6	44	0.70	10YR 3/2
SdE-64	15–20	31.24%	22	37.2	40.4	0.74	10YR 3/2
SdE-65	20–25	32.70%	36	19.2	44.8	0.77	10YR 3/2
SdE-66	30-35	69.07%				0.97	10YR 4/2
R2-P1-P2							
SdE-67	0–5	20.16%	32.4	30	37.6	0.68	10YR 3/2
SdE-68	5–10	25.67%	18	36.4	44.4	0.62	10YR 3/2
SdE-69	10–15	28.34%	32	22	46	0.67	10YR 3/2
SdE-70	15–20	44.91%	24	34.4	41.2	0.81	10YR 3/2
SdE-71	20–25	46.32%	19.6	30.4	47.2	0.75	10YR 3/2
SdE-72	30-35	68.93%				1.07	10YR 3/2
R2-P2-P1							
SdE-73	0–5	26.63%	33.6	20.8	45.6	0.69	10YR 4/2
SdE-74	5–10	35.51%	30	30.8	38.4	0.77	10YR 4/2
SdE-75	10–15	28.76%	18	42.8	37.2	0.65	10YR 3/2
SdE-76	15–20	34.86%	29.2	25.2	45.6	0.71	10YR 3/2
SdE-77	20–25	63.37%	26	34	38	1.01	10YR 3/2
R2-P2-P2							
SdE-78	0–5	31.91%	20	29.2	49.6	0.60	10YR 4/2
SdE-79	5–10	34.83%	34.4	33.6	31.6	0.71	10YR 3/2
SdE-80	10–15	31.09%	13.2	46.8	37.2	0.72	10YR 3/2
SdE-81	15–20	26.29%	34	31.6	33.2	0.67	10YR 3/2
SdE-82	20–25	34.14%	20.4	43.5	35.2	0.71	10YR 3/2

4.2.1 Bulk density

The bulk density at Location 1 (compare Figure 11) shows that the pattern from Reference 1 and Slope 1 is quite similar; the lowest bulk density is in the upper soil layer between 0.4 and 0.6 gcm^{-3} and increases with depth to values around 0.75 gcm^{-3}. In contrast, the bulk density at Slope 2 differs. There is no clear depth trend visible, and the values are higher in a range between 0.8 and 1.0 gcm^{-3}. The three observed sites at Location 2 have an almost identical pattern. The bulk density in a depth of 0-5 cm is nearby 0.65 gcm^{-3}. In the depth of 20-25 cm, the values are higher, around 0.75 gcm^{-3}. Just in a depth of 30-35 cm, the bulk density differs; while the values at Reference 2 reach values around 1.0 gcm^{-3}, the bulk density remains at Slope 4, with values around 0.75 gcm^{-3}. The displayed bulk density is the mean value of the four observed profiles from each site, and in the figure are the standard errors included. The highest standard error is at Slope 2 in the depth range from 0-5 cm. The exact values and the standard deviation are summarized in Table 27.

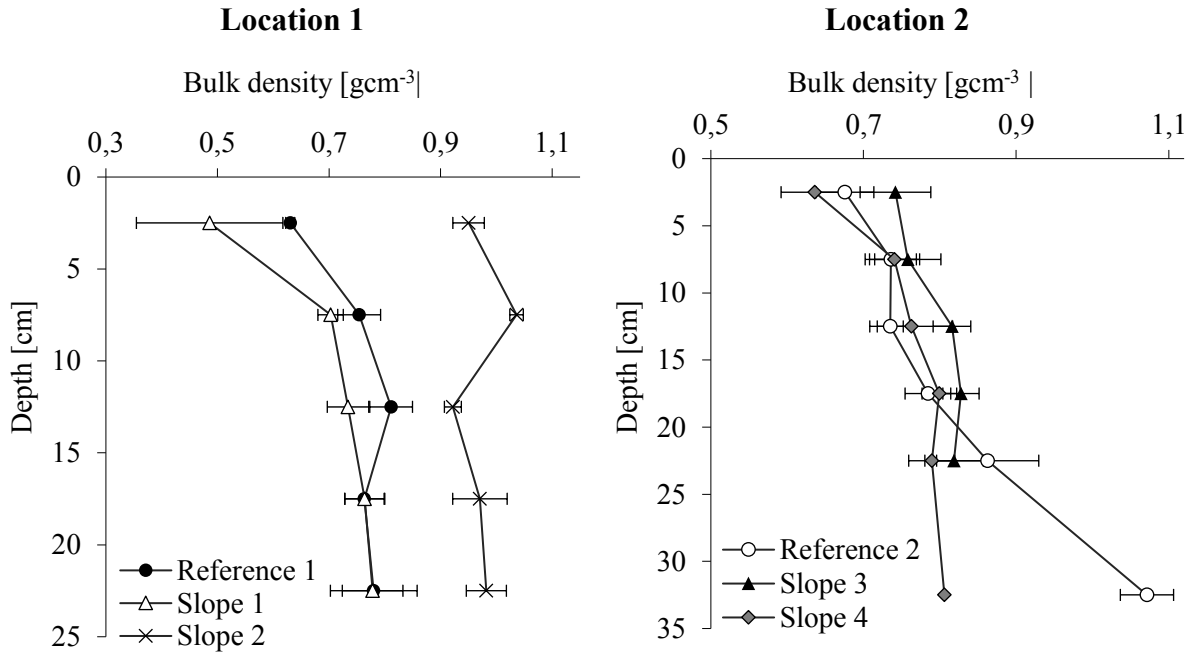

Figure 11; Bulk density of the observed soils at the two locations with standard errors, whereby n = 4

4.2.2 Grain size

The grain size distribution is shown in Figure 12. The results of the sedigraphs are classified in 7 scales, which were then assigned to a specific type of grain. The largest grain size has sand, followed by silt, and the smallest is that of clay (detailed classification in Table 4).

Table 4;Grain size results and classification

Grain size [µm]	Grain size-type
1000-2000	sand
500-1000	sand
250-500	silt
125-250	silt
63-125	clay
45-63	clay
32-45	clay

The determination of the grain size is time-consuming and was only done for the two reference sites. The graphic shows mostly the mean values of the four profiles. However, the measurement was only made for the samples with enough soil material. As a result, the mean value of some depth ranges was calculated with fewer samples. The depth range of 0-5 cm at Reference 1 or the depth range of 30-35 cm at Reference 2 could not be investigated at all. The details are shown in Table 43. The standard errors are mostly between 2 and 6 %.

Reference 1 has a similar proportion of all grain size-types; one-third is sand, one-third silt, and one-third clay. Except in the depth range of 15 - 20 cm, there is more sand and clay, but the silt amounts are only about a quarter. In Reference 2, smaller grain sizes were measured. The percentage of clay is about 40% in each depth range, whereby the lowest sand percentages are found in a depth range of 10 to 15 cm. Both investigated soils show no clear depth trend.

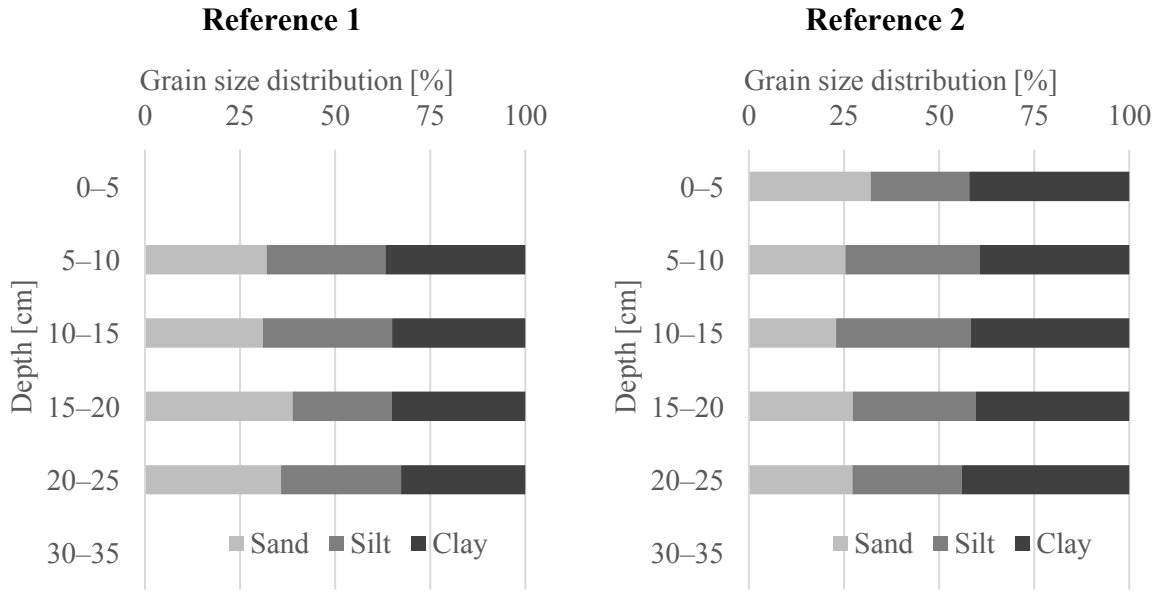

Figure 12; Grain size distribution at the two references sites, summed up to 100%

4.3 Chemical

The investigated chemical soil characteristics are summarized in Table 5 for the two references site. The data of all observed soils are in the appendix (Table 14 and Table 15). The pH- and the C/N measurements were performed twice, so the numbers listed in the table are the mean value of the two measurements. The Picarro measurement was done once to investigate the carbon amount and the δ13C values. Oxalate and Dithionite measurements are elaborately and, therefore, only done for the reference sites, whereas the number per sample differs (details in Table 14 and Table 15). The results are discussed in the following chapter in more detail.

Table 5; Chemical characteristics at the two references sites (the error margin of the red numbers in brackets are too high)

			Picarro		CHN			Oxalate				Dithionite		
Site	**Depth [cm]**	**pH [$CaCl_2$]**	**C [%]**	**δ13C [-]**	**C [gkg^{-1}]**	**N [gkg^{-1}]**	**C/N [-]**	**Al_o [gkg^{-1}]**	**Fe_o [gkg^{-1}]**	**Mn_o [$mgkg^{-1}$]**	**Si_o [$mgkg^{-1}$]**	**Al_d [gkg^{-1}]**	**Fe_d [gkg^{-1}]**	**Si_d [gkg^{-1}]**
Location 1 (non-glaciated)														
R1-P1-P1														
SdE-1	0–5	3.37	11.0	-28.4	108	7.8	13.8	1.54	3.24	27.5	109	2.90	3.91	937
SdE-2	5–10	3.40	11.5	-28.5	111	7.7	14.4	1.78	4.93	36.4	87	3.60	3.98	821
SdE-3	10–15	3.55	8.9	-28.0	96	7.2	13.3	2.50	5.12	15.0	167	4.50	4.07	1059
SdE-4	15–20	3.62	6.7	-28.3	61	4.3	14.3	1.72	5.52	7.9	105	3.39	4.62	602
SdE-5	20–25	3.66	5.5	-27.6	69	5.0	14.0	2.18	4.66	10.2	141	4.45	4.74	509
R1-P1-P2														
SdE-6	0–5	3.37	9.1	-28.0	117	8.4	14.0	1.56	5.06	15.7	89	3.43	3.95	943
SdE-7	5–10	3.39	12.3	-28.0	115	8.7	13.3	1.96	6.18	16.8	84	3.64	4.14	1047
SdE-8	10–15	3.44	9.5	-27.9	89	6.7	13.2	1.78	7.10	16.3	90	3.43	3.08	830
SdE-9	15–20	3.53	8.1	-27.7	(80)	6.1	13.2	1.71	6.66	12.5	121	4.44	4.55	785
SdE-10	20–25	3.61	6.2	-27.5	67	4.6	14.5	1.70	7.21	4.1	115	4.24	4.80	454
R1-P2-P1														
SdE-11	0–5	3.34	14.0	-28.2	134	(8.9)	15.0	1.55	3.57	10.8	49	2.39	3.98	795
SdE-12	5–10	3.47	7.6	-27.4	102	7.6	13.3	2.31	5.19	9.8	90	3.47	4.60	695
SdE-13	10–15	3.54	9.7	-27.8	77	5.8	13.3	2.17	4.09	4.6	79	2.88	4.63	347
SdE-14	15–20	3.63	7.7	-27.3	85	6.2	13.6	2.39	5.62	8.5	150	4.82	4.92	251
SdE-15	20–25	3.82	7.6	-27.1	94	6.2	15.3	4.16	8.16	8.3	110	8.89	8.33	435
R1-P2-P2														
SdE-16	0–5	3.33	10.0	-28.3	119	8.1	14.6	1.69	10.00	5.5	75	2.56	4.63	1019
SdE-17	5–10	3.51	8.8	-27.7	85	6.4	13.3	1.88	10.29	4.8	50	3.11	4.62	727
SdE-18	10–15	3.61	7.8	-27.4	(73)	5.5	13.3	2.31	12.09	5.6	104	3.62	5.04	608
SdE-19	15–20	3.74	7.7	-27.2	73	5.0	14.6	2.60	11.70	9.7	82	4.64	5.35	480
SdE-20	20–25	3.79	7.6	-27.1	69	4.8	14.4	1.89	8.17	6.8	71	5.68	6.29	361
Location 2 (glaciated)														
R2-P1-P1														
SdE-61	0–5	3.97	5.1	-28.8	69	4.9	14.1	0.95	3.27	18.5	15	1.54	4.46	584
SdE-62	5–10	3.82	5.4	-28.1	68	5.2	13.1	1.06	5.30	3.4	45	2.51	5.81	447
SdE-63	10–15	3.83	6.1	-27.6	(68)	(5.3)	12.9	1.45	4.69	4.0	123	3.09	7.00	331
SdE-64	15–20	3.91	6.2	-27.5	73	5.8	12.6	1.80	5.47	5.2	108	3.44	6.29	309
SdE-65	20–25	3.94	5.9	-27.4	62	(4.8)	12.8	2.20	2.58	5.0	101	3.79	6.97	226
SdE-66	30-35	4.13	5.6	-27.3	70	5.7	12.4	3.33	3.62	12.9	358	5.38	5.58	402
R2-P1-P2														
SdE-67	0–5	3.83	4.8	-28.1	62	4.8	13.0	1.29	4.34	4.1	65	2.38	4.52	476
SdE-68	5–10	3.88	5.2	-28.3	(63)	(4.7)	13.3	1.25	4.11	4.5	55	2.21	5.66	543
SdE-69	10–15	3.91	7.1	-27.8	70	5.3	13.3	1.75	5.90	2.6	58	3.61	6.34	392
SdE-70	15–20	3.95	8.0	-27.5	71	5.3	13.5	1.96	4.85	3.4	87	4.51	7.16	311
SdE-71	20–25	3.98	7.1	-27.4	65	4.9	13.2	2.34	4.40	5.3	62	5.12	7.45	318
SdE-72	30-35	4.12	6.1	-27.3	64	5.0	12.8	3.10	4.98	13.5	197	6.02	7.10	284
R2-P2-P1														
SdE-73	0–5	3.79	6.1	-28.6	61	4.7	12.9	1.05	4.10	5.7	26	2.41	6.55	467
SdE-74	5–10	3.81	6.8	-28.3	64	5.0	12.9	1.25	4.05	5.9	40	2.87	6.37	317
SdE-75	10–15	3.85	7.2	-28.1	72	5.6	12.8	1.65	4.18	6.0	49	3.74	7.58	429
SdE-76	15–20	3.89	5.6	-27.8	(68)	(5.4)	12.6	1.72	12.35	3.5	38	4.39	9.11	259
SdE-77	20–25	3.94	5.3	-27.7	(64)	(5.1)	12.6	2.04	5.60	3.2	50	4.52	7.74	263
R2-P2-P2														
SdE-78	0–5	3.87	6.1	-28.6	69	5.4	12.8	1.10	3.74	4.7	85	2.95	7.60	442
SdE-79	5–10	3.89	5.4	-28.2	71	5.6	12.7	1.21	5.30	3.7	86	3.46	8.17	278
SdE-80	10–15	3.86	5.4	-28.2	65	5.2	12.6	0.98	5.26	4.9	96	3.45	6.87	449
SdE-81	15–20	3.91	4.4	-27.7	69	5.4	12.7	1.30	4.88	2.6	64	5.21	7.34	257
SdE-82	20–25	3.93	5.3	-27.8	61	4.9	12.6			0.1	57	4.01	6.55	195

4.3.1 pH

The pH-values were measured twice. Consequently, the average values were determined. Figure 13 shows the average values of these two measurements from each site's four profiles (resulting mainly in n=8). The exact standard deviation and standard errors are summarized in Table 28. The standard errors are mostly low (≤ 0.05).

The pH values at the observed sites raise with increasing depth. The pH-values are in a range of 3.3 to 4.3, which can be described as acidic. While the pattern of the three sites at Location 2 shows similar properties in the depth profile, the pH at Location 1 varying more. In the formerly glaciated area, the upper soil layers' pH values are nearby 3.8 and rise to 4.1 in the deeper soil layers. The pH values at Reference 1 and Slope 1 are more acids than at the other sites. The pH is between 3.3 (at Reference 1) and 3.5 (at Slope 1) in the upper soil depths. In the lower soil depths, the values are approximately 0.4 higher. In contrast, the pH-values at Slope 2 are around 4.2 and relatively constant in the depth-profile.

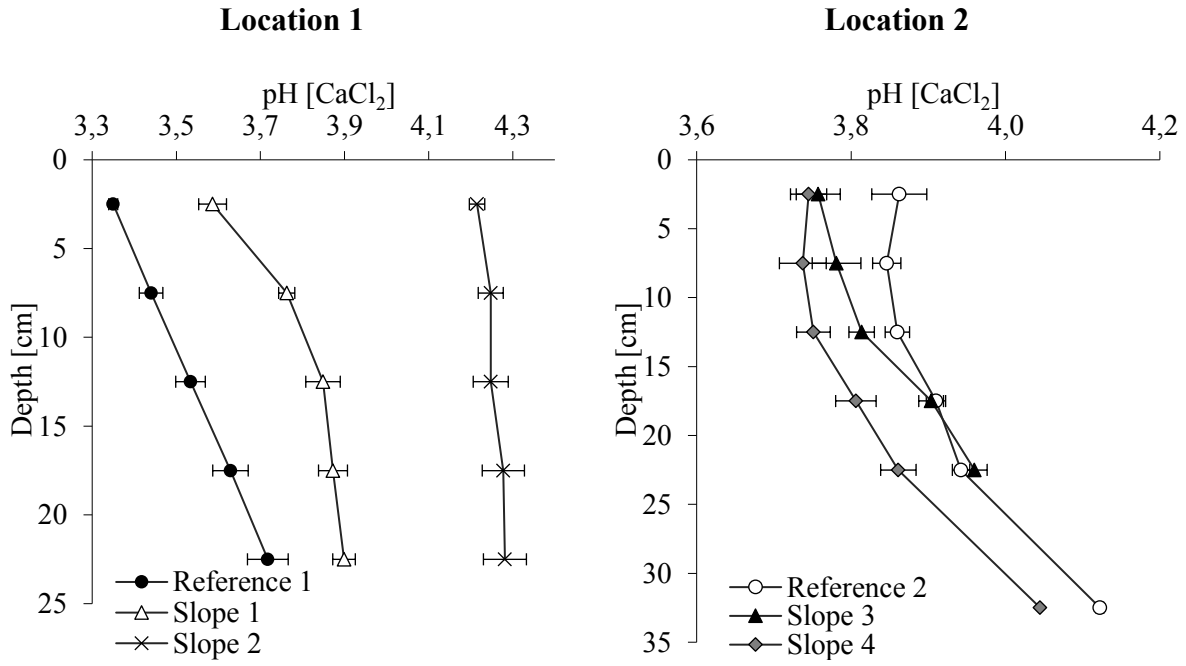

Figure 13; Plotted pH value at the observed sites with standard error, whereby n = 8

4.3.2 LOI

Figure 14 shows the average LOI-results (mainly is n = 4). The highest LOI-values (> 30%) are observed at Slope 1 in the upper soil layers and decreases to values under 15% at 7.5 cm. depth. The standard error is high at a depth of 2.5 cm (exact standard deviation and errors are summarized in Table 29). The LOI-values at Reference 1 are relatively high either, and they decrease in the depth profile. A contrasting pattern shows Slope 2; the values are smaller,

around 10%, and do not show a clear depth trend. The LOI values at Location 2 do not show a clear depth trend and are in a range between 10-16%.

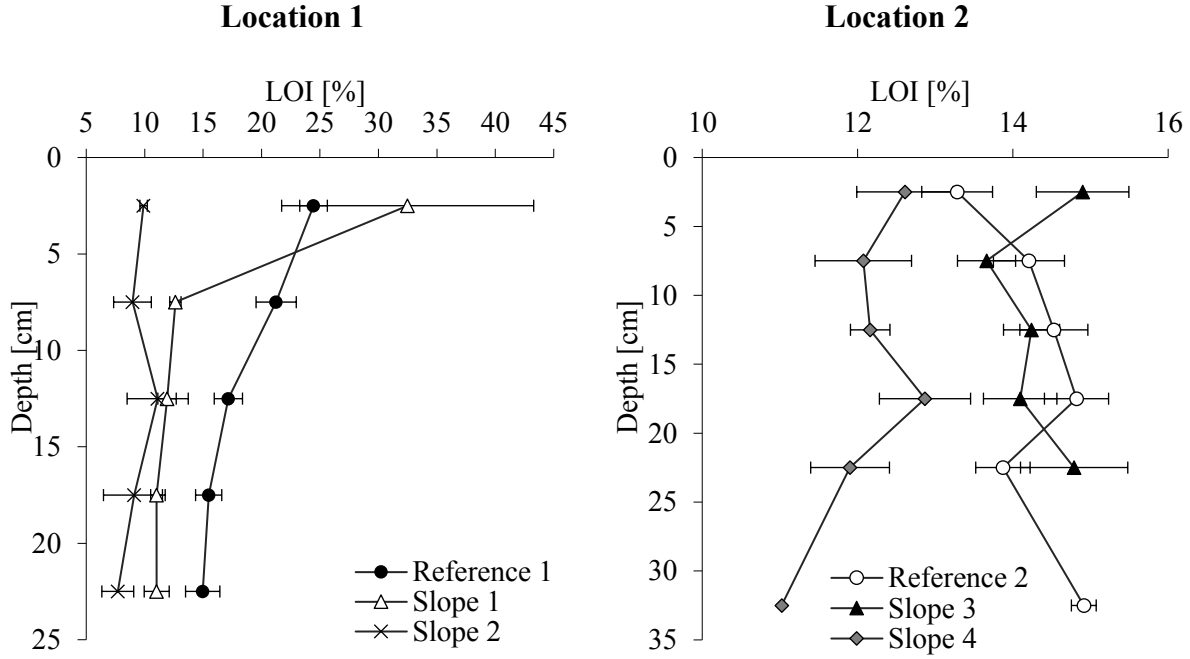

Figure 14; Loss on ignition (soil samples burned at a temperature of 550°C) for the observed sites with standard error, whereby n = 4

4.3.3 Carbon and Nitrogen

Each sample was measured twice, and the values in Figure 15 are the average of these two measurements from each site's four profiles (resulting mainly in n = 8). The exact standard deviation and standard errors are summarized in Table 30 to Table 32. An especially high standard error is visible at Slope 1 in a depth of 2.5 cm.

The highest amount of carbon values are in the upper soil layers at Slope 1, with an average value of almost 16%, and decreases in-depth to around 5%. The largest shift is between 2.5 and 7.5 cm, although the values do not change much further below. A quite similar pattern is recognizable at Reference 1, the highest values are nearby 12% in the upper soil layers, and the lowest values are in a depth of 20-25 cm. The amount of carbon is lower at Slope 2, with values between 2 and 4%. The graphics of the amount of nitrogen show similar patterns and are between 0.1 and 0.8%. The C/N-graphs do not show a depth trend and are in a range of 13 to 18. At Location 2 is no clear depth-trend visible for the total carbon and nitrogen. So is the amount of carbon of all sites between 5 and 7%. The amount of nitrogen is in a range between 0.4 and 0.6%. These values lead to a C/N ratio of approximately 13 and decrease smoothly in depth.

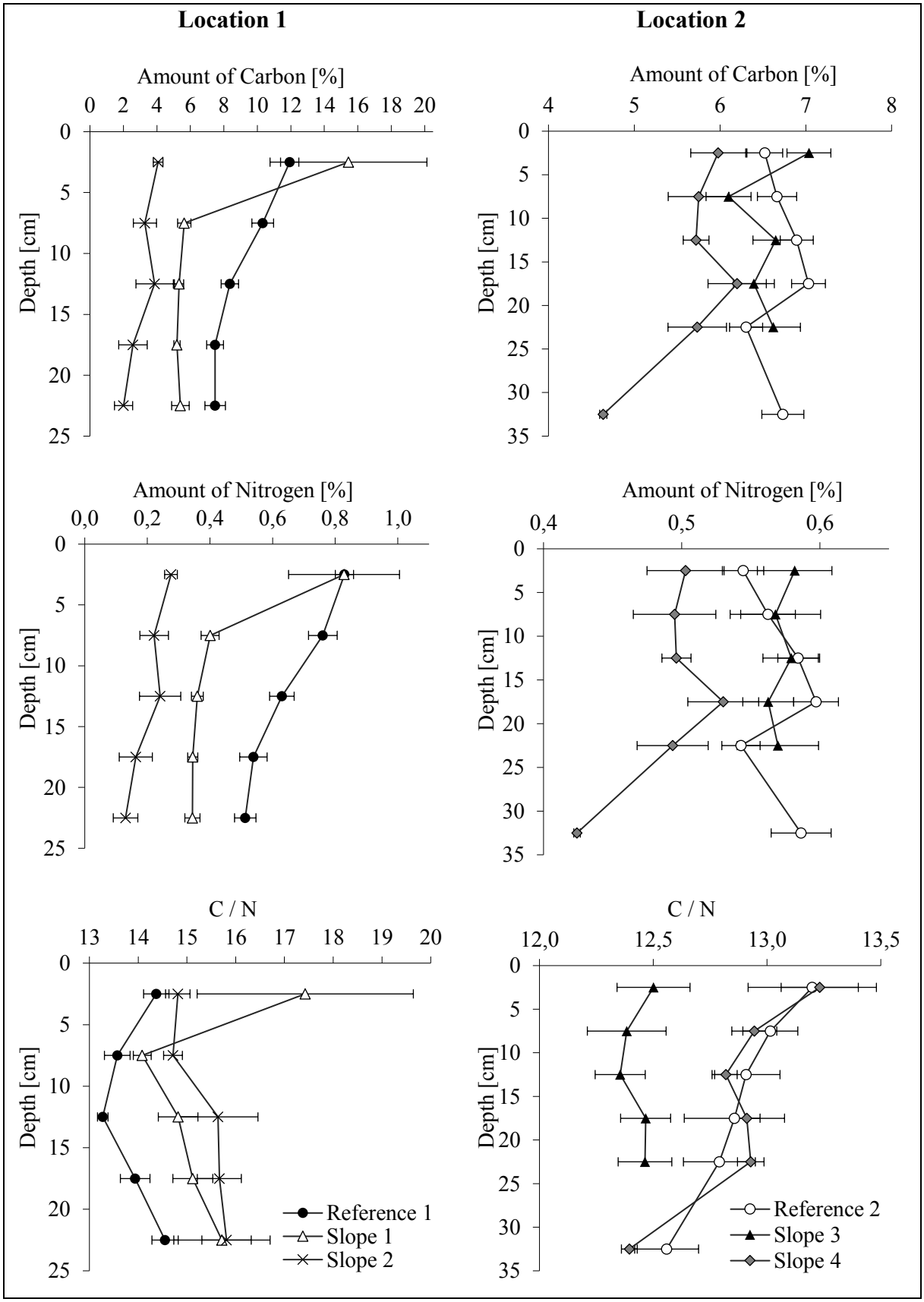

Figure 15; Amount of Carbon and Nitrogen [%] and the C/N ration with standard error, whereby n = 8

4.3.4 Picaro

Figure 17 shows the $\delta^{13}C$ values and the amount of carbon. The data originates from the picaro analyses. The trend line is added to compare the different sites better. The $\delta^{13}C$ values are in a range between - 29 and - 26.5 ‰. At Location 2 are the highest values at the reference sites. At Location 1 are the most negative values at Slope 1, whereby Reference 1 and Slope 2 have similar $\delta^{13}C$ values (see Figure 16). The standard errors are the highest at Slope 1 and 2. The exact standard errors and deviations are in Table 33.

Figure 17 shows the correlation between the C content and the $\delta^{13}C$ values. The amount of carbon shows a clear depth trend at Reference 1 and Slope 1. Besides, the $\delta^{13}C$ values become more negative by increasing depth. As a result, the trend line is slightly negative. The R^2 value for Reference 1 is almost 0.4 and therefore higher than at Slope 1 ($R^2 = 0.14$). Compared with Reference 1 and Slope 1, the depth-trend of the amount of carbon at Slope 2 is less extreme, and the $\delta^{13}C$ values do not show a clear pattern either. In total, the trend line is positive, with an R^2 value of approximately 3.3. The correlation between the amount of carbon and the $\delta^{13}C$ values at Location 2 are lower than at Location 1. The R^2 values are at all sites lower than 0.1. Neither the amount of carbon nor the $\delta^{13}C$ values show a clear depth-trend. Consequently, the data points resemble a random distribution.

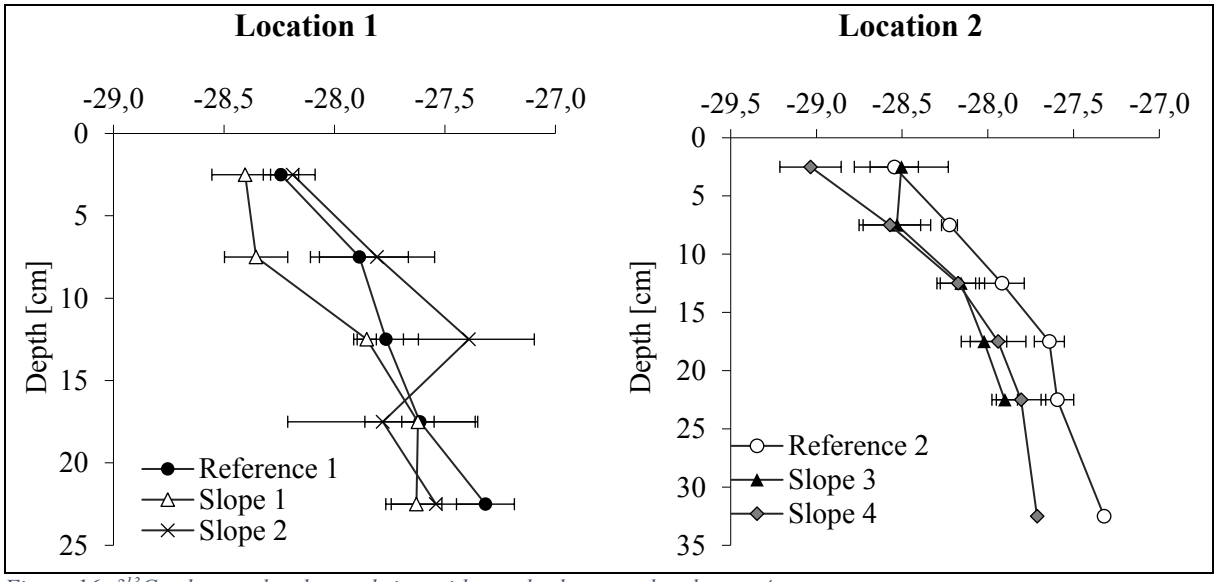

Figure 16; $\delta^{13}C$ values at the observed sites with standard error, whereby n = 4

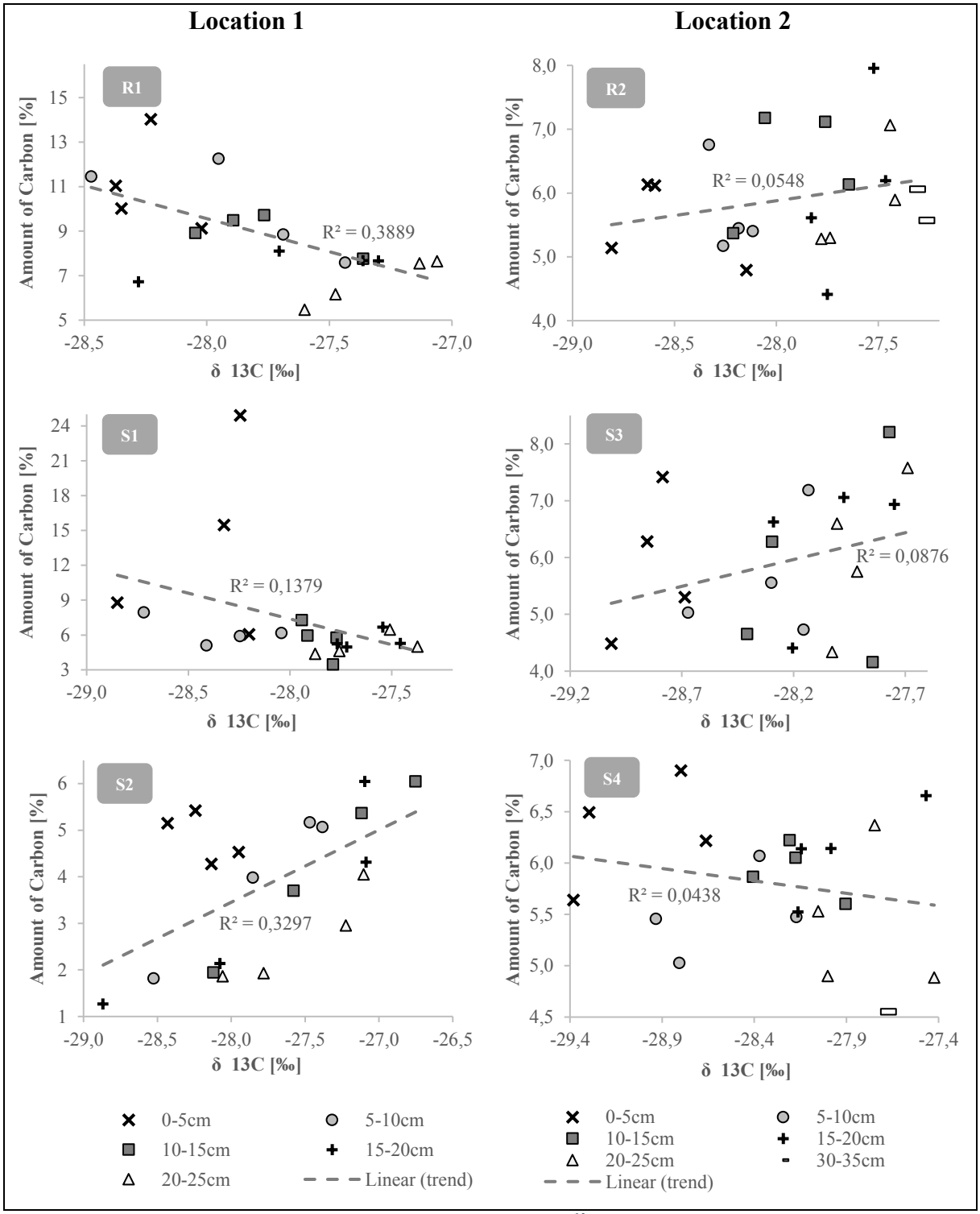

Figure 17: Correlation between Corg (amount of organic carbon) and $\delta^{13}C$ values as indicator of soil disturbance/stability. Below a concentration of 0.5% of Corg, $\delta^{13}C$ could not be measured accurately enough; these values were not considered for the correlation

4.3.5 Oxalate and dithionite extractable contents

Figure 18 shows the AAS-results. This method is elaborately and was done for the two reference sites. The oxalate extraction dissolves aluminum, iron, silicon, and manganese from the amorphous material, whereby the dithionite extraction dissolves aluminum, iron, and silicon from the amorphous and crystalline material. Therefore, the dithionite results should be higher than the oxalate extraction (McKeague & Day, 1966). The Al_o values increases in the depth profile, whereby the values at Reference 1 are higher than at Reference 2. In the upper soil layers, there are contained 1.1 (Reference 2) and 1.6 [gkg^{-1}] (Reference 1) Al_o. In a depth of 22.5 cm, the amount increases to 2.2 (Reference 2) and 2.5 [gkg^{-1}] (Reference 1). At Reference 2, the amount increases to 3.25 [gkg^{-1}] in a depth of 32.5 cm. The amount of Al_d is higher than the Al_d; in the upper soil layer, the concentration is ±2.3 [gkg^{-1}], and in the bottom, it is 6.3 [gkg^{-1}]. The values at the two sites are near to each other. In general, the standard errors and standard deviations are within the accepted range, but the highest can be detected at the Reference 1 site in a depth of 22.5 cm (Al_o and Al_d). The standard errors and standard deviation are summarized in Table 44. In the observed soils is the amount of iron higher than the amount of aluminum. The oxalate's observed range is 4-8 [gkg^{-1}], and the values at Reference 1 are higher than at Reference 2. The concentration increases slightly until 12.5 cm at Reference 1, respectively 17.5 cm at Reference 2, and decreases afterward. The pattern of the Fe_d is similar to the Fe_o, and the values are approximately 1 [gkg^{-1}] higher. At Reference 1, the results are curious; the Fe_d values are lower than the Fe_o values. The Si_o do not show a clear depth trend and range from 75 to 115 [$mgkg^{-1}$] (Reference 1) and 45 to 80 [$mgkg^{-1}$] (Reference 2). The Si_d values are significantly higher; at Reference 1, the upper soil layer's concentration is around 900 [$mgkg^{-1}$] and decreases to ±400 [$mgkg^{-1}$] in the bottom. At Reference 2, the upper soil layer concentration is around 500 [$mgkg^{-1}$] and decreases to ±250 [$mgkg^{-1}$] in 22.5 cm depth. In a 32.5 cm depth, the amount increases slightly to ±350 [$mgkg^{-1}$]. The manganese concentrations were only measured with the oxalate extraction and are in range of 3 to 15 [$mgkg^{-1}$], whereby the concentrations at Reference 1 are higher than at Reference 2. The crystalline Fe is calculated by the subtraction of Fe_o from Fe_d. The results at Reference 2 are around 2 [gkg^{-1}] and at Reference 1 in between – 4 and 0 [gkg^{-1}].

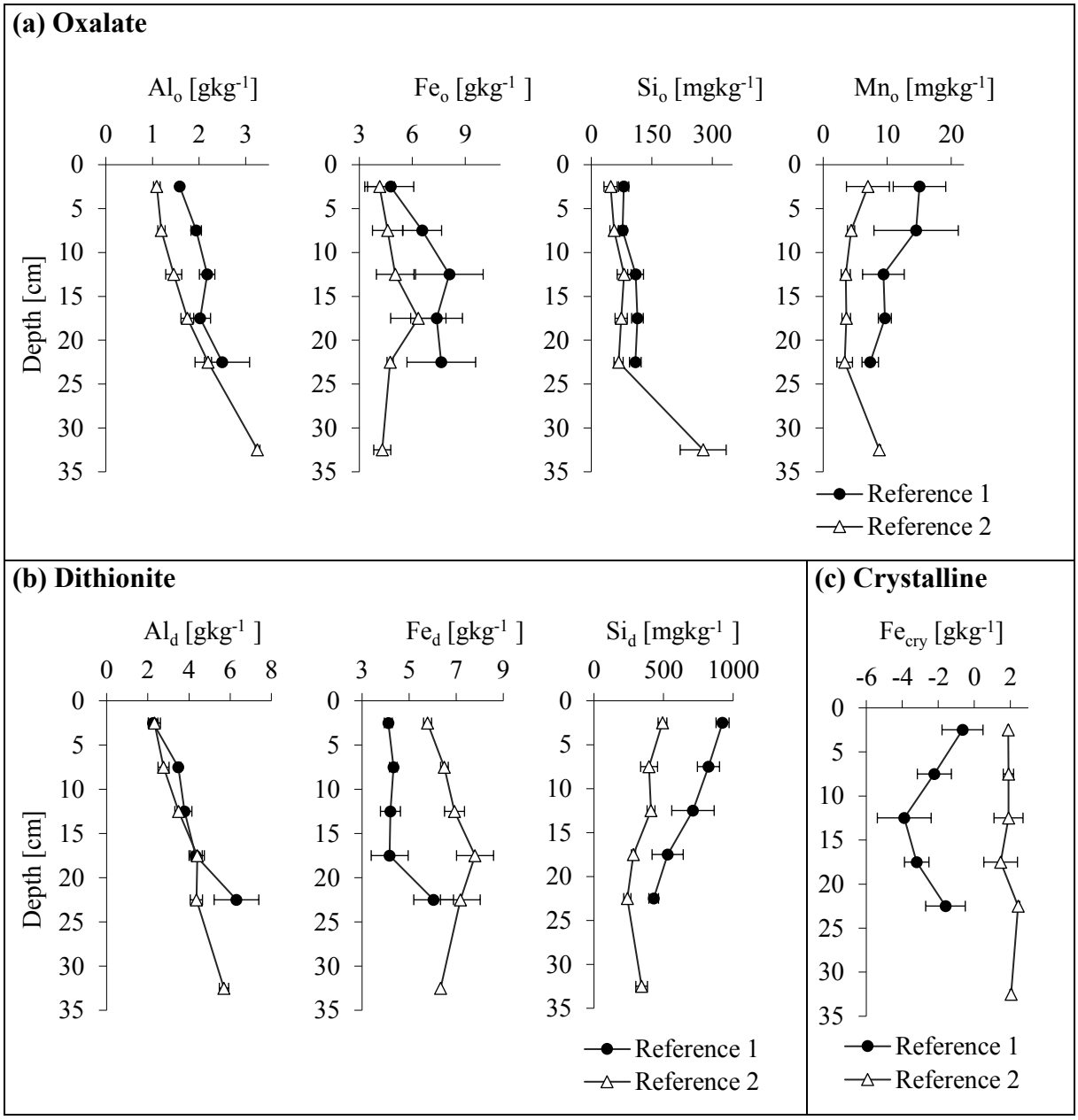

Figure 18; AAS results for the two references sites; (a) oxalate, (b) dithionite, (c) crystalline (dithionite - oxalate), with standard error, standard deviations and n are in Table 44 and Table 45

4.3.6 Elemental composition

The investigated elementary composition for the two references site is summarized in Table 1. The elemental composition of all observed sites is in the appendix (Table 21 and Table 22). The measurement was performed with XRF. The measured elements were converted to oxides, and the sum of major oxides was normalized to 100 % for easier comparison. The most common elements are SiO_2 and Al_2O_3, which are discussed in more detail, as well as TiO_2 and K_2O, which have a major impact on the used weathering indexes.

Table 6; Elementary composition of the two refernces sites

Sample	Soil Depth	Na_2O	MgO	AL_2O_3	SiO_2	P_2O_5	K_2O	CaO	TiO_2	MnO	Fe_2O3	LOI	Original Organic Matter	IVC
	[cm]	[%]	[%]	[%]	[%]	[%]	[%]	[%]	[%]	[%]	[%]	[%]	[%]	[%]
Location 1 (non-glaciated)														
R1-P1-P1														
SdE-1	0–5	4.23	0.84	22.20	40.36	1.11	5.19	0.69	0.41	0.02	4.67	20.30	18.99	4.22
SdE-2	5–10	4.01	0.82	22.14	40.73	1.09	5.33	0.69	0.41	0.02	4.52	20.24	19.72	3.98
SdE-3	10–15	4.14	0.91	25.05	40.25	1.63	5.38	0.70	0.44	0.02	5.05	16.44	15.35	3.49
SdE-4	15–20	4.32	0.98	27.53	42.41	1.81	5.66	0.77	0.51	0.02	5.28	10.73	11.57	1.03
SdE-5	20–25	3.90	0.92	26.68	40.80	2.01	6.01	0.78	0.58	0.02	5.62	12.68	9.41	4.31
R1-P1-P2														
SdE-6	0–5	3.83	0.85	21.83	36.72	1.22	4.75	0.65	0.48	0.02	5.75	23.90	15.70	8.09
SdE-7	5–10	3.99	0.86	21.77	37.62	1.39	5.03	0.72	0.47	0.02	5.33	22.81	21.09	2.30
SdE-8	10–15	4.15	0.92	24.47	40.40	1.55	5.09	0.67	0.49	0.02	5.33	16.93	16.31	2.96
SdE-9	15–20	4.43	0.96	25.99	40.05	1.85	5.45	0.69	0.50	0.02	5.56	14.50	13.94	2.59
SdE-10	20–25	4.54	1.01	27.43	42.02	1.88	5.90	0.73	0.53	0.02	5.38	10.57	10.61	1.64
R1-P2-P1														
SdE-11	0–5	4.35	0.83	20.47	38.49	0.93	4.81	0.69	0.40	0.02	4.36	24.67	24.12	3.83
SdE-12	5–10	4.47	0.94	24.05	38.49	1.41	5.08	0.65	0.47	0.02	5.26	19.17	13.05	8.59
SdE-13	10–15	4.41	0.93	25.70	41.13	1.59	5.36	0.67	0.52	0.02	5.20	14.47	16.72	-0.22
SdE-14	15–20	4.13	0.92	25.68	39.64	1.84	5.32	0.64	0.53	0.02	5.81	15.48	13.19	4.61
SdE-15	20–25	4.05	0.92	27.21	36.92	2.39	5.04	0.59	0.55	0.02	5.95	16.38	13.15	5.92
R1-P2-P2														
SdE-16	0–5	4.24	0.89	22.26	40.06	1.02	5.33	0.64	0.45	0.02	4.80	20.30	17.22	5.62
SdE-17	5–10	4.30	0.93	25.28	41.40	1.49	5.60	0.66	0.51	0.02	5.29	14.52	15.22	1.05
SdE-18	10–15	4.41	0.94	26.74	41.70	1.65	5.73	0.70	0.53	0.02	5.31	12.27	13.35	0.68
SdE-19	15–20	4.24	0.96	26.64	40.94	1.92	5.70	0.66	0.54	0.02	5.34	13.05	13.20	1.77
SdE-20	20–25	4.13	0.94	27.10	40.62	2.05	5.30	0.65	0.57	0.02	5.78	12.84	13.00	1.83
Location 2 (glaciated)														
R2-P1-P1														
SdE-61	0–5	3.73	0.78	21.75	48.86	0.62	7.45	0.33	0.40	0.02	3.73	12.33	8.84	4.96
SdE-62	5–10	3.54	0.75	22.55	47.69	0.67	7.36	0.22	0.44	0.02	4.54	12.22	9.30	4.65
SdE-63	10–15	3.55	0.74	23.15	47.05	0.66	7.45	0.21	0.46	0.01	4.58	12.14	10.56	3.22
SdE-64	15–20	3.44	0.76	23.78	45.19	0.69	7.05	0.21	0.45	0.01	5.01	13.40	10.65	4.55
SdE-65	20–25	3.75	0.74	23.87	45.96	0.65	7.43	0.19	0.44	0.01	4.92	12.05	10.13	3.24
SdE-66	30-35	3.88	0.81	26.44	42.13	0.86	6.92	0.19	0.43	0.02	4.97	13.35	9.58	5.56
R2-P1-P2														
SdE-67	0–5	3.41	0.77	23.00	48.89	0.65	7.52	0.20	0.45	0.01	4.31	10.78	8.24	4.01
SdE-68	5–10	3.55	0.78	23.24	47.07	0.68	7.51	0.22	0.45	0.02	4.59	11.90	8.90	4.30
SdE-69	10–15	3.55	0.73	23.04	47.03	0.66	7.54	0.21	0.43	0.01	4.54	12.26	12.24	1.53
SdE-70	15–20	3.66	0.75	23.86	45.65	0.68	7.41	0.21	0.45	0.01	4.84	12.49	13.69	0.23
SdE-71	20–25	3.62	0.79	24.39	45.07	0.68	7.08	0.18	0.44	0.01	4.77	12.98	12.15	2.74
SdE-72	30-35	3.63	0.83	26.11	42.95	0.79	6.95	0.20	0.44	0.02	5.26	12.83	10.42	4.27
R2-P2-P1														
SdE-73	0–5	3.65	0.79	22.91	48.44	0.56	7.47	0.19	0.46	0.02	4.47	11.05	10.55	2.28
SdE-74	5–10	3.38	0.72	22.54	47.95	0.57	7.33	0.17	0.43	0.01	4.63	12.29	11.62	2.66
SdE-75	10–15	3.76	0.76	22.95	46.00	0.63	6.99	0.17	0.46	0.02	4.98	13.28	12.35	2.85
SdE-76	15–20	3.63	0.79	23.68	45.76	0.63	7.14	0.17	0.46	0.01	5.13	12.60	9.65	4.75
SdE-77	20–25	3.65	0.77	24.52	45.25	0.65	7.21	0.16	0.49	0.01	5.14	12.15	9.11	4.66
R2-P2-P2														
SdE-78	0–5	3.26	0.84	23.16	46.98	0.60	7.31	0.19	0.47	0.02	5.04	12.14	10.52	3.74
SdE-79	5–10	3.45	0.75	22.86	46.34	0.61	7.17	0.17	0.46	0.02	4.97	13.21	9.37	6.03
SdE-80	10–15	3.47	0.77	22.86	46.58	0.60	7.29	0.17	0.43	0.01	4.72	13.09	9.24	6.13
SdE-81	15–20	3.44	0.75	23.08	45.98	0.60	6.94	0.16	0.44	0.01	5.06	13.54	7.59	8.18
SdE-82	20–25	3.42	0.78	23.99	46.38	0.66	7.19	0.16	0.45	0.02	5.13	11.81	9.08	4.37

SiO_2

The distribution of the elements shown in Figure 19 influences the weathering indexes, so they are described in more detail. SiO_2 is the most common oxide in all observed soils. The concentrations at all sites at Location 2 decrease mostly within the depth profile and are generally higher than at Location 1. The values are around 48% (Reference 2 and Slope 3) respectively ± 53% (Slope 4) in the upper soil-layers and approximately 45% in the bottom. On the other hand, the depth trend in Slope 1 is reverse. The concentration increases from 2.5 to 7.5 cm by almost 10%. However, the standard error at 2.5 cm depth is very high, so this jump could also be a measurement error. Table 33 shows the exact standard error and standard deviation. Reference 1 and Slope 2 do not show a clear depth-trend.

Al_3O_2

The second-highest concentrations are observed with Al_3O_2 oxide. Generally, the values increase in the depth profile, and they are mostly between 20 and 30%. Slope 2 can be described as an outliner; in the upper soil-layers, the values are around 32% and increases until 12.5 cm to values around 38%. Further down, the concentration remains at this level.

K_2O

The percentage frequency of K_2O is constant or slightly decreasing in the depth profile sites from Location 2. A decreasing pattern is also observed at Slope 2 until a depth of 17.5cm. But at Reference 1 and Slope 1, the K_2O concentration increases in depth. The depth range 0-5cm to 5-10 cm at Slope 1 from 5.1 to 6.4%. Similar to SiO_2, the standard error at Slope 1 at 2.5 cm depth is particularly high. The values at Location 1 are between 5 and 7% and therefore lower than at Location 2 with values between 7 and 8%.

TiO_2

The distribution of titanium oxide is comparable for almost all sites; the values are around 0.4% and are constant or slightly increasing in depth. But not for Slope 2; there is a sharp drop in the concentration from 2.5 to 12.5 cm and remains lower (± 0.27%).

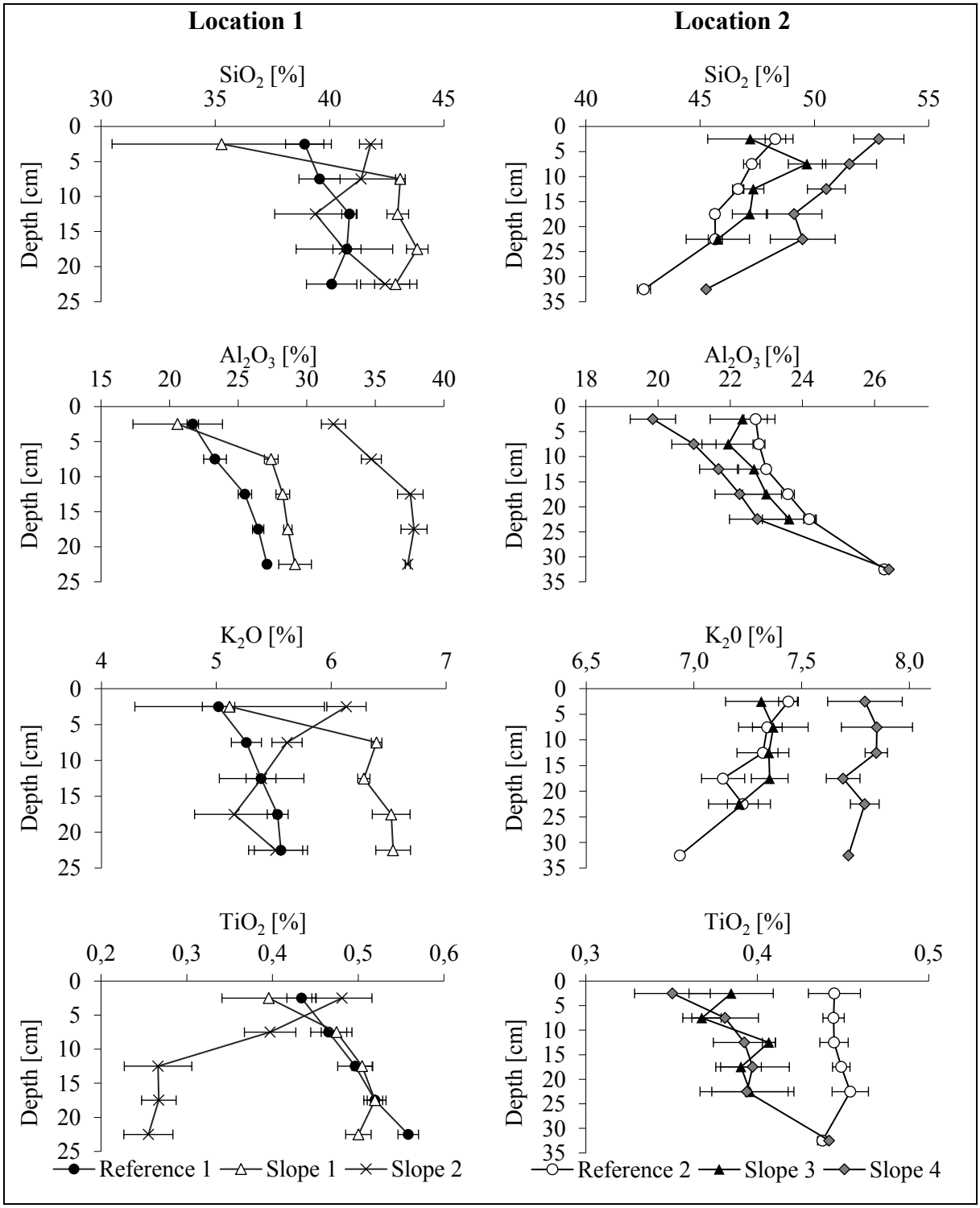

Figure 19; Sio_2, Al_2O_3, K_2O and TiO_2 (mass–%) of the observed sites with standard error, whereby n = 4

4.3.7 Weathering indexes

Table 7 shows the weathering indexes for the two references site. The calculated weathering indexes of all sites are in the appendix (Table 23 and Table 24). Depending on the used index, the weathering degree differs. The most similar weathering indexes are PIA, CPA, CIW, and CIA because the formulas use similar elements.

Table 7; Chemical weathering indexes from Reference 1 and 2: WIP = weathering index of Parker (Parker, 1970); (K + Ca)/Ti ratio (Harrington & Whitney, 1987); Index B (Kronberg and Nesbitt, 1982); CIA = chemical index of alteration (Nesbitt and Young, 1982); CIW = chemical index of weathering (Harnois, 1988); VR = Vogt ratio (Vogt, 1927); SA = Silico -aluminum ratio (Ruxton, 1968); PIA = plagioclase index of alteration (Fedo, et al., 1995); CPA = - chemical proxy of alteration (Buggle, et al., 2011).

Sample	Soil Depth [cm]	WIP	(Ca+K)/Ti	B-Index	CIA	CIW	VR	SA	PIA	CPA
Location 1 (non-glaciated)										
R1-P1-P1										
SdE-1	0–5	87.12	13.08	0.38	61.62	73.01	2.70	3.09	66.89	76.13
SdE-2	5–10	86.29	13.42	0.38	61.91	73.82	2.81	3.12	67.59	77.04
SdE-3	10–15	88.12	12.52	0.36	64.30	75.59	2.97	2.73	70.39	78.62
SdE-4	15–20	92.58	11.66	0.35	65.29	76.40	3.07	2.61	71.56	79.49
SdE-5	20–25	91.50	10.62	0.35	65.05	77.30	3.27	2.60	72.04	80.59
R1-P1-P2										
SdE-6	0–5	79.67	10.38	0.37	63.36	74.48	2.80	2.85	69.05	77.59
SdE-7	5–10	83.72	11.23	0.38	62.05	73.44	2.71	2.93	67.47	76.82
SdE-8	10–15	85.71	10.87	0.36	64.35	75.27	2.89	2.80	70.22	78.20
SdE-9	15–20	91.58	11.17	0.36	64.26	75.23	2.90	2.62	70.13	78.08
SdE-10	20–25	96.56	11.36	0.36	64.37	75.71	2.98	2.60	70.52	78.60
R1-P2-P1										
SdE-11	0–5	84.94	12.58	0.40	60.07	70.91	2.45	3.19	64.51	74.12
SdE-12	5–10	88.62	11.14	0.37	63.15	73.81	2.71	2.72	68.49	76.58
SdE-13	10–15	90.42	10.51	0.36	64.32	75.25	2.91	2.72	70.18	78.01
SdE-14	15–20	87.41	10.16	0.35	65.18	76.33	3.06	2.62	71.45	79.07
SdE-15	20–25	84.17	9.38	0.33	67.36	77.89	3.25	2.30	73.79	80.34
R1-P2-P2										
SdE-16	0–5	88.44	12.17	0.38	61.55	73.23	2.69	3.05	66.96	76.13
SdE-17	5–10	91.47	11.11	0.36	63.81	75.33	2.95	2.78	69.90	78.12
SdE-18	10–15	93.68	10.95	0.36	64.49	75.83	3.02	2.65	70.67	78.65
SdE-19	15–20	91.82	10.77	0.35	65.01	76.54	3.10	2.61	71.48	79.26
SdE-20	20–25	87.39	9.48	0.34	66.38	77.24	3.17	2.54	72.79	79.95
Location 2 (glaciated)										
R2-P1-P1										
SdE-61	0–5	100.66	16.90	0.41	59.50	76.35	3.42	3.81	67.00	78.00
SdE-62	5–10	97.79	14.82	0.39	61.38	78.37	3.76	3.59	70.09	79.46
SdE-63	10–15	98.57	14.48	0.38	61.84	78.83	3.86	3.45	70.82	79.87
SdE-64	15–20	94.23	13.92	0.36	63.50	79.76	3.95	3.22	72.80	80.78
SdE-65	20–25	100.14	14.83	0.38	62.13	78.56	3.81	3.27	70.85	79.47
SdE-66	30-35	97.28	14.16	0.35	65.01	79.69	3.87	2.70	73.76	80.54
R2-P1-P2										
SdE-67	0–5	97.92	14.81	0.38	61.97	79.38	3.94	3.61	71.32	80.40
SdE-68	5–10	99.19	14.75	0.38	61.79	78.82	3.81	3.44	70.76	79.92
SdE-69	10–15	99.32	15.53	0.38	61.56	78.73	3.87	3.46	70.50	79.77
SdE-70	15–20	99.29	14.77	0.38	62.33	78.85	3.84	3.25	71.22	79.83
SdE-71	20–25	96.15	14.30	0.36	63.62	79.52	3.87	3.14	72.69	80.38
SdE-72	30-35	95.25	13.99	0.35	65.33	80.48	3.99	2.79	74.58	81.40
R2-P2-P1										
SdE-73	0–5	99.80	14.51	0.39	61.34	78.30	3.71	3.59	70.01	79.22
SdE-74	5–10	95.79	15.08	0.38	62.03	79.35	3.97	3.61	71.35	80.22
SdE-75	10–15	96.63	13.39	0.38	62.00	77.93	3.62	3.40	70.30	78.75
SdE-76	15–20	96.73	13.64	0.37	62.83	79.04	3.80	3.28	71.75	79.86
SdE-77	20–25	97.36	13.08	0.36	63.50	79.57	3.92	3.13	72.65	80.34
R2-P2-P2										
SdE-78	0–5	94.91	13.68	0.37	62.97	80.23	3.97	3.44	72.76	81.20
SdE-79	5–10	95.20	13.89	0.38	62.45	79.25	3.88	3.44	71.62	80.11
SdE-80	10–15	96.44	14.93	0.38	62.19	79.20	3.86	3.46	71.37	80.03
SdE-81	15–20	93.08	13.96	0.37	63.16	79.50	3.90	3.38	72.35	80.32
SdE-82	20–25	95.19	14.04	0.36	63.63	80.19	4.03	3.28	73.22	81.00

Figure 20 shows the results of the different used formulas' weathering indexes as an average of the four profiles per site. The standard deviation and the exact standard errors are shown in Table 38 to Table 42. The arrows above the graphs describe the indexes' meaning: When the arrow points to the left, the weathering is more advanced lower values, and vice versa. The most weathering indexes indicate that the weathering is more advanced in the bottom than in the upper soil layers and the sites at Location 1 seem to be more weathered than the sites at Location 2. Let's have a closer look at the individual indexes.

(Ca + K) / Ti

The values of Reference 1, Slope 1, and Reference 2 are in a range of 10-15, and they decrease in the depth profile, which means that the weathering in the bottom is more advanced - according to this weathering index. Although the values are near each other, the weathering indexes from Reference 1 are lower than that of Slope 1, and the highest results are at Reference 2, so this site seems to be less weathered than the other two. Contrary to this, the weathering index at Slope 2 increases in the depth profile, especially from 7.5 to 12.5 cm is a leap. Therefore, the weathering degree in the bottom of Slope 2 seems to be much lower than at the other sites. However, the standard errors at Slope 2 are also higher than the others. The weathering indexes at Slope 3 and 4 are higher than at Reference 2, and the values decrease overall in the depth profile, although the trend is less clear than at Reference 2. In summary, the weathering degree, according to (Ca + K) / Ti, behaves as follows: The highest weathering degree is at Reference 1, followed by Slope 1, Slope 2 (0 – 10 cm), Reference 2, Slope 3, Slope 4 and the less weathering degree is at Slope 2 (10-25 cm).

WIP

Overall, the weathering indexes are higher at the sites from Location 2 than at Location 1; they are between 95 and 105, whereby the values at Slope 4 are the highest. None of the sites at Location 2 have a clear depth trend. The three sites at Location 1 shows differ pattern. The weathering index at Slope 2 drops massively from 7.5 to 12.5 cm, and the found values in the bottom are the lowest of all observed sites. However, the values at Slope 1 increase significantly from 2.5 to 7.5 cm. But the standard error at 2.5 cm is high. The indexes at Reference 1 increase smoothly in the depth profile, and the values are between Slope 1 and Slope 2. In summary, the weathering degree, according to the WIP index, behaves as follows: The highest weathering degree is at Slope 2, followed by Reference 1, Slope 1, Reference 2, and Slope 3, and the less weathering degree is at Slope 4.

B-Index

The values at all sites decrease in the depth profile. The lowest values are at Slope 2 with 0.3 in the upper layers, and they drop sharply within the first 15 cm to values around 0.24. The weathering indexes at the other five sites are near each other in a range of 0.33 to 0.42. Whereby the highest values are at Location 2. The standard errors are, compared to the WIP-Index, small. In summary, the weathering degree, according to the B-index, behaves as follows: The highest weathering degree is at Slope 2, followed by Slope 1, Reference 1, Reference 2, Slope 3, and the less weathering degree is at Slope 4.

CIA

The results of the CIA are almost the same as when using the PIA, CPA, or CIW indexes. In contrast to the other displayed weathering indexes, higher values indicate more advanced weathering. The values increase in the depth profile of all observed sites. All sites, except Slope 2, are between 57 and 67, whereby the lowest indexes are at Slope 4. The values at Slope 2 are significantly higher and increases within the first 15 cm to values around 75. If all graphs were flipped, the pattern would be almost the same as that of the B-Index.

Therefore, the sites' weathering degree shows the same order as with the B-Index: The highest weathering degree is at Slope 2, followed by Slope 1, Reference 1, Reference 2, Slope 3, and the less weathering degree is at Slope 4.

SA

The patterns resulting from the SA are similar to that one of the B-Index, although the values are higher. The highest weathering degree is at Slope 2, followed by Slope 1, Reference 1, Reference 2, Slope 3, and the less weathering degree is at Slope 4. This is the same order as already by the B-Index and the CIA. The most striking difference is that the values between the two sites are further apart, so according to this weathering index, the sites at Location 1 are also more weathered than at Location 2.

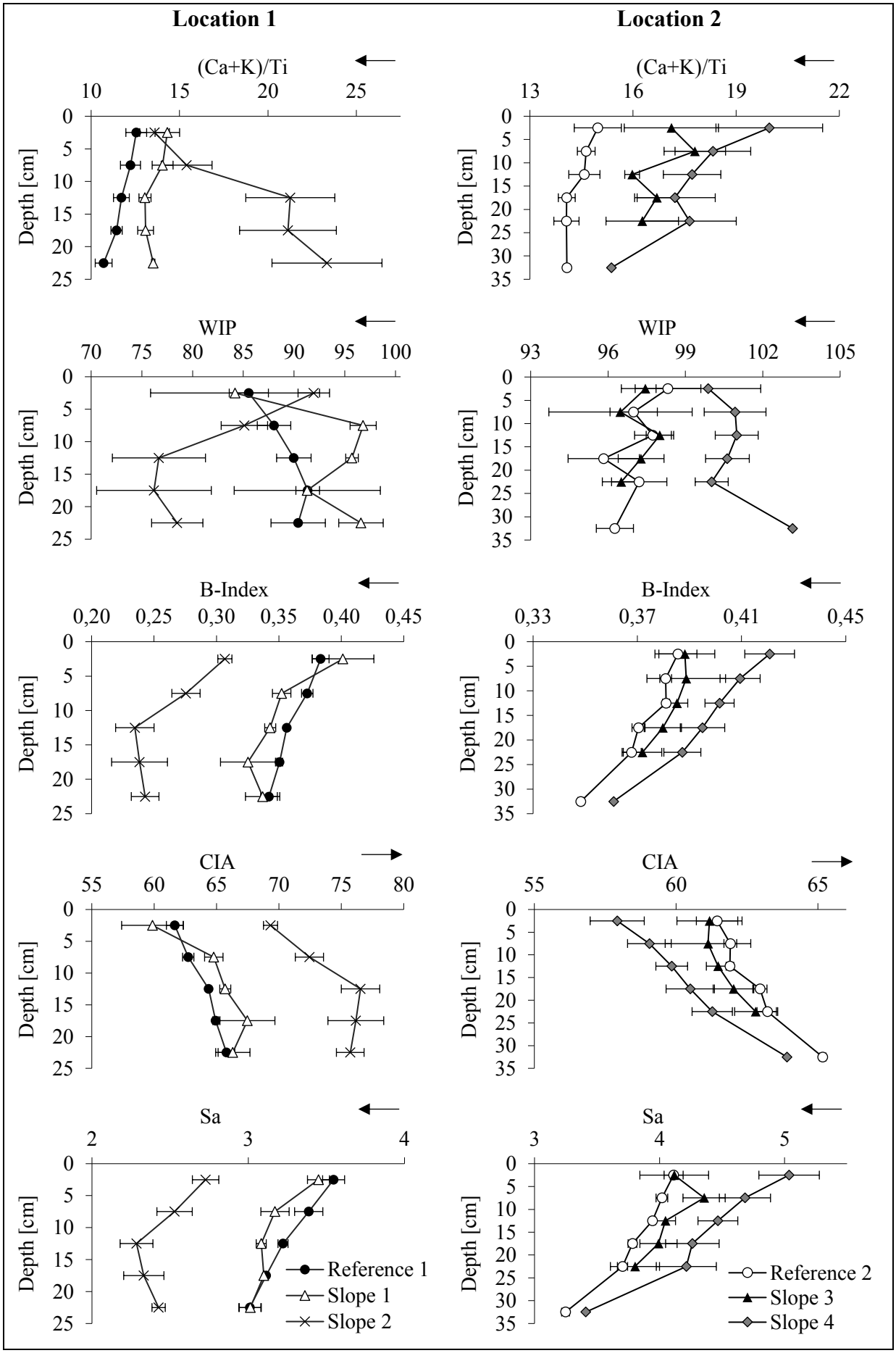

Figure 20; Weathering indexes with standard error, whereby n = 4. The arrow show in which side the weathering increases

4.4 Cosmogenic nuclides

The ^{10}Be concentration extraction was done for the two profiles in Pit 1 at the Reference 2 site. The concentration does not show a clear depth trend. The highest concentration within Profile 1 was measured at a depth range of 15 - 20 cm and reaches values about 42 x [10^8 atoms g^{-1}]. However, the maximal values at Profile 2 are in the same depth range. But the variations within Profile 2 are lower; the concentrations are between 31 and 36 x [10^8 atoms g^{-1}]. The total amount of Beryllium atoms is higher at Profile 1 than within Profile 2.

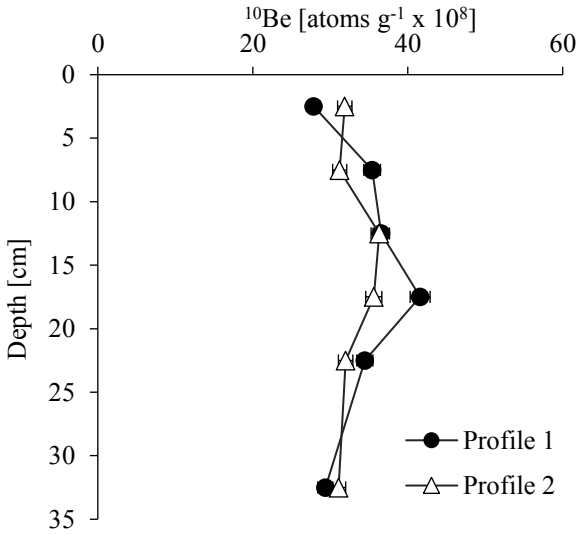

Figure 21; ^{10}Be concentration in the depth profile from profile 1 and profile 2 (Reference 2 site 2, pit 1) with standard error, whereby n = 4

4.4.1 Age estimation

The age estimation is done by the application of three different methods. The results are in Table 8. All applied formulas use the total ^{10}Be atoms per profile (details in Table 17). In the formulas by Monaghan et al. (1986) and Graley et al. (2011), the precipitation is included, resulting in different ages, up to the assumed precipitation. Increasing precipitation leads to higher deposition rates, which in turn leads to younger soil ages. According to the formula of Willenbring & von Blanckenburg (2010), the soil age is over 30 ka. Contrary, the soil age is around 15 ka by using the formula of Graley et al. (2011). By Monaghan et al. (1986), the age is about 25 ka. In general, the soil age at Profile 1 is higher than at Profile 2.

Table 8; Soil age calculations for Reference 2 by using different deposition rates (Monaghan, et al., 1986; Willenbring & von Blanckenburg, 2010; Graly, et al., 2011)

	Monaghan et al. (1986)				**Graley et al. (2011)**			**Willenbring & von Blanckenburg (2010)**
	Precipitation [mma^{-1}]				**Precipitation [mma^{-1}]**			
	1400	**1600**	**1700**	**1800**	**1400**	**1600**	**1800**	
Calculated deposition rates [atoms cm^{-2} a^{-1}]	1'694'000	1'936'000	2'057'000	2'178'000	2'684'449	3'087'249	3'451'435	1'400'000
Calculated soil age for profile 1 [ka]	28.4	24.9	23.40	22.1	17.9	15.6	13.9	34.5
Calculated soil age for profile 2 [ka]	26.2	22.9	21.56	20.4	16.5	14.3	12.8	31.8

4.4.2 Soil age estimation for Reference 1 by using the correlation between ^{10}Be and Fe_o

The soil age estimation by using the ^{10}Be is only possible for Reference 2 because we did not measure the ^{10}Be concentration for other sites (because of the high costs). Nevertheless, it is possible to estimate the ^{10}Be concentration roughly. Several authors (e.g. Willenbring & von Blanckenburg, 2010; Egli, et al., 2010; Calitri, et al., 2019) observed the correlation between ^{10}Be and organic ligands or Metallo-organic complexes.

By plotting the Fe_o and the ^{10}Be, three outliners can be seen (compare Figure 22). The linear regression was done without these three data points, resulting in a strong correlation ($R^2 = 0.93$). The functional equation allows the calculation of the ^{10}Be concentration for Reference 1. The standard errors are high (details are in Table 46). Therefore, the resulting age estimations are not very accurate. Nevertheless, it allows the determination of certain trends.

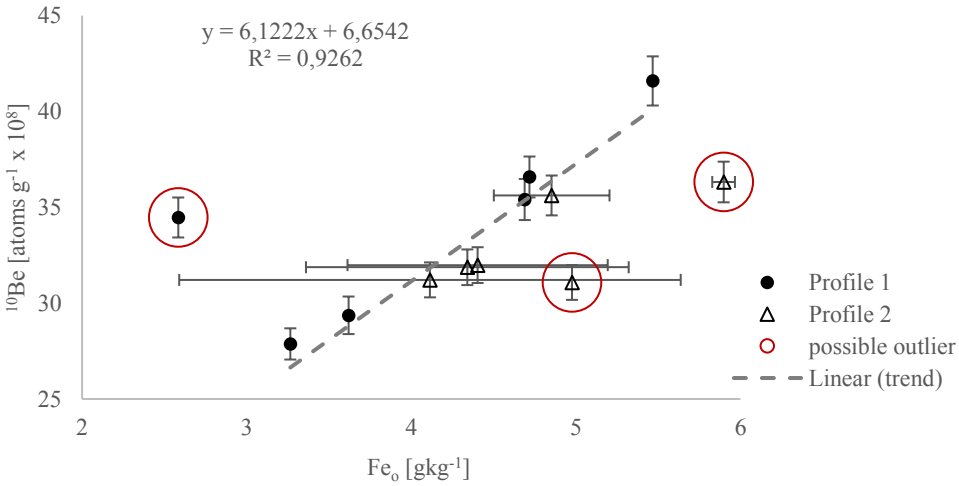

Figure 22; Correlation between meteoric ^{10}Be and Fe_o at Reference 2

The ^{10}Be concentration was calculated with the functional equation (y = 6.1222x + 6.6542). The results are shown in Figure 23, and the detailed standard deviations are summarized in Table 47. At Reference 1, the Fe_o concentrations are higher than at Reference 2, resulting in higher ^{10}Be concentrations at Reference 1 than at Reference 2. The ^{10}Be concentrations at Reference are in a range between 35 and 60 [atoms g^{-1} x 10^8].

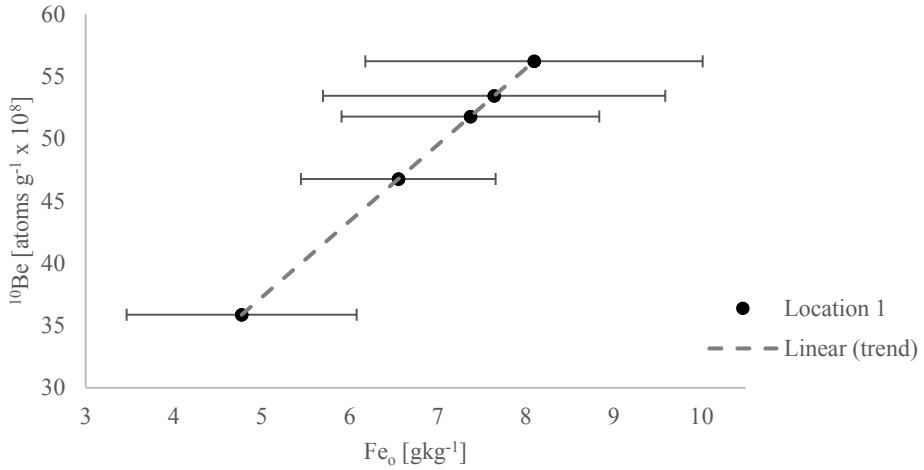

Figure 23; Correlation between meteoric ^{10}Be and Fe$_o$ at Reference 1

The obtained ^{10}Be values were used to estimate the soil age for Reference 1. The estimation was done with the same methods as for Reference 2 (details in chapter 3.4.2). Compared to Reference 2, the estimated soil age at Reference 1 is higher depending on the used method between 2.5 and 5 years older. All applied formulas use the total ^{10}Be atoms per profile (details in Table 18).

Table 9; Soil age estimations for Reference 1 by using different deposition rates (Monaghan, et al., 1986; Willenbring & von Blanckenburg, 2010; Graly, et al., 2011)

	Monaghan et al. (1986)				**Graley et al. (2011)**			**Willenbring & von Blanckenburg (2010)**
	Precipitation [mma^{-1}]				**Precipitation [mma^{-1}]**			
	1400	**1600**	**1700**	**1800**	**1400**	**1600**	**1800**	
Calculated deposition rates [atoms cm^{-2} a^{-1}]	1'694'000	1'936'000	2'057'000	2'178'000	2'684'449	3'087'249	3'451'435	1'400'000
Calculated soil age for profile 1 [ka]	31.36	27.42	25.79	24.35	19.73	17.26	15.33	38.01

4.5 Fallout Radionuclides

The $^{239+240}$Pu measurement was done for all samples, except for one sample (SdE-72), due to laboratory errors. The ^{240}Pu / ^{239}Pu ratios of most of the samples are between 0.165 and 0.200 (compare Figure 24a) and, therefore, within the global fallout range (0.180 ± 0.014).

The erosion estimates were made on the one hand with the inventory method (IM) and on the other hand with the profile distribution model (PDM). The Pu inventories of non-erosive sites (in our case, the reference sites) are compared with erosive sites (in our case, Slope 2-4). Thus, erosion rates of the last ~60 a from the slope sites can be estimated. These results are shown in Table 10. The higher (less negative) the mass redistributions, the lower are the estimated erosion rates (according to this method). The erosion rates at Location 1 are higher than at

Location 2, whereby the lowest mass redistribution are at Slope 2 with values lower than - 2000 [$tkm^{-2}a^{-1}$] (inventory method, P = 1.0). The calculated results at Slope 1 are around - 1000 [$tkm^{-2}a^{-1}$]. In contrast, the erosion rates at Location 2 are lower. The mass redistribution at Slope 4 is around + 300 [$tkm^{-2}a^{-1}$] and at Slope 3 a little higher than 0. Up to the applied method, the results differ slightly. The lowest erosion rates are estimated by using the PDM. Higher erosion rates are estimated by using the IM, whereas the highest rates erosion rates are calculated with a Particle-size correction factor of 1.0.

Table 10: Calculated soil erosion rates of $^{239+240}Pu$ at Slope 1 and Slope 2 (non-glaciated) and at Slope 3 and Slope 4 (Former glaciated). Inventory method after Lal et al. (2013) applying diverse particle size correction factors (PM), Profile Distribution Method after Walling and He (1999), and Zhang et al. (1990)

		Inventory Method (IM) P=1 [tkm^2yr^{-1}]	P=1.2 [tkm^2yr^{-1}]	P=1.5 [tkm^2yr^{-1}]	Profile Distribution Method P=1 [tkm^2yr^{-1}]
Location 1 (non-glaciated)					
S1	Average	-1'395	-1'162	-930	-891
	Std. error	39.2	38.5	34.4	34.2
S2	Average	-2'066	-1'722	-1'378	-908
	Std. error	49.6	45.3	40.5	32.5
Location 2 (glaciated)					
S3	Average	55	46	37	63
	Std. error	23.9	21.9	19.5	25.4
S4	Average	336	280	224	398
	Std. error	16.7	15.3	13.7	17.1

Because of the observed pits' varying slope angle, the mass redistribution can be plotted together with the slope angle. In Figure 24c is a strong correlation visible; the steeper the slope, the more negative are the mass losses at the observed soil. By a slope angle of 5° (Slope 3 and 4) is the mass redistribution between -100 and +400 [$tkm^{-2}a^{-1}$], whereby the mass redistribution reaches the lowest values at a slope angle of 20 ° (Slope 2).

In Figure 24d, the Pu activity depending on the depth profile, is displayed. The activity decreases in the depth profile, whereby the values in the upper soil layers are around 3 [$Bqkg^{-1}$] and decrease to values between 0.03 and 1 [$Bqkg^{-1}$] in the bottom. Pu activities below 0.3 are not detectable with this measurement method. The highest Pu-activities are observed at Location 1. The pattern from Reference 2, Slope 3, and Slope 4 are quite analogous. The total inventory at Reference 1 is around 245 [Bqm^{-2}], while the amount at Slope 1 and Slope 2 is around 70 [Bqm^{-2}], respectively nearby 90 [Bqm^{-2}]. The examined sites at the previously glaciated area do not show a clear pattern; the reference sites have the lowest total inventory (± 90 Bqm^{-2}), followed by the Slope 3 (± 130 Bqm^{-2}), and the highest amount is at Slope 4 (± 160 Bqm^{-2}).

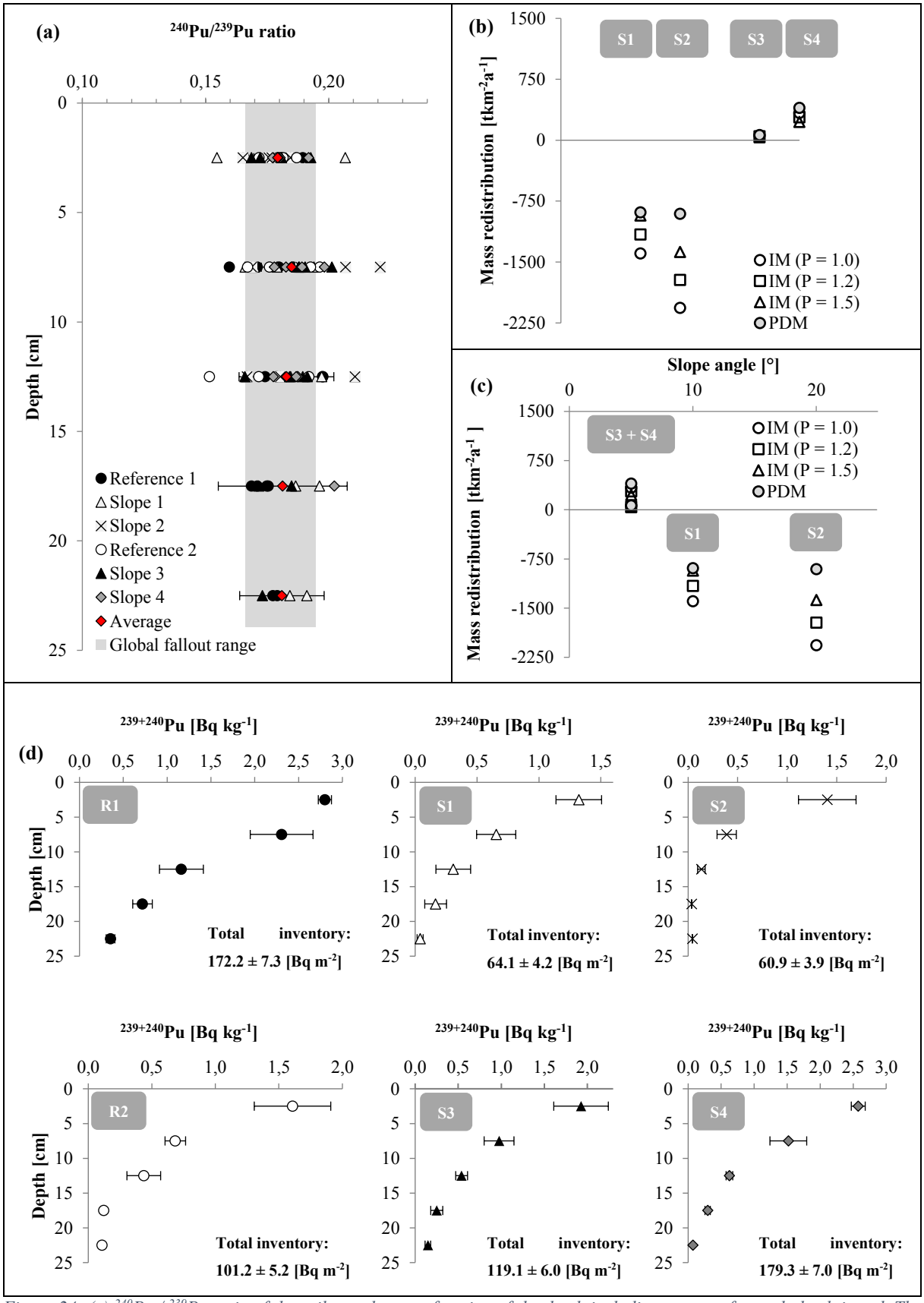

Figure 24; (a) ^{240}Pu / ^{239}Pu ratio of the soil samples as a function of the depth including average for each depth in red. The grey area indicates the global fallout range (0.180 ± 0.014) of the northern hemisphere (Kelly, Bond, & Beasley, 1999). (b) Annual soil erosion with different particle size correction factors (p = 1.0, 1.2, and 1.5) for the inventory method (IM; R Lal et al., 2013) and the profile distribution model (PDM; Walling & He, 1999; Zhang et al., 1990). (c) Calculated soil erosion ranges in relation to the slope angle (d) Depth activity profiles (±standard error) of the investigated sites.

5 Discussion

5.1 Soil properties and comparability of the sites

This master thesis aims to compare the erosion rate from a formerly glaciated and a non-glaciated area in the EAG. The comparison is only meaningful when the different sites have similar soil characteristics. Otherwise, possible differences could be caused by different soil properties. At both locations, the Munsell colors are within the brown soil range and are almost identical. The pH values from all sites are low and can be described as acidic. At Location 1, the value differs more between the sites than at Location 2, but they are still comparable. The carbon and nitrogen, as well as the elementary composition, are very similar. By regarding the AAS results, the two locations behave similarly. Although all investigated sites' chemical and physical properties are in a similar range, there are varying patterns in the depth profile: The soil profiles at Location 1 show mostly the excepted depth trend. Contrary, some soil properties within the depth profiles at Location 2 do not have the excepted depth trend. The soil seems to be mixed regularly, which could be caused by more intense cryoturbation, which occurs by frost events and changing temperature. The temperature at location 2 is lower because of the higher altitude, leading to more frost events. The different soil characteristics, including the possible explanations, are discussed in the following chapters.

In general, the observed soil sites are cambisols. Cambisols are younger soils with weak to moderate weathering. The pH is expected in a deeper range and usually increases in the depth profile. Cambisols experience plugging but no further chemical modification. Usually, cambisols do not have washed-in Al and Fe compounds (IUSS Working Group WRB, 2015). But the investigated soils show an opposite pattern; the concentration increases slightly within the depth profiles. This behavior will be discussed in more detail in chapter 5.1.2.

5.1.1 Grain size

Usually, the grain size increases in the depth profile because the weathering is more advanced in the upper soil layers, which reduces the grain size. This trend is slightly visible at Reference 1 but not at Reference 2, where the grain size distribution does not show a depth trend. The grain size distribution indicates the soil aggregates stability. Soils with a higher silt amount could be more vulnerable to erosion. In contrast, sand particles are heavy and more stable, and clay increases the soil stability because of the binding and cementing effect of clay (Morgan, 1999; Lado, et al., 2004). The silt amount at Reference 2 is higher than at Reference 1, which could increase erosion risk (Morgan, 1999). But the higher clay amount at Reference 2 increases

the aggregate stability (Lado, et al., 2004). However, the grain size composition is at both locations similar to each other, whereas conclusions on the soil aggregate stability are not clear.

5.1.2 Oxalate and dithionite extractable contents

The amorphous amount of aluminum, iron, and silicon do show a similar depth trend at both locations, whereby the values at Reference 1 are higher by a factor of 1.1 to 1.7 compared to Reference 2. According to (Stahr, et al., 2016), the Fe_o values are within the typical range for cambisols (between 4 and 8 gkg^{-1}). However, the Fe_o concentrations are expected to decrease within the depth profile (IUSS Working Group WRB, 2015; Stahr, et al., 2016). However, the observed concentrations increase slightly within the upper 15-20 cm, especially at Reference 1. The Al_o concentration also increases slightly. Such depth trends within the upper soil layers are typical for podzols. But because of the low development of the soils, advanced podzolization is unlikely. This behavior was caused more likely by cryoturbation, which mixes the soil vertically (further discussed in chapter 5.5.1). Fe_d's depth trend shows the expected pattern for cambisols (Stahr, et al., 2016).

The crystalline amount was calculated by the subtraction of the oxalate results from the dithionite results. The Al_{cry} values are in a similar range as the Al_o. The Si_{cry} amount is by a factor of 2 to 10 higher than the Si_o, whereas the Si_{cry} amount is especially high in the upper soil depths (factor 10). In contrast, the Fe_{cry} behaves strangely; the values at Reference 1 are negative. It seems like an error in the measurement. A repeat of the measurements would give certainty, but the measurement was not repeated because of limited time resources and space in the laboratory.

5.1.3 Soil disturbance and erosion according to C amount

The amount of carbon at the observed sites is higher than excepted. Apparently, there were large C inputs in the development of the soil. C accumulation is typically caused by litter input and therefore depending on plant productivity (Stahr, et al., 2016). At Location 1 is an unmistakable depth trend visible; the highest values are in the upper soil layers, whereby the concentrations decrease within the depth profile. This is an excepted pattern caused by litter inputs in the upper soil layers. The highest C amounts are at Reference 1 and Slope 1; at these sites is the vegetation denser than at the other sites, which amplified the higher C amounts in the upper soil layers. But the soil productivity in the Mediterranean climate is usually not as high, as it can explain so high C-amounts. An additional accumulation of carbon could have taken place by wildfires. The wildfire forms a layer of ash on the soil, in which very high C

contents are present. Consequently, the C content in the soil increases as a result of such fires (Bird et al., 2000).

The amount of soil organic carbon is directly influenced by erosion because the SOC is stored as small particles, which are susceptible to leaching (Meusburger, et al., 2013). Therefore, a comparison of the carbon content of the sites tells us something about erosion. Within Location 1, the reference sites have the highest amount of carbon, followed by Slope 1 and the lowest amounts are at Slope 2. This means that the two slope sites experience more erosion than the reference site without slope. At Location 2, the highest values are observed on the reference sites as well. Although the differences between the sites are lower than at Location 1: At Location 1, the values differ by 2-7 % (except for Slope 1 in the upper 5 cm), and at Location 2, only about 1 %. According to the C amounts, the highest erosions rates are at Slope 2, followed by Slope 1, then at Slope 4, and almost no erosion at Slope 3.

5.1.4 Soil disturbance and erosion according to $\delta^{13}C$ values

The $\delta^{13}C$ signatures in the upper soil layers are around - 28 ‰ and, therefore, within the typical range of C_3 plants (Kohn, 2010). According to Meusburger et al. (2013), the $\delta^{13}C$ values increase with depth if the soil is well-drained and oxic. Less negative values mean that there are more ^{13}C isotopes than ^{12}C isotopes in the soil, which is caused by aerobic decomposition. Under aerobic conditions, the micro soil organisms prefer the lighter ^{12}C isotopes, resulting in a relative accumulation of ^{13}C isotopes in the soil. The $\delta^{13}C$ values increase within the depth profiles in the observed sites as excepted. Further, Meusburger et al. (2013) write that erosive sites have more negative values than flat sites. Therefore, Slopes 3 and 4 can be characterized as erosive sites because the $\delta^{13}C$ values at the reference sites are less negative than at the slope sites. For Location 1, only Slope 1 can be described as an erosive site because Slope 2 has comparable $\delta^{13}C$ values as Reference 1.

5.1.5 Correlation between $\delta^{13}C$ values and the amount of Carbon

Various authors (e.g. Schaub & Alewell, 2009; Zollinger, et al., 2015; Meusburger, et al., 2013) examined the correlation between C content and $\delta^{13}C$. It allows the investigation of the aggregate stability and mid-term soil disturbances. However, these disturbances do not necessarily mean erosion because erosion alone does not change the correlation. Soil disturbances, like vertically mixing or accumulation, change the correlation change (Raab, et al., 2018). Zollinger et al. (2015) describe in their work that permafrost soils with a smaller R^2 value experienced more disturbances than non-permafrost soils with a higher R^2 value.

Depending on the study area, the threshold of the R^2 values differ when an observed soil can be described as erosion- or non-erosion-affected nevertheless, the lower the negative correlation, the more disturbance is expected. Among the investigated soils of the EAG, all observed correlations are only weak, whereby the strongest negative correlation is found at Reference 1.

Accordingly, this site should be the least affected by soil disturbances. The negative correlation at Slope 1 is less pronounced, which is an indication of more soil disturbances. Slope 2 has a positive correlation. A positive correlation has not been observed by the authors mentioned, so an explanation is not trivial. The most likely interpretation of this positive correlation is that Slope 2 experienced much disturbance. Other soil characteristics (for example, elemental composition) also indicate elevated disturbance at Slope 2. Location 2 has weakly positive and negative correlations. Accordingly, all sites at Site 2 could have had elevated soil disturbance. It is difficult to say if the most considerable part of soil disturbances is caused by erosion.

5.2 Chemical weathering and leaching

5.2.1 Weathering degree in the depth profile

Undisturbed soils are expected to be more weathered in the upper soil layers than in the lower layers (Stahr, et al., 2016). Contrary, the investigated soils behave the opposite. The lowest weathering degrees are found in the upper soil layers, although the depth trend is not always decisive. The WIP and the (Ca + K) / Ti index sometimes show different results. The reason for the ‘revers’ weathering degree in the depth profile could have various causes. Some elements do not always behave typically; for example, titanium can be a mobile element under tropical conditions (Cornu, et al., 1999). But these conditions do not exist in the EAG. Another possibility would be that less weathering soil overwhelmed the investigated soil, but this is unlikely at the observed sites because of the relatively flat topography. Due to the soil’s rejuvenation at the surface by litter input, a deeper weathering degree in the uppermost centimeters can be explained (Vitousek, et al., 2003). Still, it is not an explanation that the highest weathering degrees are in the deepest depth ranges.

Another way to understand the cause of the ‘reverse’ weathering is the grain size distribution. Chemical weathering occurs faster on smaller particles than with larger particles because of the higher attack’s surface. But the smaller particles are less stable in the soil and are more susceptible to erosion. However, the smallest particle sizes are usually found in the upper soil layers, and the particle size increases within the depth profile (Scheffer & Schachtschabel,

2010). But the particle size at the observed sites is relatively homogenous. Therefore, it could be that the more weathered particles are just removed from the subsoil, which leads to the lower weathering degree in the upper soil layers. Even if this explanation may be correct, it cannot fully explain the reverse weathering. The most likely explanation, in my opinion, is that the soil pores are open due to the dry and hot summers, and the precipitation soaks directly down into the bottom. Thus, the water flows downslope in the deeper soil layers, causing more leaching in the lower soil layers than in the upper ones. In summary, the best explanation for the 'reverse' pattern seems to be two processes. Firstly, the topsoil's rejuvenation by fresh organic material and, secondly, the leaching in the subsoil through the water.

5.2.2 Striking patterns in the different weathering indexes

Generally, it is not possible to nominate the best weathering index of all times. Because it depends on the observed soils. By applying several indexes, it can be seen which one fits best for the investigated soil, or at least which one does not fit at all. Most of the indexes give a similar pattern for the examined soils, except for the WIP and the (CA+K) / Ti. Therefore, the B-Index, the CIA, and SA seem to fit the best.

The WIP show different pattern at Slope 1 and Reference 1; the highest weathering degree is in the upper soil layers and degreases within the depth. The K_2O concentration influences the WIP the most, and the trend of K_2O has the same conspicuousness; especially at Slope 1, there is a sharp increase in the K_2O concentration within the uppers 10 cm. The weathering degree of Slope 2 behaves, especially by using the (Ca + K)/ Ti; the weathering degree increases massively within the first 15 cm. The titanium concentration can explain this pattern within Slope 2; In contrast to the other sites, the titanium concentration decreases sharply within the upper 15 cm.

5.3 Soil erosion estimated by Plutonium

Comparing the $^{239+240}$Pu inventories between the reference sites and the slopes sites allows a conclusion on the erosion rates within the last ~60 a. The $^{239+240}$Pu inventories at the observed sites are between 60 to 180 [Bqm^{-2}]. Compared to examinations of Alewell et al. (2014), Zollinger et al. (2015), and Xu et al. (2015) are these values relatively high but still within the expected range for the northern hemisphere. The estimation of the erosion rates is based on the assumption that soil erosion reduces the $^{239+240}$Pu inventories. Therefore, it is expected that the observed reference sites at the flat ground have the highest $^{239+240}$Pu inventories. In fact, the highest total inventories are measured at the reference site at Location 1, and the inventories at the two slope sites are much smaller. Because of these differences, the mass redistributions at Slope 1 and 2 are negative. In contrast, the highest inventory at Location 2 is measured at Slope 4, and all slope sites have a higher inventory than the reference sites, resulting in a positive mass redistribution. So the estimated soil erosion rates are higher at Location 1 than at Location 2. These results require an explanation because the hypothesis was the opposite: We expected higher soil erosion rates at the formerly glaciated area. The soils at the previously glaciated area are younger than at the non-glaciated area and, therefore, we expected less stable soil aggregates resulting in higher soil erosion rates. Maybe, this assumption was false, and the mass redistribution rates are less negative at younger soils because of increased soil formation processes.

Among others, Alewell et al. (2015) and Larsen et al. (2014) described the highest soil production rates at young soils. Enhanced soil production rates could therefore be able to neutralize higher erosion rates. Also, the mass redistribution is not only depending on the glacier history. There are a lot of other factors, such as vegetation cover, slope angle, or precipitation. The precipitation is similar at both locations, so it is not probable that the precipitation causes these differences. However, the vegetation and the slope angles differ at the observed sites (see Table 11). The densest vegetation is at Reference 1; besides grass, smaller bushes also grow there, which can stabilize the soil. Already the correlation between C amount and δ^{13}C resulted in the highest aggregate stability for Reference 1. In fact, at Reference 1 are the highest total inventory observed. At Slope 1, 3, 4, and Reference 2, there is just growing grass. At Slope 2, there is no vegetation at all, and the $^{239+240}$Pu inventory is the lowest at this site, resulting in the highest soil erosion rates. Several other studies (e.g. Mohammad, Adam, 2010; Nunes, et al., 2011) concluded that a more dense vegetation cover reduces soil erosion.

Besides the vegetation, the slope angle influences soil erosion. There is a strong correlation between slope angle and mass redistribution. The highest soil erosion is estimated for Slope 2 with a slope angle of 20°, followed by Slope 1 with a slope angle of 10°, and positive mass redistributions are observed at Slope 3 and 4, which have the lowest slope angle with 5°. the flat angle at Location 2 can also explain why the slope sites have a lot of inventory compared to the slope sites at Location 1. In summary, the estimated soil erosion rates seem to be related to the vegetation and the slope angle and not only on the glacial history.

Table 11; Vegetation types, slope angle, $^{239+240}$Pu inventory, mass redistribution according to Lal et al. (2013) with different Particle corrector, and according to Walling and He (1999) for the observed sites

Site	Vegetation	Slope	Total inventory	IM			PDM
				P=1.0	P=1.2	P=1.5	P=1.0
		[°]	[Bq m^{-2}]	[tkm^{2}yr^{-1}]	[tkm^{2}yr^{-1}]	[tkm^{2}yr^{-1}]	[tkm^{2}yr^{-1}]
Location 1 (non-glaciated)							
R1	Shrubs, grass	2	172.2				
S1	Grass	10	64.1	-1'395	-1'162	-930	-891
S2	No vegetation	20	60.9	-2'066	-1'722	-1'378	-908
Location 2 (glaciated)							
R2	frost-resistant Grass	0	101.2				
S3	frost-resistant Grass	5	119.1	55	46	37	63
S4	frost-resistant Grass	5	179.3	336	280	224	398

5.3.1 Comparison of erosion rates with other studies

Alewell et al. (2014) estimated the erosion rates between 450 and 830 [tkm^{-2}yr^{-1}] in their swiss alps study. The calculated rates in my thesis are much higher at the non-glaciated site. But compared to the calculated erosion rates in the Sila Massif upland (Italy) by Raab et al. (2018), they are similar. The Sila Massif climate is the Mediterranean as in the Geopark Estrela, whereby similar rates were expected. At some sites in the Sila Massif upland are the erosion rates significantly higher than in the EAG. The more intense land use, before the Sila Massif became a national park, could cause these higher values. The European Soil Data Centre estimated the soil loss rates for most parts of Europe (Eurosat, 2015).

Figure 25 shows the Iberian peninsula's erosion rates, and the region of the EAG is classified in the second-highest class, in which the erosion rates are between 10 and 20 [tha^{-1}yr^{-1}] (=1000 – 2000 tkm^{-2}yr^{-1}). Thus, the calculated erosion rates of Location 1 are within the expected range. In contrast, the estimated erosion rates for Location 2 are positive. Positive erosion rates are not found in the study by Alewell et al. (2014), nor by Xu et al. (2015) in northeast China, and also not by Raab et al. (2018) in the Sila Massif upland (Italy). I can imagine that the erosion values obtained from Location 2 are not meaningful because the slope angle at Slope 3 and 4 are not steep enough to experience significantly more erosion than the reference site.

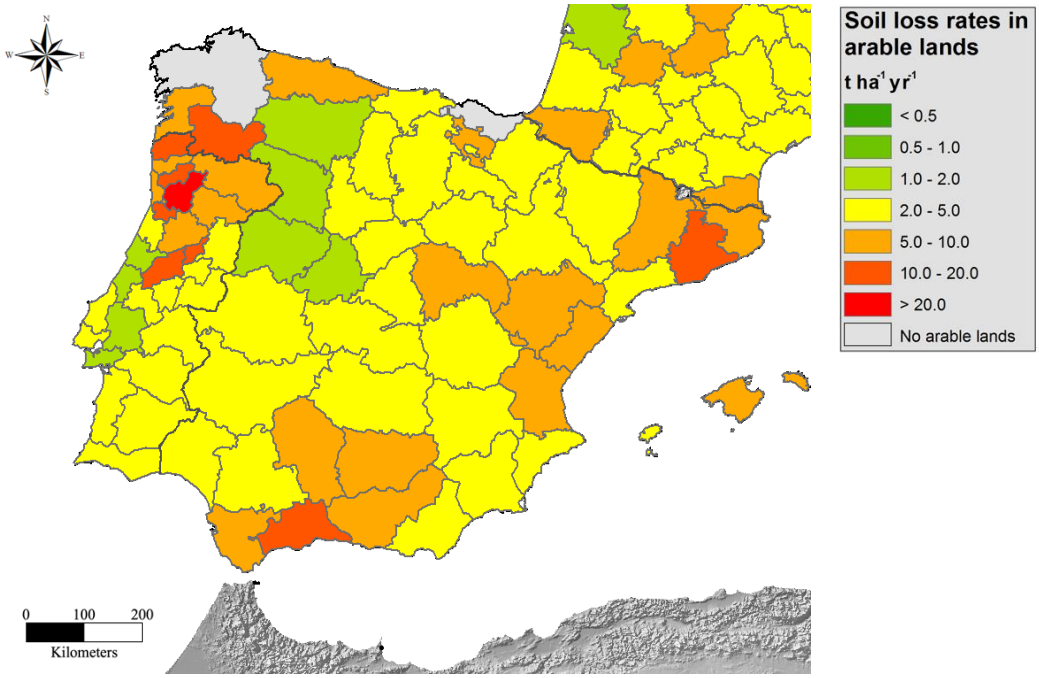

Figure 25; Soil loss rates on the Iberian peninsula (Eurosat, 2015)

5.3.2 Development of mass redistribution over time

Comparing the actual erosion rates at Location 1 with older erosion rates is not yet possible because the overarching project is still in progress. However, erosion rates at Location 1 are most likely higher than in the past. Other studies (Raab, et al., 2018; Scarciglia, 2015) calculated long-term erosion rates in the Sila upland (Italy). The erosion rates are in a range of 8 to 250 [$tkm^{-2}yr^{-1}$] and, therefore, significantly lower than current soil erosion rates. The highest erosion rates are observed at the transition from the Pleistocene to the Holocene. The Sila upland's climatic conditions are similar to the climatic conditions in the EAG with an average temperature of 9–12 °C and annual precipitation of 1000–1800 mm (Le Pera and Sorriso-Valvo, 2000). Thus, the expected erosion rates in the EAG are in a similar range as that of the Sila upland. The current higher erosion rates could result from climate warming because the soils are drying out more in the summer months, and the rain intensity is increasing in the winter months. Also, Nearing et al. (2004) observed increased erosion rates under warming conditions. Besides, the soil production rates influence mass redistribution. Alewell et al. (2015), Larsen et al. (2015), and Dixon and von Blanckenburg (2012) observed the highest soil production rates at young soils (>1–10 ka). With long-term soil erosion rates, it would be possible to estimate the soil production rates in the EAG. If we assume erosion rates of about 200 [$tkm^{-2}yr^{-1}$], soil production rates should be slightly higher (estimated between 210 and 220 [$tkm^{-2}yr^{-1}$]). These rates are consistent with the values in the papers mentioned above.

5.4 Estimated soil age

The total inventory of Beryllium was used to estimate the absolute soil age at one pit of Reference 2. Up to the used formula, the soil age varying between 13 and 35 ka. The most significant uncertainty in the formula from Maejima, et al. (2004) is the annual deposition rate of ^{10}Be. Depending on the estimation of this deposition, the results differ. The highest ages were calculated by the deposition rate, according to Willenbring & von Blanckenburg (2010). They created a world map with individuals deposition rates, but the resolution is not high. The observed location's deposition rate is higher than displayed on the map because the precipitation is over the average in this climate because of the altitude (Vieira, et al., 2017). If the assumed deposition rates are too low, the resulting age is too high. The soil age is much lower by using the deposition determination by Graley et al. (2011). In this formula, the precipitation is included, resulting in different results, up to the assumed precipitation. The higher the assumed precipitation, the higher the deposition rates, and the younger the calculated age. The most likely precipitation is around 1600 mma^{-1}, which leads to an age of 14.3 a. This result is more immature than expected. The formula by Monaghan et al. (1986) calculates the deposition rates with a constant beryllium concentration in the rain, multiplicated by the precipitation at the observed site. The result with 1600 mma^{-1} precipitation led to a soil age of 22.5 ka. This soil age was expected because the soil formation at Location 2 began most probably after the LGM. The measured soil age by using the TEA is in the same range of a nearby moraine boulder with 22.5 ka would support this age range. Accordingly, the deposition rate by using the formula by Monaghan et al. (1986) with precipitation of 1700 mma^{-1} seems to fit the best.

The correlation between ^{10}Be and Fe_o allowed the roughly estimation of the ^{10}Be concentration for Reference 1. Accordingly, the soil age was roughly estimated. The soil age at Reference 1 is 25.8 ka by using the formula by Monaghan et al. (1986) with precipitation of 1700 mma^{-1}. This soil age must be considered with caution because there are many uncertainties in the estimation. Nevertheless, it is likely that this age is approximately correct. The TEA determined ages of ~20 ka at the subsurface and 29 ka in the bottom from Tor 1, which is next to Reference 1. Therefore, a soil age of ~26 ka is consistent with these results. Besides, the weathering degree at Reference 1 is higher than at Reference 2. Usually, the weathering degree increases with time (Stahr, et al., 2016). Accordingly, the soil age at Reference 1 seems to be higher than at Reference 2. Also, the general soil development is more advanced at Reference 1 than at Reference 2. The differences between the soil development at the two locations are low, whereby a much higher soil age at Location 1 is not likely.

5.5 Soil disturbance

Undisturbed soil has continuous growth; in the upper soil layers is humification, and in the bottom, the bedrock gets slightly weathered. These soil formations lead to a typical depth trend of the different soil characteristics (Graham, et al., 2010). But if the soil is disturbed, the depth trends of the individual soil properties are changing. Therefore, the soil disturbances can be estimated by using the depth profile's characteristics at each site. Typically soil disturbances in the EAG are wildfires, which cause the high C-amount in the observed soils (Nunes, et al., 2010). Another soil disturbance is cryoturbation, whereby the soil layers are mixed. Besides, anthropogenic influences can lead to soil disturbances. Deforestation or grazing changes the vegetation covers, which influences soil erosion (Egli & Poulenard, 2016; Nunes et al., 2010). Soil disturbances can change over time due to changes in climatic conditions or through anthropogenic influences. The analysis of the beryllium concentration in the soil tells us something about the long-term soil disturbances. In contrast, the plutonium analysis indicates soil disturbances of the last ~60 a. These changes in soil disturbance over time are discussed in the next chapters and are summarized in Figure 26.

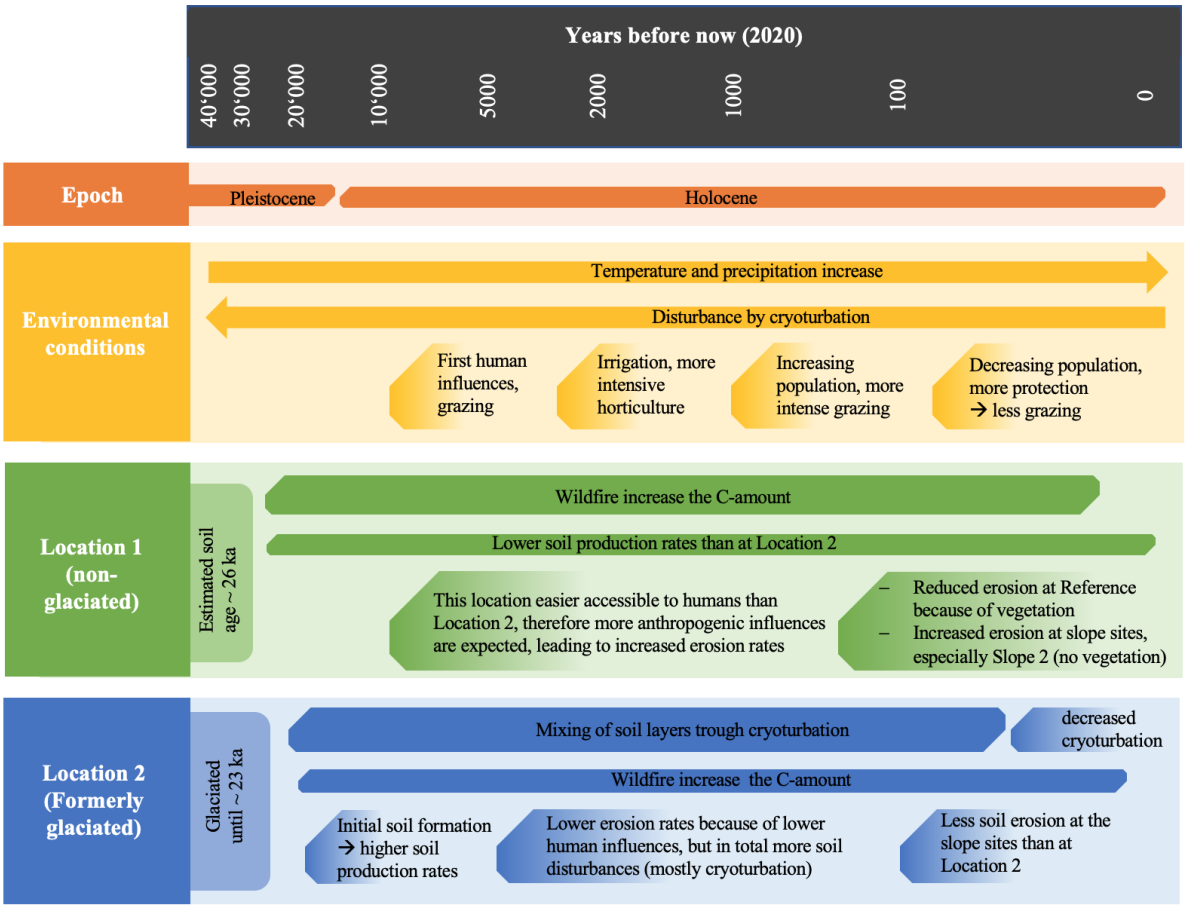

Figure 26; Summary of the factors affecting the two studied locations

5.5.1 Long- and mid-term soil disturbances

At Reference 2, the meteoric ^{10}Be was measured, and the observed age of the pit is estimated at 22.5 ka. Therefore, any irregularities in the soil profile mean soil disturbances within the last 22.5 ka (long-term soil disturbances). Undisturbed cambisols have the highest ^{10}Be concentration in the upper soil layers, decreasing within the depth (Graly, et al., 2010). The studied pit does not show a clear depth trend; the highest concentration is in a depth range of 10-15 cm. Several authors (e.g. Willenbring & von Blanckenburg, 2010; Egli, et al., 2010; Calitri, et al., 2019) observed the correlation between ^{10}Be and organic ligands or Metallo-organic complexes. By regarding this correlation, initial translocations could explain the unexpected depth trend within the upper soil depth of Fe_o and ^{10}Be. But because of the young age of the soil (22.5 ka), translocation is not likely. Accordingly, it is more likely that the site experienced other disturbances, most probably cryoturbation. During the winter month, the temperature sinks below 0°C, why frost is not uncommon. The aggregate stability estimates mid-term soil disturbances. These results are available for all sites and illustrate more soil disturbances at Location 2 than at Location 1. The disturbances are probably caused by cryoturbation because there is no clear depth trend of carbon at the observed sites. But also at Location 1 are some mid-term soil disturbances (even if less than at Location 2). In contrast to Location 2, the carbon amount at Location 1 does show a clear depth trend. Therefore, soil disturbances caused by cryoturbation are not likely. Location 1 is at a lower altitude than Location 2, so these results are not surprising. Instead of disturbances by cryoturbation, the sites could be more affected by wild-fires. The higher carbon amount at Location 1 compared to Location 2 could be caused by such fires.

5.5.2 Recent soil disturbance

The $^{239+240}Pu$ was released during the nuclear weapon tests in the atmosphere and accumulated in the upper soil layers since 1963. Undisturbed soils have the highest $^{239+240}Pu$ concentration in the upper soil layers, and the amount decreases within the depth profile. Susceptible irregularities in the depth profile indicate disturbances, which occurred during the last ~60 a. The $^{239+240}Pu$ measurements were done for all sites. The expected depth trends are visible in every observed pit; the highest $^{239+240}Pu$ concentrations are in the upper soil layers, and the concentration decreases strongly. Therefore, the estimated area was not affected by more considerable soil disturbance in the last ~60 a. More considerable disturbances are processes, which mix the soil layers vertically, such as cryoturbation.

Besides, there is an increase in forest fires in Portugal in the last decades (Nunes, et al., 2010; Nunes, 2012; Vieira, et al., 2017). The anthropogenic influence on nature decreases in the previous century because of environmental protection, and many people are moving into the cities. Therefore, certain areas become overgrown, making them more susceptible to fire (Nunes, 2012). Andreu et al. (2001) observed forest fires' influence on soil aggregate stability in Spain. During the summer months, the fire events destroy the soil aggregate in the upper soil layers, making the soil more vulnerable to erosion during the autumn and winter month. Estimating the frequency of fire events with the methods used in this work is not entirely possible. According to Bird et al. (2000), the amount of carbon in the fine soil increases due to wildfires. Especially Reference 1 and Site 1 have high carbon amounts in the upper soil layers. Maybe there was a forest fire within the last few years at Location 1. Further research would provide more clarity in the frequencies of forest fires — for example, the measurement of pyrogenic carbon or dendrochronological studies.

Compared to the earlier soil disturbances (discussed in chapter 5.5.1), fewer cryoturbation-events occurred at Location 2. Hence, the ^{10}Be concentrations do not show a clear depth trend caused by soil disturbances; there is an unmistakable depth trend in the $^{239+240}$Pu results. This change can be explained by climatic warming; the temperature increases during the last millennia, which reduces the frequency of frost events.

6 Conclusions

This work aimed to compare the soil erosion rates of the last ~60 years and the long-, mid, and short-term soil disturbances in a formerly glaciated and non-glaciated area in the Geopark Estrela. The soil development and the weathering degrees in the non-glaciated area are higher than at the formerly glaciated sites. The soil age at Reference 2 (formerly glaciated area) is about 22.5 ka. At Reference 1 (non-glaciated area), the soil age is roughly estimated at 26 ka, which confirms the higher soil age and more advanced soil development at Location 1.

The Plutonium analyses allow identifying short-term soil disturbances and the estimation of erosion rates within the last ~60 years. Higher erosion rates were hypothesized for the formerly glaciated area, but the results are reversed; the highest erosion rates are at Location 1. The results are around 1100 [$tkm^{-2}yr^{-1}$] at Slope 1 and 1700 [$tkm^{2}yr^{-1}$] at Slope 2. At Location 2, the mass redistributions are positive; accordingly, the soil deposition seem to be higher than the erosion rates. But to what extent the glacial history influenced these calculated erosion rates is questionable. More likely are explanations by other factors such as vegetation density or varying slope angle. The slope angles at the slope sites at Location 2 are significantly lower (5°) than at Location 1 (10-20°). Slope 2, with the highest erosion rates, is also the site with no vegetation, which makes the soil particularly vulnerable to erosion. Besides, the soil production rates are higher at younger soils than at more developed soils. Overall, the $^{239+240}Pu$ method is well suited to determine soil erosion rates. But for a meaningful comparison, is the choice of similar sites important.

By comparing the long-, mid-, and short-term soil disturbances, some changes were identified. The long-term soil disturbances were detected with ^{10}Be and were done for Reference 2. The results confirm the hypothesis of high soil disturbances. The ^{10}Be concentration within the depth profiles does not show the typical pattern. Probably, the soils at this location underwent vertical mixing caused by cryoturbation. The mid-term soil disturbances were analyzed with the correlation between the carbon amount and the $\delta^{13}C$. These results also indicate increased soil disturbance. Especially the slope sites seem to be affected by soil disturbances. In this period, the soil disturbances at Location 2 could be caused by cryoturbation. At Location 1, human impacts such as deforestation or pasture could be the causes of the disturbances.
In contrast, the $^{239+240}Pu$ concentrations do show a clear depth trend at both locations. Therefore, the short-term soil disturbances seems to be lower than in the past. Global climatic warming leads to fewer frost events, which reduces the soil disturbances by cryoturbation. Besides, the

anthropogenetic influences decrease through increased protections of the Geopark. Nevertheless, the number of forest fires increases, which in turn makes the soil more vulnerable to erosion. The erosion rates at the non-glaciated sites are much higher than in the past. Wildfire events and global warming could cause these high rates.

To better determine the influence of cryoturbation and wildfire on the soil, some further studies could be done. Studies with climatic reconstructions would identify the frequency of frost events in the past. Besides, the ^{10}Be could be measured at more locations to estimate the long-term soil disturbances. The influence of forest fires on the soil aggregate stability could be determined with long-term studies, whereas the soil properties would be described before and after a fire event. With dendrochronological methods, previous fire events could be identified. The risk of erosion in the Geopark is high because of the climatic and topographical conditions and will probably increase in the future. Therefore, I recommend maintaining the vegetation to reduce the risk of forest fires and better protect the soil from erosion.

Acknowledgement

During writing my master thesis, I received generous support from various people, and I would like to thank them all.

Prof. Dr. Markus Egli supervised me from the Context to the submission of the master thesis. Besides explaining methods and calculations and furthermore interpreting all the results, he always motivated me with his enthusiastic manner.

I want to thank Dr. Gerald Raab for his support during the entire master thesis, on the field, in the laboratory, until the finalization of my thesis. He helped me handling a large amount of data. He always had time for moral support and great tips to interpret the results, whether physical or via zoom.

The fieldwork was only possible through Dr. Gonçalo Vieira (University of Lisbon), who knows the Geopark Estrella perfectly, and Prof. Dr. hab. Piotr Migoń (University of Wroclaw), who traveled all the way from Poland to Portugal. Many thanks also to Dr. Gerald Raab, Prof. Dr. Markus Egli, and Fabio Scarciglia (PhD at Università della Calabria) for their physically challenging work in the field - despite the heat.

I would like to thank Dr. Michael E. Ketterer and his team (Northern Arizona University) for the Plutonium extraction and the measurements. The beryllium measurements were done at the ETH Zürich, thanks also to this team.

Finally, I want to thank all the lovely people from the laboratory (Geochronology and Soil Science and Biogeochemistry staff).

References

AEMet (Agencia Estatal de Meteorología), IM (Insitituto de Meteorologia). 2011. Iberian Climate Atlas: Air Temperature and Precipitation (1971-2000). *Ministerio de Medio Ambiente y Medio Rural y Marino*.

Alewell C, Egli M, Meusburger K. 2015. An attempt to estimate tolerable soil erosion rates by matching soil formation with denudation in Alpine grasslands. *Journal of Soils and Sediments*, 15(6). 1383–1399. DOI: 10.1007/s11368-014-0920-6

Alewell C, Meusburger K, Juretzko G, Mabit L, Ketterer M. 2014. Suitability of $^{239+240}$Pu and ^{137}Cs as tracers for soil erosion assessment in mountain grasslands. *Chemosphere, 103*. 274-280. DOI: 10.1016/j.chemosphere.2013.12.016

Alfeld M, Requena G, Boesenberg U, Bauckhage C, Wellenreuther G, Falkenberg G, Whabza M. 2016. Non-negative matrix factorization for the near real-time interpretation of absorption effect in elemental distribution images acquired by X-ray fluorescence imaging. *Journal of Synchrotron Radiation, 23*. 579-589. DOI: 10.1107/S1600577515023528

Andreu V, Imeson AC, Rubio JL. 2001. Temporal changes in soil aggregates and water erosion after a wildfire in a Mediterranean pine forest. *Catena,* 44. 69–84. DOI: 10.1016/S0341-8162(00)00177-6

Bashour I, Sayegh AH. 2007. Methods of analysis for soil of arid and semi-arid. In *16.2.2. Measurement of Element Concentration Using Atomic Absorption Spectroscopy.* Beirut, Lebanon: American University of Beirut.

Beckhoff B, Kanngießer B, Langhoff N, Wedell R, Wolff H. 2006. *Handbook of Practical X-ray Fluorescence Analysis. Springer, Berlin.* Springer, Berlin.

Bird M, Veenendaal E, Moyo C, Frost LP. 2000. Effect of fire and soil texture on soil carbon in a sub-humid savanna (Matopos, Zimbabwe). *Geoderma*, 94(1). 71-90. DOI: 10.1016/S0016-7061(99)00084-1

Bochet E, Rubio J. 1998. Relative efficiency of three representative matorral species in reducing water erosion at the microscale in a semi-arid climate (Valencia, Spain). *Geomorphology*, 23. 139-150. DOI: 10.1016/S0169-555X(97)00109-8

Braun-Blanquet J, Pinto da Silva A, Rozeira A, Fontes F. 1952. Resultats de deuxexcursions géobotaniques a travers le Portugal septentrional et moyen: 1 uneincursion dans la Serra da Estrela. *Agronomia Lusitana, 14*. 303-323.

References

Buggle B, Glaser B, Hambach U, Gerasimenko N, Markovic S. 2011. An evaluation of geochemical weathering indices in loess–paleosol studies. *Quat. Int*., 240. 12–21. DOI: 10.1016/j.quaint.2010.07.019

Calitri F, Sommer M, Norton K, Temme A, Brandová D, Portes R, Christl M, Ketterer ME, Egli M. 2019. Tracing the temporal evolution of soil redistribution rates in an agricultural landscape using $^{239+240}$Pu and ^{10}Be. *Earth Surf. Process. Landforms* 44. 1783–1798. DOI: 10.1002/esp.4612

Chmeleff J, von Blanckenburg F, Kossert K, Jakob D. 2010. Determination of the ^{10}Be half-life by multicollector ICP-MS and liquid scintillation counting. Nuclear Instruments and Methods. *Physics Research Section B: Beam Interactions with Materials and Atoms*, 268 (2). 192- 199. DOI: 10.1016/j.nimb.2009.09.012

Christl M, Vockenhuber C, Kubik P, Wacker L, Lachner J, Alfimov V, Synal H. 2013. The ETH Zurich AMS facilities: Performance parameters and reference materials. Nuclear Instruments and Methods. *Physics Research B, 294*. 29–38. DOI: 10.1016/j.nimb.2012.03.004

Connor S, Araújo J, van der Knaap W, van Leeuwen J. 2012. A long-term perspective on biomass burning in the Serra da Estrela, Portuga. *Quaternary Science Reviews, 55*. 114-124. DOI: 10.1016/j.quascirev.2012.08.007

Cornu S, Lucas Y, Lebon E, Ambrosi J, Luizão F, Rouiller J, Bonnay M, Neal C. 1999. Evidence of titanium mobility in soil profiles, Manaus, central Amazonia. *Geoderma, 91*. 281–295. DOI: 10.1016/S0016-7061(99)00007-5

Díez A, Balda M, Vegas R, González LF. 1990. Central Iberian zone (autochthonoussequences) 2.2 structure. R. Dallmeyer, & Martínez-Garcia (ed.). *Pre-Mesozoic Geology of Iberia*. Springer-Verlag, Heidelberg. 172–188

Dixon JL, von Blanckenburg F. 2012. Soils as pacemakers and limiters of global silicate weathering. *Comptes Rendus Geoscience, 344*. 597–609. DOI: 10.1016/j.crte.2012.10.012

EEA. 2009. *Assessment of the actual soil erosion risk in Southern Europe by combining four sets of factors: soil, climate, slopes, vegetation. European Environment Agency.* https://www.eea.europa.eu/data-and-maps/figures/soil-erosi [access on 11.12.2020]

Egli M, Poulenard J. 2016. Soils of mountainous landscapes. *International Encyclopedia of Geography: People, the Earth, Environment and Technology*. 1-10. DOI: 10.1002/9781118786352.wbieg0197

References

Egli M, Kraut T, Tikhomirov D, Keller T. 2020. *Geochronology laboratory methods*. University of Zurich, Department of Geography.

Eurosat. 2015. *European Soil Data Centre (ESDAC). Mean soil erosion rates at NUTS 3 level for arable lands (tonnes per ha per year), 2010, EU-28 Graph created with data from 2010.* https://ec.europa.eu/eurostat/statisticsexplained/index.php?title=File:Mean_soil_erosion_rates_at_NUTS_3_level_for_arable_lands_(tonnes_per_ha_per_year),_2010,_EU-28.png&oldid=255762 [access on 07. 01 2021]

Fedo CM, Nesbitt HW, Young GM. 1995. Unraveling the effects of potassium metasomatism in sedimentary rocks and paleosols, with implications for paleoweathering conditions and provenance. *Geology, 23*. 921–924. DOI: 10.1130/0091-7613(1995)023<0921:UTEOPM>2.3.CO;2

Flottweg. 2020. *Gesetz von Stokes (Laminare Strömung um eine Kugel)*. https://www.flottweg.com/de/wiki/trenntechnik/gesetz-von-stokes-laminare stroemung-um-eine-kugel/ [access on 06. 10 2020]

Giani L, Witte S, Wark M. 2015. Bodenkundliches Grundpraktikum. *Fakultät V Institut für Biologie und Umweltwissenschaften AG Bodenkunde*.

Graham R, Rossi A, Kenneth R. 2010. Rock to regolith conversion: Producing hospitable substrates for terrestrial ecosystems. *GSA today, 20*. 4-9. DOI: 10.1130/GSAT57A.1

Graly JA, Reusser LJ, Bierman PR. 2011. Short and long-term delivery rates of meteoric ^{10}Be to terrestrial soils. *Earth and Planetary Science Letters, 302*. 329–336. DOI: 10.1016/j.epsl.2010.12.020

Graly J, Bierman PR, Reusser L, Pavich M. 2010. Meteoric ^{10}Be in soil profiles – A global meta-analysis. *Geochimica et Cosmochimica Acta, 74*. 6814-6829. DOI: 10.1016/j.gca.2010.08.036

Grotzinger J, Jordan T. 2016. *Allgemeine Geologie* (7). Press / Siever, Springer Spektrum.

Harnois L. 1988. The CIW index: a new chemical index of weathering. *Sediment. Geol, 55*. 319–322. DOI: 10.1016/0037-0738(88)90137-6

Harrington CD, Whitney JW. 1987. Scanning electron microscope method for rock- varnish dating. *Geology, 15*. 967-970. DOI: 10.1130/0091-7613(1987)15<967:SEMMFR>2.0.CO;2

ICNB. 2007. Plano deOrdenamento do Parque Natural da Serra da Estrela: II, Caracterização dosValores Naturais. *Ministério do Ambiente, do Ordenamento do Território e doDesenvolvimento Regional, Lisboa*.

Imeson A. 1990. Climate fluctuations and soil erosion under Mediterranean conditions. *Technical Report. International University, Menéndez Pelayo, Valencia, Spain*.

IPMA. 2021. Instituto Português do Mar e da Atmosfera. Monthly Averages for Penhas Douradas (1982–2010). http://www.ipma.pt/pt/oclima/series.longas/list.jsp [access on 01. 02 2021]

IUSS Working Group WRB. 2015. World Reference Base for Soil Resources 2014, Update 2015. International Soil Classification System for Naming Soils and Creating Legends for Soil Maps. World Soil Resources Reports 106 FAO, Rome.Kabata-Pendias A. 2011. Trace elements in soils and plants. Boca Raton (Florida): CRC Press.

Ketterer ME, Hafer KM, Link CL, Kolwaite D, Wilson J, Mietelskic JW. 2004. Resolving global versus local/regional Pu sources in the environment using sector ICP-MS. *Journal of Analytical Atomic Spectrometry, 19*. 241–245. DOI: 10.1039/B302903D

Kohn J. 2010. Carbon isotope compositions of terrestrial C^3 plants as indicators of (paleo)ecology and (paleo)climate. *Proceedings of the National Academy of Sciences of the USA, 107*. 19691–19695. DOI: 10.1073/pnas.1004933107

Korschinek G, Bergmaier A, Faestermann T, Gerstmann U, Knie K, Rugel G, Wallner A, Dillmann I, Dollinger G, Lierse von Gostomski Ch, Kossert K, Maiti M, Poutivtsev M, Remmert A. (2010). A new value for the half-life of ^{10}Be by Heavy-Ion Elastic Recoil Detection and liquid scintillation counting. *Nuclear Instruments and Methods in Physics Research B*, 268. 187–191. DOI: 10.1016/j.nimb.2009.09.020

Kronberg B, Nesbitt H. 1981. Quantification of weathering, soil geochemistry and soil fertility. *Journal of Soil Science*. 453-459. DOI: 10.1111/j.1365-2389.1981.tb01721.x

Lado M, Hur MB, Shainberg I. 2004. Soil Wetting and Texture Effects on Aggregate Stability, Seal Formation, and Erosion. *Soil Science Society of America Journal*, 68(6). 1992–1999. DOI: 10.2136/sssaj2004.1992

Lal R, Tims SG, Fifield LK, Wasson RJ, Howe D. 2013. Applicability of ^{239}Pu as a tracer for soil erosion in the wet-dry tropics of northern Australia. Nuclear Instruments and Methods. *Physics Research Section B: Beam Interactions with Materials and Atoms*, 294. 577-583. DOI: 10.1016/j.nimb.2012.07.041

Larsen I J, Almond P C, Eger A, Stone J O, Montgomery D R, Malcolm B. (2014). Rapid soil production and weathering in the Western Alps, New Zealand. *Science*, 1244908. 637–640. DOI: 10.1126/science.1244908

Le Pera E, Sorriso-Valvo M. 2000. Weathering and morphogenesis in a Mediterranean

climate Clabria, Italy. *Geomorphology*, 34. 251–270. DOI: /10.1016/S0169-555X(00)00012-X

Mabit L, Meusburger K, Fulajtar E, Alewell C. 2013. The usefulness of ^{137}Cs as a tracerfor soil erosion assessment: a critical reply to Parsons and Foster. *Earth-Science Reviews*, 127. 300–307. DOI: 10.1016/j.earscirev.2013.05.008

Maejima Y, Matsuzaki H, Nakano C. 2004. Be concentrations of Red soils in Southwest Japan and its possibility of dating. *Nuclear Instruments and Methods in Physics Research Section B: Beam Interactions with Materials and Atoms*, 223-224. 596–600. DOI: 10.1016/j.nimb.2004.04.110

McHargue L, Damon P. 1991. The global beryllium 10 cycle. *Reviews of Geophysics*, 29. 141-158. DOI: 10.1029/91RG00072

McKeague JA, Day JH. 1966. Dithionite- and oxalate-extractable fe and al as aids in differentiating various classes of soils. *Canadian Journal of Soil Science*, 46. 13-22. DOI: 10.4141/cjss66-003

Meusburger K, Mabit L, Park JH, Sandor T, Alewell C. 2013. Combined use of stable isotopes and fallout radionuclides as soil erosion indicators in a forested mountain site, South Korea. *Biogeosciences*, 10. 5627-5638. DOI: 10.5194/bg-10-5627-2013

Migoń P, Vieira G. 2014. Granite geomorphology and its geological controls, Serra da Estrela, Portugal. *Geomorphology*, 226. 1-14. DOI: 10.1016/j.geomorph.2014.07.027

Mohammad AG, Adam MA. 2010. The impact of vegetative cover type on runoff and soil erosion under different land uses. *Catena,* 81 (2). 97-103. DOI: 10.1016/j.catena.2010.01.008

Mohd Fairulnizal M, Vimala B, Rathi D, Mohd Naeem M. 2019. Atomic absorption spectroscopy for food quality evaluation. *Woodhead Publishing Series in Food Science, Technology and Nutrition, Evaluation Technologies for Food Quality, Woodhead Publishing*. 145-173. DOI: 10.1016/B978-0-12-814217-2.00001-9

Monaghan MC, Krishnaswami S, Turekian KK. 1986. The global-average production rate of ^{10}Be. *Earth and Planetary Science Letters, 76*. 279-287. DOI: 10.1016/0012-821X(86)90079-8

Mora C, Vieira G, Alcoforado M. 2001. Daily minimum air temperatures in theSerra da Estrela, Portugal. *Finisterra, 71*. 49-60. DOI: 10.18055/Finis1647

Morgan R. 1999. Soil Erosion and Conservation. *Soil Erosion and Conservation. Blackwell Publishing*. 45–65.

Nearing MA, Pruski FF, O'neal MR. 2004. Expected climate change impacts on soil erosion

rates: a review. *Journal of soil and water conservation,* 59 (1). 43-50.

Nesbitt H, Young G. 1982. Early Proterozoic climates and plate motions inferred from major element chemistry of lutites. *Nature*, 299. 715–717.

Nunes A. 2012. Regional variability and driving forces behind forest fires in Portugal an overview of the last three decades (1980–2009). *Applied Geography*, 34. 576-586. DOI: 10.1016/j.apgeog.2012.03.002

Nunes A, Coelho C, de Almeida A, Figueiredo A. 2010. Soil erosion and hydrological response to land abandonment in a central inland area of Portugal . *Land Degredation & Development*, 21. 260–273. DOI: 10.1002/ldr.973

Nunes A, de Almeida A, Coelho C. 2011. Impacts of land use and cover type on runoff and soil erosion in a marginal area of Portugal. *Applied Geography*, 31. 687-699. DOI: 10.1016/j.apgeog.2010.12.006

Pansu M, Gautheyron J. 2006. *Handbook of soil analysis. Mineral, organic and inorganic methods.* Springer Verlag, Berlin, Heidelberg.

Parker A. 1970. An index of weathering for silicate rocks. *Geology Magazine*, 107. 501–504. DOI: 10.1017/S0016756800058581

Price J, Velbel M. 2003. Chemical weathering indices applied to weathering profiles developed on heterogeneous felsic metamorphic parent rocks. *Chemical Geology*, 202. 397-416. DOI: 10.1016/j.chemgeo.2002.11.001

Raab G, Scarciglia F, Norton K, Dahms D, Brandová D, Portes R, Christl M, Ketterer ME, Ruppli A, Egli M. 2018. Denudation Variability of the Sila Massif Upland (Italy) from decades to millennia using ^{10}Be and $^{239+240}$Pu. *Land Degradation and Development*. 3736-3752. DOI: 10.1002/ldr.3120

Ribeiro A, Antunes M, Ferreira M, Rocha R, Soares A, Zbyszewski G, Almeida FM, Carvalho D, Monteiro JH. 1979. Introduction a la géologie générale du Portugal. *Serviços Geológicos de Portugal, Lisboa*, 114.

Ribeiro A, Pereira E, Dias R. 1990. Structure in the northwest of the Iberian Peninsula. In R. Dallmeyer, & E. Martínez Garcia (Ed.), *Pre-Mesozoic Geology of Iberia*. Springer-Verlag, Berlin, Heidelberg. 220–236.

Ruxton BP. 1968. Measures of the Degree of Chemical Weathering of Rocks. *The Journal of Geology*. 518-527. DOI: 10.1086/627357

Sant'Ovaia H, Olivier P, Ferreira N, Noronha F, Leblanc D. 2010. Magmatic structuresand kinematics emplacement of the Variscan granites from Central Portugal (Serrada Estrela

and Castro Daire areas). *Journal of Structural Geology, 32*. 1450–1465. DOI: 10.1016/j.jsg.2010.09.003

Scarciglia F. 2015. Weathering and exhumation history of the Sila Massif upland plateaus, southern Italy: a geomorphological and pedological perspective. *Journal of Soils and Sediments* 15: 1278–1291. DOI: 10.1007/s11368-014-0923-3.

Schaub M, Alewell C. 2009. Stable carbon isotopes as an indicator for soil degradation in an alpine environment (Urseren Valley, Switzerland). *Rapid Communications in Mass Spectrometry*, 23. 1499-1507. DOI: 10.1002/rcm.4030

Scheffer F, Schachtschabel P. 2010. *Lehrbuch der Bodenkunde* (16). Heidelberg: Spektrum Akademischer Verlag.

Stahr K, Kanderler E, Herrmann L, Streck T. 2016. *Bodenkunde und Standortlehre* (3). Eugen Ulmer Stuttgard.

Vieira G, Castro E, Loureiro F, Patrocínio F, Firminio G, Gomes H, Fernandes M, Forte J. 2017. *TEAMSNET: Aspiring Geopark Estrela, Application Dossier for UNESCO global Geopark.* https://teamsnet.unesco.org/UNESCO%20Geoparks/Estrela%20–%20PORTUGAL/Application_dossier/Estrela-PORTUGAL-Application_Dossier.pdf [access on 20. 08 2020]

Vitousek P, Chadwick OA, Matson P, Allison S, Derry LA, Kettley L, Luers A, Mecking E, Monastra V, Porder S. 2003. Erosion and the rejuvenation of weathering-derived nutrient supply in an old tropical landscape. *Ecosystems* 6. 762–772. DOI: 10.1007/s10021-003-0199-8

Vogt T. 1927. Geochemistry of Palaeoproterozoic Rocks of Aravalli Supergroup: Implications for Weathering History and Depositional Sequence. *Norges Geologiske Undersokelse*, 8. 1-560. DOI: 10.4236/ijg.2017.810074

von Blanckenburg F, Belshaw N, O'Nions R. 1996. Separation of 9Be and cosmogenic ^{10}Be from environmental materials and SIMS isotope dilution analysis. *Chemical Geology, 129* (1-2). 93-99. DOI: 10.1016/0009-2541(95)00157-3

von Blanckenburg F, Hewawasam T, Kubik P. 2004. Cosmogenic nuclide evidence for low weathering and denudation in the wet, tropical highlands of Sri Lanka. *Journal of Geophysical Research, 109*. 1-22. DOI: 10.1029/2003JF000049

Wagner G. 1998. Cosmogenic Nuclides. Springer, Berlin, Heidelberg.

Walling D, He Q. 1999. Improved models for estimating soil erosion rates from cesium-137 measurements. *Journal of Environmental Quality*, 28. 611–622. DOI: 10.2134/jeq1999.00472425002800020027x

References

Wartel S, Barusseau J, Cornand L. 1995. Improvement of grain-size analyses using the automated SEDIGRAPH 5100. *Geological Survey of Belgium, Professional Paper*. 400-426.

Willenbring JK, von Blanckenburg F. 2010. Meteoric cosmogenic Beryllium-10 adsorbed to river sediment and soil: Applications for Earth-surface dynamics. *Earth-Science Reviews (Elsevier)*, 98. 105-122. DOI: 10.1016/j.earscirev.2009.10.008

Xu Y, Qiao J, Pan S, Hou X, Roos P, Cao L. 2015. Plutonium as a tracer for soil erosion assessment in northeast China. *Science of the Total Environment*, 511. 176-185. DOI: 10.1016/j.scitotenv.2014.12.006

Zhang X, Higgitt DL, Walling DE. 1990. A preliminary assessment of the potential for using caesium-137 to estimate rates of soil erosion in the Loess Plateau of China. *Hydrological Science Journal*, 35. 43–252. DOI: 10.1080/02626669009492427

Zollinger B, Alewell C, Kneisel C, Meusburger K, Brandová D, Kubik P, Schaller M, Ketterer M, Egli M. 2015. The effect of permafrost on time-split soil erosion using radionuclides (^{137}Cs, $^{239+240}$Pu, meteoric ^{10}Be) and stable isotopes ($\delta\ ^{13}$C) in the eastern Swiss Alps. *Journal of Soils and Sediments*, 15. 1400–1419. DOI: 10.1007/s11368-014-0881-9

Appendix

Table 12; Physical characteristics of the investigated sites at Location 1

Sample	Depth [cm]	Soil skeleton (> 2 mm) [wt%]	Sand [%]	Silt [%]	Clay [%]	Bulk density [g/cm3]	Munsell colour [dry]
Location 1 (non-glaciated)							
R1-P1-P1							
SdE-1	0–5	0.57				0.58	10YR 3/2
SdE-2	5–10	0.76				0.73	10YR 4/2
SdE-3	10–15	0.51	40.80	28.80	29.20	0.71	10YR 4/2
SdE-4	15–20	0.54				0.65	10YR 4/2
SdE-5	20–25	0.57				0.60	10YR 4/2
R1-P1-P2							
SdE-6	0–5	0.43				0.59	10YR 4/2
SdE-7	5–10	0.61				0.75	10YR 4/2
SdE-8	10–15	0.54	29.20	36.40	33.20	0.79	10YR 3/2
SdE-9	15–20	0.57				0.80	10YR 4/2
SdE-10	20–25	0.54				0.90	10YR 4/2
R1-P2-P1							
SdE-11	0–5	0.57				0.59	10YR 4/2
SdE-12	5–10	0.32	32.00	31.20	36.80	0.59	10YR 3/2
SdE-13	10–15	0.48	29.20	32.80	36.40	0.68	10YR 3/2
SdE-14	15–20	0.49				0.66	10YR 3/2
SdE-15	20–25	0.38	33.20	27.60	39.20	0.60	10YR 3/2
R1-P2-P2							
SdE-16	0–5	0.47				0.56	10YR 4/2
SdE-17	5–10	0.52				0.74	10YR 3/2
SdE-18	10–15	0.49	24.80	36.00	39.20	0.85	10YR 3/2
SdE-19	15–20	0.50	38.80	26.00	35.20	0.74	10YR 3/2
SdE-20	20–25	0.51	38.40	34.80	25.60	0.82	10YR 3/2
S1-P1-P1							
SdE-21	0–5	0.47				0.59	
SdE-22	5–10	0.37				0.67	
SdE-23	10–15	0.40				0.65	
SdE-24	15–20	0.38				0.64	
SdE-25	20–25	0.39				0.63	
S1-P1-P2							
SdE-26	0–5	0.32				0.73	
SdE-27	5–10	0.40				0.63	
SdE-28	10–15	0.36				0.60	
SdE-29	15–20	0.36				0.67	
SdE-30	20–25	0.39				0.79	
S1-P2-P1							
SdE-31	0–5	0.50				0.18	
SdE-32	5–10	0.52				0.60	
SdE-33	10–15	0.61				0.76	
SdE-34	15–20	0.49				0.75	
SdE-35	20–25	0.46				0.85	
S1-P2-P2							
SdE-36	0–5	0.27				0.25	
SdE-37	5–10	0.45				0.71	
SdE-38	10–15	0.49				0.73	
SdE-39	15–20	0.36				0.79	
SdE-40	20–25	0.56				0.65	
S2-P1-P1							
SdE-41	0–5	0.44				0.96	
SdE-42	5–10	0.59				0.99	
SdE-43	10–15	0.49				0.84	
SdE-44	15–20	0.42				0.90	
SdE-45	20–25	0.42				0.86	
S2-P1-P2							
SdE-46	0–5	0.46				0.90	
SdE-47	5–10	0.55				1.02	
SdE-48	10–15	0.63				0.89	
SdE-49	15–20	0.47				0.80	
SdE-50	20–25	0.57				1.02	
S2-P2-P1							
SdE-51	0–5	0.59				0.83	
SdE-52	5–10	0.79				0.96	
SdE-53	10–15	0.70				0.85	
SdE-54	15–20	0.67				1.02	
SdE-55	20–25	0.73				0.88	
S2-P2-P2							
SdE-56	0–5	0.71				0.91	
SdE-57	5–10	0.76				0.97	
SdE-58	10–15	0.67				0.91	
SdE-59	15–20	0.72				0.97	
SdE-60	20–25	0.69				0.97	

Table 13; Physical characteristics of the investigated sites at Location 2

Sample	Depth [cm]	Soil skeleton (> 2 mm) [wt%]	Sand [%]	Silt [%]	Clay [%]	Bulk density [g/cm3]	Munsell colour [dry]
Location 2 (glaciated)							
R2-P1-P1							
SdE-61	0–5	0.17	42.00	22.80	34.80	0.53	10YR 3/2
SdE-62	5–10	0.30	19.20	39.60	40.80	0.64	10YR 3/2
SdE-63	10–15	0.23	28.40	27.60	44.00	0.70	10YR 3/2
SdE-64	15–20	0.31	22.00	37.20	40.40	0.74	10YR 3/2
SdE-65	20–25	0.33	36.00	19.20	44.80	0.77	10YR 3/2
SdE-66	30-35	0.69				0.97	10YR 4/2
R2-P1-P2							
SdE-67	0–5	0.20	32.40	30.00	37.60	0.68	10YR 3/2
SdE-68	5–10	0.26	18.00	36.40	44.40	0.62	10YR 3/2
SdE-69	10–15	0.28	32.00	22.00	46.00	0.67	10YR 3/2
SdE-70	15–20	0.45	24.00	34.40	41.20	0.81	10YR 3/2
SdE-71	20–25	0.46	19.60	30.40	47.20	0.75	10YR 3/2
SdE-72	30-35	0.69				1.07	10YR 3/2
R2-P2-P1							
SdE-73	0–5	0.27	33.60	20.80	45.60	0.69	10YR 4/2
SdE-74	5–10	0.36	30.00	30.80	38.40	0.77	10YR 4/2
SdE-75	10–15	0.29	18.00	42.80	37.20	0.65	10YR 3/2
SdE-76	15–20	0.35	29.20	25.20	45.60	0.71	10YR 3/2
SdE-77	20–25	0.63	26.00	34.00	38.00	1.01	10YR 3/2
R2-P2-P2							
SdE-78	0–5	0.32	20.00	29.20	49.60	0.60	10YR 4/2
SdE-79	5–10	0.35	34.40	33.60	31.60	0.71	10YR 3/2
SdE-80	10–15	0.31	13.20	46.80	37.20	0.72	10YR 3/2
SdE-81	15–20	0.26	34.00	31.60	33.20	0.67	10YR 3/2
SdE-82	20–25	0.34	20.40	43.50	35.20	0.71	10YR 3/2
S3-P1-P1							
SdE-83	0–5	0.45				0.69	
SdE-84	5–10	0.51				0.80	
SdE-85	10–15	0.40				0.80	
SdE-86	15–20	0.39				0.78	
SdE-87	20–25	0.42				0.69	
S3-P1-P2							
SdE-88	0–5	0.27				0.63	
SdE-89	5–10	0.36				0.68	
SdE-90	10–15	0.36				0.78	
SdE-91	15–20	0.41				0.84	
SdE-92	20–25	0.46				0.72	
S3-P2-P1							
SdE-93	0–5	0.30				0.62	
SdE-94	5–10	0.61				0.76	
SdE-95	10–15	0.56				0.69	
SdE-96	15–20	0.63				0.77	
SdE-97	20–25	0.67				0.82	
S3-P2-P2							
SdE-98	0–5	0.29				0.60	
SdE-99	5–10	0.49				0.79	
SdE-100	10–15	0.46				0.72	
SdE-101	15–20	0.70				0.84	
SdE-102	20–25	0.69				0.85	
S4-P1-P1							
SdE-103	0–5	0.22				0.58	
SdE-104	5–10	0.31				0.71	
SdE-105	10–15	0.46				0.76	
SdE-106	15–20	0.51				0.81	
SdE-107	20–25	0.33				0.65	
SdE-108	30-35	0.51				0.76	
S4-P1-P2							
SdE-109	0–5	0.24				0.70	
SdE-110	5–10	0.36				0.77	
SdE-111	10–15	0.38				0.83	
SdE-112	15–20	0.39				0.75	
SdE-113	20–25	0.37				0.79	
S4-P2-P1							
SdE-114	0–5	0.20				0.57	
SdE-115	5–10	0.24				0.65	
SdE-116	10–15	0.26				0.58	
SdE-117	15–20	0.36				0.73	
SdE-118	20–25	0.36				0.76	
S4-P2-P2							
SdE-119	0–5	0.20				0.49	
SdE-120	5–10	0.30				0.63	
SdE-121	10–15	0.37				0.68	
SdE-122	15–20	0.32				0.71	
SdE-123	20–25	0.44				0.76	

Appendix

Table 14; Chemical characteristics of the investigated sites at Location 1 (numbers in red and brackets are out of the accepted range)

Site	Depth	pH	Picarro		CHN			Oxalate									Dithionite						Crystaline	
			C	δ13C	C	N	C/N	Al_o	n	Fe_o	n	Mn_o	n	Si_o	n	Al_o +1/2Fe_o		Al_d	n	Fe_d	n	Si_d	n	Fe_{cry}	Fe_o/Fe_d
	[cm]	[$CaCl_2$]	[%]	[-]	[gkg^{-1}]	[gkg^{-1}]	[-]	[gkg^{-1}]		[gkg^{-1}]		[$mgkg^{-1}$]		[$mgkg^{-1}$]		[gkg^{-1}]		[gkg^{-1}]		[gkg^{-1}]		[$mgkg^{-1}$]		[gkg^{-1}]	[-]
Location 1 (non-glaciated)																								
R1-P1-P1		**n=2**	**n=1**	**n=1**	**n=2**	**n=2**																		
SdE-1	0–5	3.37	11.04	-28.37	107.6	7.78	13.82	1.54	1	3.24	3	27.5	1	108.7	1	3.16		2.90	1	3.91	1	937	1	0.67	0.83
SdE-2	5–10	3.40	11.46	-28.47	111.0	7.71	14.39	1.78	2	4.93	1	36.4	1	87.1	1	4.24		3.60	2	3.98	1	821	1	-0.96	1.24
SdE-3	10–15	3.55	8.93	-28.05	95.7	7.22	13.25	2.50	2	5.12	1	15.0	1	166.6	1	5.06		4.50	2	4.07	1	1059	1	-1.05	1.26
SdE-4	15–20	3.62	6.73	-28.28	60.9	4.25	14.32	1.72	1	5.52	1	7.9	1	104.9	1	4.48		3.39	1	4.62	1	602	1	-0.90	1.19
SdE-5	20–25	3.66	5.47	-27.60	69.3	4.96	13.97	2.18	1	4.66	2	10.2	1	140.6	1	4.51		4.45	1	4.74	1	509	1	0.08	0.98
R1-P1-P2								0.00		0.00								0.00		0.00					
SdE-6	0–5	3.37	9.13	-28.02	117.3	8.36	14.03	1.56	1	5.06	2	15.7	2	88.9	1	4.09		3.43	1	3.95	1	943	1	-1.11	1.28
SdE-7	5–10	3.39	12.26	-27.95	115.5	8.69	13.29	1.96	1	6.18	2	16.8	1	83.6	1	5.04		3.64	1	4.14	1	1047	1	-2.04	1.49
SdE-8	10–15	3.44	9.48	-27.89	88.9	6.74	13.18	1.78	2	7.10	1	16.3	1	90.1	1	5.33		3.43	1	3.08	1	830	1	-4.02	2.30
SdE-9	15–20	3.53	8.11	-27.70	(80.2)	6.06	13.24	1.71	2	6.66	1	12.5	1	120.7	1	5.04		4.44	1	4.55	2	785	1	-2.11	1.46
SdE-10	20–25	3.61	6.17	-27.47	66.8	4.60	14.52	1.70	3	7.21	1	4.1	1	115.1	1	5.30		4.24	1	4.80	1	454	2	-2.41	1.50
R1-P2-P1								0.00		0.00								0.00		0.00					
SdE-11	0–5	3.34	14.02	-28.23	133.7	(8.93)	14.96	1.55	1	3.57	1	10.8	1	48.8	1	3.34		2.39	1	3.98	1	795	1	0.42	0.90
SdE-12	5–10	3.47	7.59	-27.44	101.7	7.65	13.30	2.31	1	5.19	1	9.8	1	89.9	1	4.91		3.47	1	4.60	1	695	1	-0.59	1.13
SdE-13	10–15	3.54	9.72	-27.77	76.9	5.77	13.34	2.17	1	4.09	1	4.6	1	78.5	1	4.22		2.88	1	4.63	1	347	1	0.54	0.88
SdE-14	15–20	3.63	7.67	-27.30	85.2	6.25	13.64	2.39	1	5.62	1	8.5	1	150.3	1	5.20		4.82	1	4.92	1	251	1	-0.70	1.14
SdE-15	20–25	3.82	7.65	-27.06	94.4	6.18	15.27	4.16	2	8.16	1	8.3	1	110.2	1	8.24		8.89	2	8.33	1	435	2	0.17	0.98
R1-P2-P2								0.00		0.00								0.00		0.00					
SdE-16	0–5	3.33	10.01	-28.35	118.7	8.11	14.65	1.69	1	10.00	1	5.5	1	75.1	1	6.69		2.56	1	4.63	1	1019	1	-5.37	2.16
SdE-17	5–10	3.51	8.85	-27.69	84.7	6.37	13.30	1.88	1	10.29	1	4.8	2	50.0	1	7.02		3.11	1	4.62	1	727	1	-5.68	2.23
SdE-18	10–15	3.61	7.76	-27.36	(72.8)	5.46	13.34	2.31	1	12.09	2	5.6	2	104.2	1	8.35		3.62	1	5.04	1	608	1	-7.06	2.40
SdE-19	15–20	3.74	7.67	-27.17	72.7	4.99	14.56	2.60	1	11.70	1	9.7	1	81.8	1	8.45		4.64	1	5.35	1	480	1	-6.35	2.19
SdE-20	20–25	3.79	7.56	-27.13	68.8	4.77	14.43	1.89	1	8.17	2	6.8	1	70.8	1	5.97		5.68	2	6.29	1	361	2	-1.88	1.30

Appendix

Table 15; Chemical characteristics of the investigated sites at Location 2 (numbers in red and brackets are out of the accepted range)

Site	Depth [cm]	pH [$CaCl_2$]	Picarro C [%]	Picarro δ13C [-]	CHN C [gkg^{-1}]	CHN N [gkg^{-1}]	CHN C/N [-]	Oxalate Al_o [gkg^{-1}]	n	Oxalate Fe_o [gkg^{-1}]	n	Oxalate Mn_o [$mgkg^{-1}$]	n	Oxalate Si_o [$mgkg^{-1}$]	n	Oxalate Al_o +1/2Fe_o [gkg^{-1}]	Dithionite Al_d [gkg^{-1}]	n	Dithionite Fe_d [gkg^{-1}]	n	Dithionite Si_d [$mgkg^{-1}$]	n	Crystaline Fe_{cry} [gkg^{-1}]	Fe_o/Fe_d [-]
Location 2 (glaciated)																								
R2-P1-P1																								
SdE-61	0–5	3.97	5.14	-28.81	69.0	4.91	14.07	0.95	1	3.27	1	18.5	1	15.2	1	2.58	1.54	1	4.46	1	584	1	1.20	0.73
SdE-62	5–10	3.82	5.41	-28.12	68.4	5.22	13.11	1.06	1	5.30	2	3.4	1	44.9	1	3.71	2.51	1	5.81	1	447	1	0.51	0.91
SdE-63	10–15	3.83	6.14	-27.64	(68.3)	(5.31)	12.87	1.45	1	4.69	1	4.0	1	123.0	1	3.80	3.09	1	7.00	1	331	1	2.30	0.67
SdE-64	15–20	3.91	6.19	-27.46	73.2	5.80	12.61	1.80	1	5.47	1	5.2	1	108.3	1	4.54	3.44	1	6.29	1	309	2	0.82	0.87
SdE-65	20–25	3.94	5.89	-27.42	61.5	(4.82)	12.76	2.20	1	2.58	1	5.0	1	100.9	1	3.49	3.79	1	6.97	1	226	1	4.38	0.37
SdE-66	30-35	4.13	5.57	-27.30	70.3	5.69	12.36	3.33	2	3.62	1	12.9	1	358.0	1	5.14	5.38	1	5.58	1	402	1	1.96	0.65
R2-P1-P2																								
SdE-67	0–5	3.83	4.79	-28.15	62.3	4.81	12.96	1.29	1	4.34	2	4.1	2	65.3	1	3.46	2.38	1	4.52	1	476	1	0.17	0.96
SdE-68	5–10	3.88	5.17	-28.26	(62.8)	(4.73)	13.29	1.25	1	4.11	2	4.5	1	55.5	1	3.31	2.21	1	5.66	2	543	1	1.54	0.73
SdE-69	10–15	3.91	7.12	-27.76	70.3	5.27	13.34	1.75	1	5.90	2	2.6	1	58.4	1	4.70	3.61	2	6.34	1	392	1	0.44	0.93
SdE-70	15–20	3.95	7.96	-27.52	71.4	5.28	13.52	1.96	2	4.85	2	3.4	2	86.5	1	4.39	4.51	2	7.16	1	311	2	2.30	0.68
SdE-71	20–25	3.98	7.06	-27.44	65.5	4.95	13.24	2.34	1	4.40	2	5.3	1	62.0	1	4.54	5.12	1	7.45	1	318	1	3.04	0.59
SdE-72	30-35	4.12	6.06	-27.34	64.4	5.04	12.77	3.10	1	4.98	1	13.5	1	196.9	1	5.59	6.02	1	7.10	1	284	1	2.12	0.70
R2-P2-P1																								
SdE-73	0–5	3.79	6.13	-28.63	60.6	4.68	12.93	1.05	1	4.10	1	5.7	1	26.5	1	3.10	2.41	1	6.55	1	467	1	2.45	0.63
SdE-74	5–10	3.81	6.76	-28.33	64.2	4.96	12.94	1.25	1	4.05	1	5.9	1	39.6	1	3.27	2.87	1	6.37	1	317	1	2.32	0.64
SdE-75	10–15	3.85	7.18	-28.06	71.9	5.63	12.78	1.65	1	4.18	2	6.0	1	48.5	1	3.74	3.74	1	7.58	1	429	1	3.40	0.55
SdE-76	15–20	3.89	5.61	-27.83	(68.1)	(5.40)	12.60	1.72	1	12.35	1	3.5	2	37.9	1	7.90	4.39	1	9.11	2	259	1	-3.24	1.36
SdE-77	20–25	3.94	5.30	-27.74	(63.9)	(5.07)	12.61	2.04	1	5.60	3	3.2	2	50.2	1	4.84	4.52	1	7.74	1	263	1	2.14	0.72
R2-P2-P2																								
SdE-78	0–5	3.87	6.12	-28.60	69.0	5.37	12.83	1.10	1	3.74	3	4.7	2	84.8	1	2.97	2.95	1	7.60	1	442	1	3.86	0.49
SdE-79	5–10	3.89	5.45	-28.19	71.2	5.59	12.73	1.21	2	5.30	2	3.7	1	86.3	1	3.85	3.46	1	8.17	1	278	1	2.87	0.65
SdE-80	10–15	3.86	5.37	-28.21	65.3	5.16	12.64	0.98	1	5.26	2	4.9	1	96.3	1	3.61	3.45	1	6.87	2	449	2	1.61	0.77
SdE-81	15–20	3.91	4.41	-27.75	68.5	5.40	12.70	1.30	1	4.88	2	2.6	1	63.7	1	3.74	5.21	1	7.34	1	257	2	2.47	0.66
SdE-82	20–25	3.93	5.28	-27.78	61.2	4.88	12.56	0.00		0.00		0.1	1	57.3	1	0.00	4.01	1	6.55	1	195	2	6.55	0.00

Table 16; Beryllium results in more detail of the Reference 2 site

											Corrected to sample preparation blank, Error includes AMS standard error				
Sample	**Soil Depth**	**^{10}Be counts**	**^{9}Be (LE)**	**Trans.**	**^{10}Be/^{9}Be final**	**error**	**Abs. error**	**^{10}Be**	**^{10}Be**	**err abs.**	**^{10}Be/^{9}Be corr Lab blk**	**Abs error**	**^{10}Be**	**Err ^{10}Be**	**Err ^{10}Be**
	[cm]		**[n atoms]**	**[%]**	**[10^{-12}]**	**[%]**	**[10^{-12}]**	**[cps]**	**[atoms g^{-1} x 10^{4}]**		**[10^{-12}]**	**[10^{-12}]**	**[atoms g^{-1} x 10^{4}]**	**[atoms g^{-1} x 10^{4}]**	**[%]**
Location 2 (glaciated)															
R2-P1-P1															
SdE-61	0–5	5'088	1935	37.0	8.335	1.5%	0.125	434	27918	428	8.322	0.243	27873.34	813.93	2.9%
SdE-62	5–10	4'236	1337	33.0	10.622	1.7%	0.181	297	35454	606	10.609	0.321	35408.81	1071.82	3.0%
SdE-63	10–15	9'328	3236	34.8	10.913	1.5%	0.164	377	36627	549	10.900	0.318	36583.34	1067.87	2.9%
SdE-64	15–20	5'444	1410	33.6	12.419	1.8%	0.224	253	41639	768	12.406	0.383	41594.57	1282.72	3.1%
SdE-65	20–25	9'881	3123	36.4	10.228	1.7%	0.174	522	34514	576	10.215	0.309	34470.52	1043.47	3.0%
SdE-66	30-35	7'051	1677	33.4	8.737	2.2%	0.192	424	29411	660	8.724	0.291	29366.65	979.43	3.3%
R2-P1-P2															
SdE-67	0–5	11'272	4053	36.5	9.479	1.5%	0.142	625	31918	479	9.466	0.276	31874.27	930.58	2.9%
SdE-68	5–10	8'182	2714	35.7	9.342	1.5%	0.140	430	31260	469	9.329	0.272	31214.86	911.35	2.9%
SdE-69	10–15	8'408	2406	35.5	10.829	1.5%	0.162	421	36367	546	10.816	0.316	36322.51	1060.26	2.9%
SdE-70	15–20	7'201	2277	35.0	10.563	1.5%	0.158	428	35664	535	10.550	0.308	35620.37	1039.80	2.9%
SdE-71	20–25	5'867	1838	35.4	9.492	1.5%	0.142	324	32029	480	9.479	0.277	31985.97	933.84	2.9%
SdE-72	30-35	6'944	2332	37.8	9.240	1.5%	0.139	512	31124	467	9.227	0.269	31080.11	907.43	2.9%

Table 17; Calculation of total ^{10}Be per horizon for Reference 2

Sample	**Depth range [cm]**	**Thickness [cm]**	**density [g cm^{-3}]**	**Weight [g cm^{-2}]**	**10Be [atoms g^{-1} x 10^{8}]**	**Skeleton [%]**	**10Be [atoms g^{-1} cm^{-2} x 10^{8}]**
R2-P1-P1							
SdE61	0–5	5	0.53	2.6500	28	17	61.1
SdE62	5–10	5	0.64	3.2000	35	30	79.8
SdE63	10–15	5	0.70	3.5000	37	23	98.4
SdE64	15–20	5	0.74	3.7000	42	31	105.8
SdE65	20–25	5	0.77	3.8500	34	33	89.3
SdE66	30-35	5	0.97	4.8500	29	69	44.1
						Total ^{10}Be [atoms g^{-1} cm^{-2} x 10^{8}]	**478.5**
R2-P1-P2							
SdE67	0–5	5	0.68	3.4000	32	20	86.5
SdE68	5–10	5	0.62	3.1000	31	26	71.9
SdE69	10–15	5	0.67	3.3500	36	28	87.2
SdE70	15–20	5	0.81	4.0500	36	45	79.5
SdE71	20–25	5	0.75	3.7500	32	46	64.4
SdE72	30-35	5	1.07	5.3500	31	69	51.7
						Total ^{10}Be [atoms g^{-1} cm^{-2} x 10^{8}]	**441.2**

Table 18; Calculation of total ^{10}Be per horizon for Reference 1

Sample	Depth range [cm]	Thickness [cm]	density [g cm^{-3}]	Weight [g cm^{-2}]	10Be [atoms g^{-1} x 10^{8}]	Skeleton [%]	10Be [atoms g^{-1} cm^{-2} x 10^{8}]
Reference 1 (average from all profiles)							
	0–5	5	0.58	2.9025	36	51	51.0
	5–10	5	0.70	3.5200	47	55	73.9
	10–15	5	0.76	3.8067	56	50	106.3
	15–20	5	0.71	3.5675	52	53	87.5
	20–25	5	0.73	3.6508	53	50	97.0
estimation	*25-30*	*5*	*1.00*	*5.0000*	*50*	*55*	*111.4*
						Total ^{10}Be [atoms g^{-1} cm^{-2} x 10^{8}]	**527.2**

Table 19; Picarro and C/N results of the investigated sites at Location 1 (numbers in red and brackets are outside the acceptable ranges of errors)

			Picarro		CHN		
Site	**Depth [cm]**	**pH [CaCl2]**	**C [%]**	**δ13C [-]**	**C [gkg-1]**	**N [gkg-1]**	**C/N [-]**
Location 1 (non-glaciated)							
R1-P1-P1		**n=2**	**n=1**	**n=1**	**n=2**	**n=2**	
SdE-1	0–5	3.37	11.04	-28.37	107.6	7.78	13.82
SdE-2	5–10	3.40	11.46	-28.47	111.0	7.71	14.39
SdE-3	10–15	3.55	8.93	-28.05	95.7	7.22	13.25
SdE-4	15–20	3.62	6.73	-28.28	60.9	4.25	14.32
SdE-5	20–25	3.66	5.47	-27.60	69.3	4.96	13.97
R1-P1-P2							
SdE-6	0–5	3.37	9.13	-28.02	117.3	8.36	14.03
SdE-7	5–10	3.39	12.26	-27.95	115.5	8.69	13.29
SdE-8	10–15	3.44	9.48	-27.89	88.9	6.74	13.18
SdE-9	15–20	3.53	8.11	-27.70	(80.2)	6.06	13.24
SdE-10	20–25	3.61	6.17	-27.47	66.8	4.60	14.52
R1-P2-P1							
SdE-11	0–5	3.34	14.02	-28.23	133.7	(8.93)	14.96
SdE-12	5–10	3.47	7.59	-27.44	101.7	7.65	13.30
SdE-13	10–15	3.54	9.72	-27.77	76.9	5.77	13.34
SdE-14	15–20	3.63	7.67	-27.30	85.2	6.25	13.64
SdE-15	20–25	3.82	7.65	-27.06	94.4	6.18	15.27
R1-P2-P2							
SdE-16	0–5	3.33	10.01	-28.35	118.7	8.11	14.65
SdE-17	5–10	3.51	8.85	-27.69	84.7	6.37	13.30
SdE-18	10–15	3.61	7.76	-27.36	(72.8)	5.46	13.34
SdE-19	15–20	3.74	7.67	-27.17	72.7	4.99	14.56
SdE-20	20–25	3.79	7.56	-27.13	68.8	4.77	14.43
S1-P1-P1							
SdE-21	0–5	3.57	8.78	-28.85	86.4	5.99	14.42
SdE-22	5–10	3.72	6.18	-28.04	48.3	3.43	14.09
SdE-23	10–15	3.76	5.94	-27.91	54.4	3.88	14.03
SdE-24	15–20	3.78	6.67	-27.54	53.7	3.73	14.39
SdE-25	20–25	3.84	6.46	-27.51	(52.4)	(3.69)	14.19
S1-P1-P2							
SdE-26	0–5	3.68	6.04	-28.20	(57.4)	(4.11)	13.99
SdE-27	5–10	3.75	5.91	-28.25	50.1	3.53	14.17
SdE-28	10–15	3.80	5.78	-27.77	55.1	3.80	14.49
SdE-29	15–20	3.85	4.96	-27.72	51.2	3.45	14.83
SdE-30	20–25	3.94	4.36	-27.88	46.0	3.36	13.69
S1-P2-P1							
SdE-31	0–5	3.51	24.89	-28.24	275.9	11.35	24.32
SdE-32	5–10	3.81	7.94	-28.72	64.1	4.44	14.42
SdE-33	10–15	3.91	7.28	-27.94	58.2	3.65	15.94
SdE-34	15–20	3.94	5.22	-27.77	(50.6)	(3.09)	16.41
SdE-35	20–25	3.95	4.61	-27.76	(48.6)	(2.81)	17.27
S1-P2-P2							
SdE-36	0–5	3.60	15.45	-28.32	198.1	11.69	16.95
SdE-37	5–10	3.79	5.11	-28.41	63.0	4.61	13.65
SdE-38	10–15	3.94	3.45	-27.79	(45.1)	(3.05)	14.78
SdE-39	15–20	3.93	5.26	-27.46	52.4	3.53	14.87
SdE-40	20–25	3.87	4.98	-27.37	69.1	3.89	17.78
S2-P1-P1							
SdE-41	0–5	4.17	4.03	-27.95	(42.0)	(2.75)	15.24
SdE-42	5–10	4.20	4.57	-27.38	40.3	2.67	15.09
SdE-43	10–15	4.13	5.55	-26.75	62.0	4.03	15.38
SdE-44	15–20	4.17	3.81	-27.09	37.3	2.52	14.81
SdE-45	20–25	4.14	3.55	-27.10	37.6	2.57	14.62
S2-P1-P2							
SdE-46	0–5	4.26	4.92	-28.24	41.6	2.76	15.08
SdE-47	5–10	4.20	4.67	-27.47	45.7	3.10	14.75
SdE-48	10–15	4.24	3.20	-27.58	24.6	1.67	14.73
SdE-49	15–20	4.21	5.55	-27.10	45.3	2.71	16.73
SdE-50	20–25	4.26	2.45	-27.22	15.6	0.96	16.30
S2-P2-P1							
SdE-51	0–5	4.22	4.65	-28.43	38.8	2.69	14.38
SdE-52	5–10	4.27	3.49	-27.85	(33.0)	(2.24)	14.73
SdE-53	10–15	4.33	1.45	-28.12	12.1	0.85	14.25
SdE-54	15–20	4.36	0.77	-28.87	7.8	0.52	15.09
SdE-55	20–25	4.38	1.36	-28.06	14.4	0.85	16.92
S2-P2-P2							
SdE-56	0–5	4.22	3.77	-28.13	40.6	(2.81)	14.43
SdE-57	5–10	4.33	1.32	-28.53	(12.3)	0.86	14.34
SdE-58	10–15	4.30	4.87	-27.12	55.9	3.08	18.16
SdE-59	15–20	4.38	1.64	-28.08	12.4	0.78	16.03
SdE-60	20–25	4.35	1.43	-27.78	12.8	0.83	15.38

Table 20; Picarro and C/N results of the investigated sites at Location 2 (numbers in red and brackets are outside the acceptable ranges of errors)

			Picarro		CHN		
Site	**Depth [cm]**	**pH [CaCl2]**	**C [%]**	**δ13C [-]**	**C [gkg-1]**	**N [gkg-1]**	**C/N [-]**
Location 2 (glaciated)							
R2-P1-P1							
SdE-61	0–5	3.97	5.14	-28.81	69.0	4.91	14.07
SdE-62	5–10	3.82	5.41	-28.12	68.4	5.22	13.11
SdE-63	10–15	3.83	6.14	-27.64	(68.3)	(5.31)	12.87
SdE-64	15–20	3.91	6.19	-27.46	73.2	5.80	12.61
SdE-65	20–25	3.94	5.89	-27.42	61.5	(4.82)	12.76
SdE-66	30-35	4.13	5.57	-27.30	70.3	5.69	12.36
R2-P1-P2							
SdE-67	0–5	3.83	4.79	-28.15	62.3	4.81	12.96
SdE-68	5–10	3.88	5.17	-28.26	(62.8)	(4.73)	13.29
SdE-69	10–15	3.91	7.12	-27.76	70.3	5.27	13.34
SdE-70	15–20	3.95	7.96	-27.52	71.4	5.28	13.52
SdE-71	20–25	3.98	7.06	-27.44	65.5	4.95	13.24
SdE-72	30-35	4.12	6.06	-27.34	64.4	5.04	12.77
R2-P2-P1							
SdE-73	0–5	3.79	6.13	-28.63	60.6	4.68	12.93
SdE-74	5–10	3.81	6.76	-28.33	64.2	4.96	12.94
SdE-75	10–15	3.85	7.18	-28.06	71.9	5.63	12.78
SdE-76	15–20	3.89	5.61	-27.83	(68.1)	(5.40)	12.60
SdE-77	20–25	3.94	5.30	-27.74	(63.9)	(5.07)	12.61
R2-P2-P2							
SdE-78	0–5	3.87	6.12	-28.60	69.0	5.37	12.83
SdE-79	5–10	3.89	5.45	-28.19	71.2	5.59	12.73
SdE-80	10–15	3.86	5.37	-28.21	65.3	5.16	12.64
SdE-81	15–20	3.91	4.41	-27.75	68.5	5.40	12.70
SdE-82	20–25	3.93	5.28	-27.78	61.2	4.88	12.56
S3-P1-P1							
SdE-83	0–5	3.85	5.30	-28.69	64.7	5.20	12.45
SdE-84	5–10	3.87	5.56	-28.30	(62.4)	(5.08)	12.28
SdE-85	10–15	3.86	4.65	-28.41	61.3	4.91	12.48
SdE-86	15–20	3.92	4.40	-28.21	60.9	4.86	12.52
SdE-87	20–25	3.96	4.33	-28.03	(62.3)	4.88	12.75
S3-P1-P2							
SdE-88	0–5	3.75	6.28	-28.86	66.9	5.16	12.98
SdE-89	5–10	3.76	5.03	-28.67	55.7	4.31	12.91
SdE-90	10–15	3.81	6.28	-28.30	62.5	4.99	12.53
SdE-91	15–20	3.86	6.62	-28.29	62.1	4.90	12.67
SdE-92	20–25	3.92	5.75	-27.92	61.6	4.93	12.49
S3-P2-P1							
SdE-93	0–5	3.71	7.41	-28.79	74.9	6.13	12.22
SdE-94	5–10	3.80	7.18	-28.13	(66.8)	(5.47)	12.22
SdE-95	10–15	3.82	8.20	-27.77	71.2	5.75	12.38
SdE-96	15–20	3.92	6.93	-27.75	(66.5)	(5.31)	12.52
SdE-97	20–25	3.96	7.58	-27.69	74.9	6.02	12.43
S3-P2-P2							
SdE-98	0–5	3.74	4.48	-29.02	59.0	4.78	12.35
SdE-99	5–10	3.71	4.73	-28.16	70.9	5.85	12.12
SdE-100	10–15	3.77	4.16	-27.85	66.4	5.52	12.03
SdE-101	15–20	3.93	7.05	-27.97	66.1	5.43	12.18
SdE-102	20–25	4.01	6.59	-28.01	(60.3)	(4.94)	12.19
S4-P1-P1							
SdE-103	0–5	3.74	6.49	-29.30	60.4	4.45	13.58
SdE-104	5–10	3.79	5.46	-28.94	49.2	3.79	13.00
SdE-105	10–15	3.80	5.87	-28.41	53.4	4.21	12.67
SdE-106	15–20	3.88	5.52	-28.16	53.6	4.18	12.84
SdE-107	20–25	3.91	5.53	-28.05	52.3	4.02	13.00
SdE-108	30-35	4.05	4.55	-27.71	46.4	3.74	12.40
S4-P1-P2							
SdE-109	0–5	3.82	5.64	-29.38	50.7	3.78	13.41
SdE-110	5–10	3.79	5.03	-28.81	54.1	4.09	13.21
SdE-111	10–15	3.78	6.22	-28.21	58.7	4.56	12.89
SdE-112	15–20	3.82	6.14	-28.15	58.4	4.52	12.92
SdE-113	20–25	3.90	4.90	-28.00	50.1	3.92	12.78
S4-P2-P1							
SdE-114	0–5	3.70	6.90	-28.80	67.2	5.19	12.94
SdE-115	5–10	3.65	6.07	-28.37	60.2	4.71	12.77
SdE-116	10–15	3.69	6.05	-28.18	56.6	4.39	12.88
SdE-117	15–20	3.74	6.14	-27.99	68.7	5.31	12.94
SdE-118	20–25	3.81	6.37	-27.75	62.6	4.83	12.96
S4-P2-P2							
SdE-119	0–5	3.73	6.22	-28.66	60.9	4.69	12.98
SdE-120	5–10	3.73	5.47	-28.17	66.5	5.20	12.79
SdE-121	10–15	3.74	5.60	-27.91	60.1	4.68	12.84
SdE-122	15–20	3.79	6.66	-27.47	67.2	5.19	12.94
SdE-123	20–25	3.84	4.89	-27.42	64.4	4.97	12.97

Table 21; Total elemental content (given as oxides) of the investigated sites at Location 1. LOI = loss on ignition.

Sample	Soil Depth [cm]	Na_2O [%]	MgO [%]	AL_2O_3 [%]	SiO_2 [%]	P_2O_5 [%]	K_2O [%]	CaO [%]	TiO_2 [%]	MnO [%]	Fe_2O_3 [%]	LOI [%]	Organic Matter [%]	IVC [%]
Location 1 (non-glaciated)														
R1-P1-P1														
SdE-1	0–5	4.23	0.84	22.20	40.36	1.11	5.19	0.69	0.41	0.02	4.67	20.30	18.99	4.22
SdE-2	5–10	4.01	0.82	22.14	40.73	1.09	5.33	0.69	0.41	0.02	4.52	20.24	19.72	3.98
SdE-3	10–15	4.14	0.91	25.05	40.25	1.63	5.38	0.70	0.44	0.02	5.05	16.44	15.35	3.49
SdE-4	15–20	4.32	0.98	27.53	42.41	1.81	5.66	0.77	0.51	0.02	5.28	10.73	11.57	1.03
SdE-5	20–25	3.90	0.92	26.68	40.80	2.01	6.01	0.78	0.58	0.02	5.62	12.68	9.41	4.31
R1-P1-P2														
SdE-6	0–5	3.83	0.85	21.83	36.72	1.22	4.75	0.65	0.48	0.02	5.75	23.90	15.70	8.09
SdE-7	5–10	3.99	0.86	21.77	37.62	1.39	5.03	0.72	0.47	0.02	5.33	22.81	21.09	2.30
SdE-8	10–15	4.15	0.92	24.47	40.40	1.55	5.09	0.67	0.49	0.02	5.33	16.93	16.31	2.96
SdE-9	15–20	4.43	0.96	25.99	40.05	1.85	5.45	0.69	0.50	0.02	5.56	14.50	13.94	2.59
SdE-10	20–25	4.54	1.01	27.43	42.02	1.88	5.90	0.73	0.53	0.02	5.38	10.57	10.61	1.64
R1-P2-P1														
SdE-11	0–5	4.35	0.83	20.47	38.49	0.93	4.81	0.69	0.40	0.02	4.36	24.67	24.12	3.83
SdE-12	5–10	4.47	0.94	24.05	38.49	1.41	5.08	0.65	0.47	0.02	5.26	19.17	13.05	8.59
SdE-13	10–15	4.41	0.93	25.70	41.13	1.59	5.36	0.67	0.52	0.02	5.20	14.47	16.72	-0.22
SdE-14	15–20	4.13	0.92	25.68	39.64	1.84	5.32	0.64	0.53	0.02	5.81	15.48	13.19	4.61
SdE-15	20–25	4.05	0.92	27.21	36.92	2.39	5.04	0.59	0.55	0.02	5.95	16.38	13.15	5.92
R1-P2-P2														
SdE-16	0–5	4.24	0.89	22.26	40.06	1.02	5.33	0.64	0.45	0.02	4.80	20.30	17.22	5.62
SdE-17	5–10	4.30	0.93	25.28	41.40	1.49	5.60	0.66	0.51	0.02	5.29	14.52	15.22	1.05
SdE-18	10–15	4.41	0.94	26.74	41.70	1.65	5.73	0.70	0.53	0.02	5.31	12.27	13.35	0.68
SdE-19	15–20	4.24	0.96	26.64	40.94	1.92	5.70	0.66	0.54	0.02	5.34	13.05	13.20	1.77
SdE-20	20–25	4.13	0.94	27.10	40.62	2.05	5.30	0.65	0.57	0.02	5.78	12.84	13.00	1.83
S1-P1-P1														
SdE-21	0–5	4.08	0.87	24.67	42.49	1.04	6.31	0.65	0.50	0.02	4.54	14.83	15.11	2.16
SdE-22	5–10	3.79	0.97	28.05	43.20	1.51	6.29	0.65	0.53	0.02	5.00	10.00	10.62	1.18
SdE-23	10–15	3.89	1.00	28.27	42.08	1.67	6.27	0.65	0.53	0.02	5.34	10.27	10.21	1.84
SdE-24	15–20	1.29	0.64	28.98	44.14	1.56	6.45	0.66	0.53	0.02	5.20	10.53	11.47	0.56
SdE-25	20–25	3.96	0.97	28.29	43.38	1.34	6.56	0.65	0.50	0.02	4.97	9.39	11.10	0.00
S1-P1-P2														
SdE-26	0–5	4.22	0.91	26.86	43.76	1.30	6.67	0.67	0.47	0.02	4.61	10.50	10.39	2.04
SdE-27	5–10	4.04	0.94	28.46	42.63	1.51	6.48	0.67	0.45	0.02	4.83	9.98	10.16	1.64
SdE-28	10–15	3.95	0.87	27.31	43.19	1.26	6.44	0.69	0.50	0.02	5.10	10.68	9.94	2.89
SdE-29	15–20	3.97	0.97	29.17	42.85	1.22	6.49	0.64	0.48	0.02	4.94	9.25	8.53	2.47
SdE-30	20–25	3.55	1.00	32.61	40.51	1.07	6.33	0.58	0.47	0.02	5.05	8.83	7.50	3.12
S1-P2-P1														
SdE-31	0–5	3.50	0.83	12.38	23.62	0.56	3.23	1.02	0.27	0.03	2.79	51.77	42.82	15.62
SdE-32	5–10	4.25	0.91	26.78	42.94	1.19	6.34	0.70	0.48	0.02	4.69	11.71	13.66	0.00
SdE-33	10–15	4.24	0.94	27.80	42.43	1.12	6.23	0.73	0.48	0.02	4.79	11.23	12.53	0.59
SdE-34	15–20	4.29	0.95	27.82	45.00	0.88	6.97	0.76	0.52	0.02	4.52	8.28	8.97	0.67
SdE-35	20–25	4.09	0.93	28.57	44.98	0.90	6.96	0.79	0.54	0.02	4.81	7.42	7.93	0.71
S1-P2-P2														
SdE-36	0–5	3.84	0.74	18.45	31.25	0.87	4.25	0.60	0.34	0.02	3.77	35.86	26.57	15.31
SdE-37	5–10	4.29	0.88	26.36	43.62	1.27	6.47	0.71	0.45	0.02	4.40	11.55	8.79	4.49
SdE-38	10–15	4.17	1.02	29.63	44.22	1.07	6.20	0.71	0.51	0.02	4.82	7.64	5.94	3.72
SdE-39	15–20	4.01	0.93	28.53	43.36	1.05	6.18	0.72	0.54	0.02	4.97	9.71	9.05	2.35
SdE-40	20–25	4.11	0.93	27.13	42.71	1.07	6.31	0.69	0.50	0.02	4.61	11.94	8.57	5.26
S2-P1-P1														
SdE-41	0–5	3.69	1.10	31.43	41.70	0.88	6.38	0.63	0.54	0.03	5.73	7.89	6.93	2.47
SdE-42	5–10	3.40	0.97	33.05	41.09	0.89	6.01	0.54	0.46	0.02	4.81	8.76	7.86	2.74
SdE-43	10–15	2.28	0.91	35.53	37.54	0.98	5.71	0.25	0.36	0.01	4.45	11.99	9.55	5.05
SdE-44	15–20	2.07	0.87	36.96	38.35	0.92	5.91	0.16	0.30	0.01	4.26	10.20	6.56	6.07
SdE-45	20–25	2.05	0.85	36.91	39.42	0.83	6.21	0.14	0.29	0.01	4.05	9.25	6.11	5.49
S2-P1-P2														
SdE-46	0–5	3.33	1.00	30.22	42.89	0.87	6.29	0.67	0.54	0.02	5.13	9.07	8.46	2.36
SdE-47	5–10	2.96	0.91	36.39	37.62	1.00	5.54	0.49	0.42	0.02	4.85	9.81	8.03	4.00
SdE-48	10–15	2.95	0.81	38.29	39.93	0.77	5.85	0.47	0.30	0.01	4.28	6.35	5.50	2.51
SdE-49	15–20	2.44	0.72	40.07	35.91	0.72	4.24	0.43	0.27	0.01	3.69	11.52	9.54	5.09
SdE-50	20–25	2.88	0.74	37.44	42.39	0.61	5.21	0.66	0.32	0.01	4.03	5.73	4.22	3.18
S2-P2-P1														
SdE-51	0–5	4.07	1.01	31.74	42.05	0.88	6.24	0.73	0.43	0.02	4.71	8.12	8.00	1.84
SdE-52	5–10	3.69	1.00	35.33	40.86	0.96	5.47	0.88	0.39	0.02	4.36	7.03	6.00	2.60
SdE-53	10–15	3.66	0.69	36.61	44.12	0.67	5.73	0.87	0.24	0.01	3.20	4.21	2.49	2.93
SdE-54	15–20	3.61	0.68	38.54	43.47	0.69	5.19	1.08	0.21	0.01	3.06	3.44	1.32	3.08
SdE-55	20–25	3.78	0.63	37.31	44.20	0.75	5.41	1.03	0.20	0.01	2.46	4.23	2.34	3.06
S2-P2-P2														
SdE-56	0–5	3.98	1.00	34.40	40.54	0.86	5.63	0.81	0.41	0.02	4.60	7.75	6.49	3.09
SdE-57	5–10	4.07	0.81	34.07	45.94	0.71	5.45	0.99	0.32	0.02	3.98	3.65	2.27	2.33
SdE-58	10–15	2.80	0.77	39.78	35.92	0.84	4.29	0.36	0.17	0.01	2.53	12.52	8.37	8.03
SdE-59	15–20	4.04	0.71	35.71	44.86	0.66	5.28	1.20	0.30	0.02	3.41	3.82	2.82	1.98
SdE-60	20–25	3.24	0.71	37.80	43.71	0.61	5.24	0.68	0.22	0.02	2.88	4.90	2.46	3.94

Table 22; Total elemental content (given as oxides) of the investigated sites at Location 2. LOI = loss on ignition

Sample	Soil Depth [cm]	Na_2O [%]	MgO [%]	AL_2O_3 [%]	SiO_2 [%]	P_2O_5 [%]	K_2O [%]	CaO [%]	TiO_2 [%]	MnO [%]	Fe_2O_3 [%]	LOI [%]	Organic Matter [%]	IVC [%]
Location 2 (glaciated)														
R2-P1-P1														
SdE-61	0–5	3.73	0.78	21.75	48.86	0.62	7.45	0.33	0.40	0.02	3.73	12.33	8.84	4.96
SdE-62	5–10	3.54	0.75	22.55	47.69	0.67	7.36	0.22	0.44	0.02	4.54	12.22	9.30	4.65
SdE-63	10–15	3.55	0.74	23.15	47.05	0.66	7.45	0.21	0.46	0.01	4.58	12.14	10.56	3.22
SdE-64	15–20	3.44	0.76	23.78	45.19	0.69	7.05	0.21	0.45	0.01	5.01	13.40	10.65	4.55
SdE-65	20–25	3.75	0.74	23.87	45.96	0.65	7.43	0.19	0.44	0.01	4.92	12.05	10.13	3.24
SdE-66	30-35	3.88	0.81	26.44	42.13	0.86	6.92	0.19	0.43	0.02	4.97	13.35	9.58	5.56
R2-P1-P2														
SdE-67	0–5	3.41	0.77	23.00	48.89	0.65	7.52	0.20	0.45	0.01	4.31	10.78	8.24	4.01
SdE-68	5–10	3.55	0.78	23.24	47.07	0.68	7.51	0.22	0.45	0.02	4.59	11.90	8.90	4.30
SdE-69	10–15	3.55	0.73	23.04	47.03	0.66	7.54	0.21	0.43	0.01	4.54	12.26	12.24	1.53
SdE-70	15–20	3.66	0.75	23.86	45.65	0.68	7.41	0.21	0.45	0.01	4.84	12.49	13.69	0.23
SdE-71	20–25	3.62	0.79	24.39	45.07	0.68	7.08	0.18	0.44	0.01	4.77	12.98	12.15	2.74
SdE-72	30-35	3.63	0.83	26.11	42.95	0.79	6.95	0.20	0.44	0.02	5.26	12.83	10.42	4.27
R2-P2-P1														
SdE-73	0–5	3.65	0.79	22.91	48.44	0.56	7.47	0.19	0.46	0.02	4.47	11.05	10.55	2.28
SdE-74	5–10	3.38	0.72	22.54	47.95	0.57	7.33	0.17	0.43	0.01	4.63	12.29	11.62	2.66
SdE-75	10–15	3.76	0.76	22.95	46.00	0.63	6.99	0.17	0.46	0.02	4.98	13.28	12.35	2.85
SdE-76	15–20	3.63	0.79	23.68	45.76	0.63	7.14	0.17	0.46	0.01	5.13	12.60	9.65	4.75
SdE-77	20–25	3.65	0.77	24.52	45.25	0.65	7.21	0.16	0.49	0.01	5.14	12.15	9.11	4.66
R2-P2-P2														
SdE-78	0–5	3.26	0.84	23.16	46.98	0.60	7.31	0.19	0.47	0.02	5.04	12.14	10.52	3.74
SdE-79	5–10	3.45	0.75	22.86	46.34	0.61	7.17	0.17	0.46	0.02	4.97	13.21	9.37	6.03
SdE-80	10–15	3.47	0.77	22.86	46.58	0.60	7.29	0.17	0.43	0.01	4.72	13.09	9.24	6.13
SdE-81	15–20	3.44	0.75	23.08	45.98	0.60	6.94	0.16	0.44	0.01	5.06	13.54	7.59	8.18
SdE-82	20–25	3.42	0.78	23.99	46.38	0.66	7.19	0.16	0.45	0.02	5.13	11.81	9.08	4.37
S3-P1-P1														
SdE-83	0–5	3.29	0.75	22.82	47.88	0.87	7.52	0.21	0.39	0.02	4.04	12.22	9.12	4.77
SdE-84	5–10	2.97	0.71	24.06	49.00	0.82	6.99	0.16	0.38	0.01	3.88	11.02	9.56	4.10
SdE-85	10–15	3.70	0.79	23.75	46.82	0.81	7.37	0.19	0.41	0.02	4.40	11.75	8.00	5.65
SdE-86	15–20	3.35	0.78	24.51	46.26	0.79	7.36	0.18	0.42	0.02	4.60	11.74	7.58	6.00
SdE-87	20–25	3.46	0.77	24.30	45.73	0.75	7.30	0.18	0.40	0.02	4.46	12.64	7.45	7.12
S3-P1-P2														
SdE-88	0–5	3.57	0.67	20.56	50.75	0.71	7.57	0.20	0.33	0.01	3.46	12.17	10.80	3.14
SdE-89	5–10	3.70	0.62	20.70	51.79	0.63	7.75	0.18	0.34	0.01	3.46	10.83	8.65	4.03
SdE-90	10–15	3.39	0.73	22.92	48.28	0.81	7.44	0.18	0.40	0.02	4.17	11.66	10.80	2.88
SdE-91	15–20	3.41	0.73	23.10	48.29	0.77	7.54	0.19	0.38	0.02	4.12	11.46	11.39	1.63
SdE-92	20–25	3.48	0.77	24.21	47.07	0.75	7.53	0.18	0.40	0.02	4.29	11.32	9.89	3.13
S3-P2-P1														
SdE-93	0–5	3.64	0.72	21.36	48.21	0.82	7.33	0.20	0.37	0.01	3.89	13.46	12.75	2.68
SdE-94	5–10	3.79	0.73	21.74	47.93	0.97	7.25	0.21	0.39	0.02	4.18	12.80	12.36	2.13
SdE-95	10–15	3.73	0.74	22.22	46.33	0.97	7.24	0.18	0.41	0.02	4.53	13.63	14.11	1.06
SdE-96	15–20	3.95	0.73	23.16	45.51	0.88	7.13	0.20	0.40	0.01	4.64	13.41	11.93	3.02
SdE-97	20–25	3.75	0.78	24.64	41.94	0.95	6.84	0.19	0.45	0.02	5.64	14.82	13.03	3.30
S3-P2-P2														
SdE-98	0–5	3.22	0.71	21.31	49.99	0.85	7.49	0.20	0.37	0.02	3.64	12.22	7.71	6.12
SdE-99	5–10	3.53	0.73	21.76	47.89	1.05	7.34	0.19	0.40	0.02	4.27	12.82	8.14	6.32
SdE-100	10–15	3.33	0.69	21.26	48.66	0.99	7.37	0.18	0.36	0.01	4.17	12.97	7.15	7.68
SdE-101	15–20	3.53	0.66	21.42	48.35	0.87	7.18	0.17	0.34	0.01	4.42	13.05	12.13	3.10
SdE-102	20–25	3.57	0.69	23.32	45.81	1.02	6.89	0.18	0.35	0.01	4.53	13.61	11.34	4.32
S4-P1-P1														
SdE-103	0–5	3.37	0.49	18.06	55.41	0.38	7.85	0.19	0.31	0.01	3.08	10.85	11.17	1.43
SdE-104	5–10	3.42	0.66	20.83	52.81	0.53	8.19	0.20	0.38	0.01	3.59	9.39	9.39	1.37
SdE-105	10–15	3.45	0.63	20.48	52.72	0.49	7.85	0.17	0.34	0.01	3.71	10.16	10.09	1.76
SdE-106	15–20	3.62	0.59	20.34	52.72	0.44	7.87	0.16	0.33	0.01	3.78	10.15	9.50	2.37
SdE-107	20–25	3.27	0.57	20.54	53.25	0.42	7.84	0.15	0.32	0.01	3.68	9.95	9.51	2.26
SdE-108	30-35	3.79	0.81	26.40	45.27	0.75	7.72	0.18	0.44	0.02	4.86	9.77	7.83	3.20
S4-P1-P2														
SdE-109	0–5	3.62	0.66	20.27	53.43	0.53	8.24	0.21	0.32	0.01	3.09	9.62	9.70	1.23
SdE-110	5–10	3.49	0.66	21.00	52.55	0.54	8.01	0.19	0.36	0.01	3.45	9.74	8.65	2.66
SdE-111	10–15	3.46	0.77	23.03	48.71	0.63	7.94	0.20	0.43	0.01	4.42	10.40	10.70	1.05
SdE-112	15–20	3.64	0.78	23.56	48.22	0.65	7.75	0.19	0.41	0.01	4.36	10.44	10.56	1.36
SdE-113	20–25	3.45	0.68	23.06	50.10	0.57	7.84	0.17	0.38	0.01	4.06	9.69	8.43	2.73
S4-P2-P1														
SdE-114	0–5	3.50	0.76	20.98	50.16	0.65	7.42	0.20	0.41	0.01	3.75	12.17	11.87	2.02
SdE-115	5–10	3.38	0.62	19.58	52.79	0.61	7.76	0.18	0.35	0.01	3.46	11.26	10.44	2.38
SdE-116	10–15	3.60	0.67	21.59	50.44	0.66	7.90	0.18	0.40	0.01	3.81	10.74	10.41	1.77
SdE-117	15–20	3.46	0.72	22.64	48.10	0.69	7.66	0.17	0.41	0.01	4.30	11.85	10.56	2.86
SdE-118	20–25	3.50	0.76	23.25	47.19	0.68	7.60	0.17	0.43	0.01	4.52	11.90	10.96	2.42
S4-P2-P2														
SdE-119	0–5	3.15	0.66	20.13	52.27	0.67	7.67	0.21	0.36	0.01	3.46	11.42	10.69	2.34
SdE-120	5–10	3.57	0.74	22.57	47.99	0.84	7.43	0.19	0.44	0.01	4.40	11.82	9.42	3.99
SdE-121	10–15	3.38	0.67	21.59	50.23	0.70	7.70	0.17	0.40	0.01	3.93	11.22	9.64	3.24
SdE-122	15–20	3.57	0.73	22.52	47.40	0.67	7.50	0.17	0.43	0.01	4.49	12.52	11.45	2.81
SdE-123	20–25	3.46	0.74	24.19	47.42	0.74	7.89	0.16	0.44	0.01	4.69	10.26	8.40	2.91

Table 23; Chemical weathering indexes along the investigated soil profiles at Location 1: WIP = weathering index of Parker (Parker, 1970); (K + Ca)/Ti ratio (Harrington & Whitney, 1987); Index B (Kronberg and Nesbitt, 1982); CIA = chemical index of alteration (Nesbitt and Young, 1982); CIW = chemical index of weathering (Harnois, 1988); VR = Vogt ratio (Vogt, 1927); SA = Silico -aluminum ratio (Ruxton, 1968); PIA = plagioclase index of alteration (Fedo, et al., 1995); CPA = - chemical proxy of alteration (Buggle, et al., 2011).

Sample	Soil Depth [cm]	WIP	(Ca+K)/Ti	B-Index	CIA	CIW	VR	SA	PIA	CPA
Location 1 (non-glaciated)										
R1-P1-P1										
SdE-1	0–5	87.12	13.08	0.38	61.62	73.01	2.70	3.09	66.89	76.13
SdE-2	5–10	86.29	13.42	0.38	61.91	73.82	2.81	3.12	67.59	77.04
SdE-3	10–15	88.12	12.52	0.36	64.30	75.59	2.97	2.73	70.39	78.62
SdE-4	15–20	92.58	11.66	0.35	65.29	76.40	3.07	2.61	71.56	79.49
SdE-5	20–25	91.50	10.62	0.35	65.05	77.30	3.27	2.60	72.04	80.59
R1-P1-P2										
SdE-6	0–5	79.67	10.38	0.37	63.36	74.48	2.80	2.85	69.05	77.59
SdE-7	5–10	83.72	11.23	0.38	62.05	73.44	2.71	2.93	67.47	76.82
SdE-8	10–15	85.71	10.87	0.36	64.35	75.27	2.89	2.80	70.22	78.20
SdE-9	15–20	91.58	11.17	0.36	64.26	75.23	2.90	2.62	70.13	78.08
SdE-10	20–25	96.56	11.36	0.36	64.37	75.71	2.98	2.60	70.52	78.60
R1-P2-P1										
SdE-11	0–5	84.94	12.58	0.40	60.07	70.91	2.45	3.19	64.51	74.12
SdE-12	5–10	88.62	11.14	0.37	63.15	73.81	2.71	2.72	68.49	76.58
SdE-13	10–15	90.42	10.51	0.36	64.32	75.25	2.91	2.72	70.18	78.01
SdE-14	15–20	87.41	10.16	0.35	65.18	76.33	3.06	2.62	71.45	79.07
SdE-15	20–25	84.17	9.38	0.33	67.36	77.89	3.25	2.30	73.79	80.34
R1-P2-P2										
SdE-16	0–5	88.44	12.17	0.38	61.55	73.23	2.69	3.05	66.96	76.13
SdE-17	5–10	91.47	11.11	0.36	63.81	75.33	2.95	2.78	69.90	78.12
SdE-18	10–15	93.68	10.95	0.36	64.49	75.83	3.02	2.65	70.67	78.65
SdE-19	15–20	91.82	10.77	0.35	65.01	76.54	3.10	2.61	71.48	79.26
SdE-20	20–25	87.39	9.48	0.34	66.38	77.24	3.17	2.54	72.79	79.95
S1-P1-P1										
SdE-21	0–5	95.28	12.62	0.37	62.61	75.75	3.12	2.92	69.31	78.62
SdE-22	5–10	92.69	11.93	0.34	66.35	79.10	3.54	2.61	74.13	81.83
SdE-23	10–15	93.50	11.74	0.34	66.31	78.86	3.47	2.53	73.92	81.55
SdE-24	15–20	70.06	12.00	0.26	73.78	89.72	7.30	2.58	86.89	93.19
SdE-25	20–25	96.45	13.03	0.34	65.69	78.65	3.49	2.60	73.40	81.30
S1-P1-P2										
SdE-26	0–5	99.80	13.95	0.36	63.58	76.69	3.25	2.76	70.63	79.46
SdE-27	5–10	96.55	14.22	0.34	65.67	78.35	3.46	2.54	73.16	81.08
SdE-28	10–15	95.26	12.84	0.35	64.98	77.89	3.44	2.68	72.41	80.76
SdE-29	15–20	96.03	13.32	0.34	66.45	79.11	3.57	2.49	74.20	81.71
SdE-30	20–25	90.74	13.23	0.30	70.35	82.55	4.19	2.11	78.89	84.80
S1-P2-P1										
SdE-31	0–5	64.61	15.71	0.47	52.69	61.89	1.64	3.24	53.83	68.24
SdE-32	5–10	97.30	13.41	0.36	63.91	76.43	3.19	2.72	70.68	79.30
SdE-33	10–15	96.42	13.31	0.35	64.90	77.02	3.23	2.59	71.75	79.96
SdE-34	15–20	103.27	13.36	0.36	63.52	76.74	3.26	2.75	70.63	79.77
SdE-35	20–25	101.44	13.02	0.35	64.52	77.75	3.43	2.67	72.01	80.92
S1-P2-P2										
SdE-36	0–5	75.06	12.94	0.39	60.59	71.37	2.48	2.87	65.17	74.49
SdE-37	5–10	98.71	14.61	0.37	63.19	75.93	3.15	2.81	69.85	78.88
SdE-38	10–15	95.69	12.29	0.33	66.60	78.42	3.39	2.53	73.77	81.20
SdE-39	15–20	93.85	11.63	0.34	66.15	78.29	3.44	2.58	73.41	81.22
SdE-40	20–25	95.75	12.75	0.35	64.65	77.21	3.28	2.67	71.72	80.06
S2-P1-P1										
SdE-41	0–5	92.83	11.60	0.31	69.00	81.33	3.83	2.25	77.27	83.83
SdE-42	5–10	86.35	12.70	0.28	71.66	83.41	4.38	2.11	80.16	85.55
SdE-43	10–15	72.65	14.58	0.23	77.39	89.43	6.43	1.79	87.48	90.44
SdE-44	15–20	72.06	17.58	0.21	78.55	90.91	7.36	1.76	89.21	91.56
SdE-45	20–25	74.33	18.85	0.22	78.11	91.06	7.54	1.81	89.28	91.64
S2-P1-P2										
SdE-46	0–5	88.48	11.67	0.31	69.15	81.90	4.02	2.41	77.81	84.67
SdE-47	5–10	78.01	12.82	0.24	75.61	86.37	5.27	1.75	84.11	88.22
SdE-48	10–15	80.27	18.83	0.24	76.09	87.03	5.75	1.77	84.85	88.76
SdE-49	15–20	61.57	15.80	0.19	81.03	89.31	6.76	1.52	88.09	90.88
SdE-50	20–25	74.45	16.87	0.24	76.41	86.33	5.53	1.92	84.29	88.78
S2-P2-P1										
SdE-51	0–5	95.16	14.56	0.32	68.25	79.83	3.64	2.25	75.71	82.57
SdE-52	5–10	85.54	15.24	0.28	72.20	82.15	4.04	1.96	79.29	85.32
SdE-53	10–15	86.47	25.60	0.27	72.64	82.82	4.58	2.05	80.02	85.89
SdE-54	15–20	82.03	28.18	0.26	74.01	82.96	4.59	1.91	80.62	86.64
SdE-55	20–25	85.10	30.57	0.27	72.80	82.18	4.46	2.01	79.54	85.72
S2-P2-P2										
SdE-56	0–5	89.32	14.52	0.29	70.91	81.09	3.84	2.00	77.92	84.01
SdE-57	5–10	88.52	18.84	0.30	70.30	80.03	3.79	2.29	76.82	83.57
SdE-58	10–15	65.33	24.05	0.20	80.04	88.30	6.16	1.53	86.95	89.62
SdE-59	15–20	87.11	20.97	0.29	71.06	80.19	3.90	2.13	77.27	84.31
SdE-60	20–25	78.07	25.06	0.24	75.55	85.21	5.20	1.96	83.04	87.65

Table 24; Chemical weathering indexes along the investigated soil profiles at Location 2: WIP = weathering index of Parker (Parker, 1970); (K + Ca)/Ti ratio (Harrington & Whitney, 1987); Index B (Kronberg and Nesbitt, 1982); CIA = chemical index of alteration (Nesbitt and Young, 1982); CIW = chemical index of weathering (Harnois, 1988); VR = Vogt ratio (Vogt, 1927); SA = Silico -aluminum ratio (Ruxton, 1968); PIA = plagioclase index of alteration (Fedo, et al., 1995); CPA = - chemical proxy of alteration (Buggle, et al., 2011).

Sample	Soil Depth [cm]	WIP	(Ca+K)/Ti	B-Index	CIA	CIW	VR	SA	PIA	CPA
Location 2 (glaciated)										
R2-P1-P1										
SdE-61	0–5	100.66	16.90	0.41	59.50	76.35	3.42	3.81	67.00	78.00
SdE-62	5–10	97.79	14.82	0.39	61.38	78.37	3.76	3.59	70.09	79.46
SdE-63	10–15	98.57	14.48	0.38	61.84	78.83	3.86	3.45	70.82	79.87
SdE-64	15–20	94.23	13.92	0.36	63.50	79.76	3.95	3.22	72.80	80.78
SdE-65	20–25	100.14	14.83	0.38	62.13	78.56	3.81	3.27	70.85	79.47
SdE-66	30-35	97.28	14.16	0.35	65.01	79.69	3.87	2.70	73.76	80.54
R2-P1-P2										
SdE-67	0–5	97.92	14.81	0.38	61.97	79.38	3.94	3.61	71.32	80.40
SdE-68	5–10	99.19	14.75	0.38	61.79	78.82	3.81	3.44	70.76	79.92
SdE-69	10–15	99.32	15.53	0.38	61.56	78.73	3.87	3.46	70.50	79.77
SdE-70	15–20	99.29	14.77	0.38	62.33	78.85	3.84	3.25	71.22	79.83
SdE-71	20–25	96.15	14.30	0.36	63.62	79.52	3.87	3.14	72.69	80.38
SdE-72	30-35	95.25	13.99	0.35	65.33	80.48	3.99	2.79	74.58	81.40
R2-P2-P1										
SdE-73	0–5	99.80	14.51	0.39	61.34	78.30	3.71	3.59	70.01	79.22
SdE-74	5–10	95.79	15.08	0.38	62.03	79.35	3.97	3.61	71.35	80.22
SdE-75	10–15	96.63	13.39	0.38	62.00	77.93	3.62	3.40	70.30	78.75
SdE-76	15–20	96.73	13.64	0.37	62.83	79.04	3.80	3.28	71.75	79.86
SdE-77	20–25	97.36	13.08	0.36	63.50	79.57	3.92	3.13	72.65	80.34
R2-P2-P2										
SdE-78	0–5	94.91	13.68	0.37	62.97	80.23	3.97	3.44	72.76	81.20
SdE-79	5–10	95.20	13.89	0.38	62.45	79.25	3.88	3.44	71.62	80.11
SdE-80	10–15	96.44	14.93	0.38	62.19	79.20	3.86	3.46	71.37	80.03
SdE-81	15–20	93.08	13.96	0.37	63.16	79.50	3.90	3.38	72.35	80.32
SdE-82	20–25	95.19	14.04	0.36	63.63	80.19	4.03	3.28	73.22	81.00
S3-P1-P1										
SdE-83	0–5	96.74	17.03	0.38	62.10	79.78	4.03	3.56	71.73	80.85
SdE-84	5–10	89.11	16.38	0.35	65.38	82.30	4.53	3.46	76.12	83.13
SdE-85	10–15	99.35	15.73	0.38	62.25	78.69	3.76	3.34	71.04	79.59
SdE-86	15–20	95.98	15.47	0.36	63.98	80.79	4.17	3.20	73.95	81.66
SdE-87	20–25	96.47	16.27	0.36	63.59	80.18	4.05	3.19	73.19	81.03
S3-P1-P2										
SdE-88	0–5	99.59	20.12	0.41	58.75	76.72	3.63	4.19	66.46	77.76
SdE-89	5–10	102.08	20.19	0.42	58.30	76.33	3.64	4.25	65.73	77.26
SdE-90	10–15	96.97	16.51	0.38	62.14	79.51	4.00	3.57	71.56	80.42
SdE-91	15–20	97.99	17.34	0.38	62.08	79.52	4.01	3.55	71.52	80.45
SdE-92	20–25	98.61	16.66	0.37	63.04	80.01	4.04	3.30	72.64	80.86
S3-P2-P1										
SdE-93	0–5	98.25	17.80	0.40	59.93	77.08	3.59	3.83	67.90	78.10
SdE-94	5–10	99.01	16.49	0.40	60.06	76.69	3.50	3.74	67.76	77.73
SdE-95	10–15	98.35	15.53	0.39	60.85	77.47	3.61	3.54	69.00	78.38
SdE-96	15–20	99.46	16.01	0.39	61.38	77.15	3.55	3.33	69.25	78.09
SdE-97	20–25	95.24	13.51	0.36	63.92	79.11	3.79	2.89	72.60	79.99
S3-P2-P2										
SdE-98	0–5	95.74	18.13	0.39	60.76	79.02	3.94	3.98	70.00	80.10
SdE-99	5–10	97.38	16.12	0.39	60.68	77.96	3.72	3.73	69.18	78.94
SdE-100	10–15	95.69	17.94	0.39	60.65	78.53	3.87	3.88	69.55	79.51
SdE-101	15–20	95.76	18.63	0.39	60.66	77.77	3.74	3.83	69.03	78.67
SdE-102	20–25	93.81	17.39	0.37	63.06	78.99	3.87	3.33	71.88	79.88
S4-P1-P1										
SdE-103	0–5	99.60	22.14	0.44	55.65	75.39	3.72	5.21	61.86	76.50
SdE-104	5–10	103.42	19.17	0.42	58.37	77.68	3.88	4.30	66.65	78.73
SdE-105	10–15	100.62	20.11	0.41	58.60	77.43	3.84	4.37	66.74	78.32
SdE-106	15–20	102.22	20.65	0.42	57.95	76.52	3.73	4.40	65.45	77.36
SdE-107	20–25	98.66	21.39	0.41	59.23	78.43	4.10	4.40	68.09	79.26
SdE-108	30-35	103.16	15.37	0.36	63.91	80.11	4.04	2.91	73.35	80.89
S4-P1-P2										
SdE-109	0–5	105.67	22.76	0.43	57.07	76.21	3.65	4.47	64.21	77.31
SdE-110	5–10	102.50	19.50	0.41	58.74	77.56	3.83	4.25	66.98	78.54
SdE-111	10–15	101.92	16.30	0.39	61.14	79.20	3.95	3.59	70.49	80.18
SdE-112	15–20	101.96	16.59	0.38	61.55	78.81	3.85	3.47	70.55	79.73
SdE-113	20–25	100.72	17.93	0.39	61.44	79.40	4.09	3.69	70.90	80.23
S4-P2-P1										
SdE-114	0–5	97.83	16.07	0.40	59.74	77.44	3.61	4.06	67.94	78.49
SdE-115	5–10	99.28	19.58	0.42	57.82	76.90	3.75	4.57	65.52	77.87
SdE-116	10–15	102.60	17.53	0.41	59.32	77.52	3.79	3.96	67.57	78.46
SdE-117	15–20	99.35	16.26	0.39	61.31	79.07	3.96	3.61	70.53	79.91
SdE-118	20–25	99.26	15.60	0.38	61.96	79.34	3.95	3.44	71.29	80.17
S4-P2-P2										
SdE-119	0–5	96.47	18.88	0.41	59.24	78.37	3.94	4.41	68.05	79.54
SdE-120	5–10	98.51	15.03	0.39	61.29	78.42	3.79	3.61	70.06	79.37
SdE-121	10–15	98.82	16.94	0.40	60.32	78.63	3.95	3.95	69.31	79.54
SdE-122	15–20	98.99	15.37	0.39	61.18	78.49	3.82	3.57	70.00	79.32
SdE-123	20–25	101.43	15.64	0.38	62.45	80.13	4.16	3.33	72.29	80.93

Table 25; Plutonium results of the investigated sites at Location 1

Site	Depth [cm]	Pu inventory [Bqkg^{-1}]	Section Mass [kgm^{-2}]	Section Activity - FE [Bqm^{-2}]	Section Activity - SD [Bqm^{-2}]	Pu-Inv. Sum. [Bqm^{-2}]	Incre.Sum. [Bqm^{-2}]	Activity Sum. [Bqm^{-2}]	Std. Dev. [Bqm^{-2}]	$^{239+240}$Pu 240/239	$^{239+240}$Pu sd 240239	$^{239+240}$Pu Average
Location 1 (non-glaciated)												
R1-P1-P1												
SdE-1	0–5	2.692	19.30	51.97	78.07		1.56			0.181	0.002	0.179
SdE-2	5–10	3.427	13.70	46.96	125.09		4.06			0.171	0.011	0.160
SdE-3	10–15	1.337	26.64	35.62	47.46		5.01			0.179	0.009	0.170
SdE-4	15–20	0.694	22.87	15.87	22.56		5.46			0.176	0.005	0.171
SdE-5	20–25	0.509	19.36	9.85	15.27	160	5.77	288	58	0.179	0.024	0.155
R1-P1-P2												
SdE-6	0–5	3.033	25.88	78.48	89.47		1.79			0.186	0.003	0.183
SdE-7	5–10	2.202	22.56	49.69	82.58		1.65			0.160	0.004	0.156
SdE-8	10–15	1.894	28.07	53.16	74.81		3.29			0.174	0.015	0.160
SdE-9	15–20	1.053	26.13	27.52	42.12		4.13			0.175	0.022	0.153
SdE-10	20–25	0.343	31.43	10.78	15.44	220	4.44	304	61	0.177	0.006	0.172
R1-P2-P1												
SdE-11	0–5	2.646	19.30	51.08	78.06		1.56			0.190	0.012	0.178
SdE-12	5–10	2.167	30.61	66.34	63.93		1.28			0.180	0.007	0.173
SdE-13	10–15	0.832	27.40	22.80	28.29		2.13			0.198	0.013	0.184
SdE-14	15–20	0.704	25.82	18.18	23.23		2.59			0.169	0.040	0.128
SdE-15	20–25	0.235	28.58	6.72	7.05	165	2.73	201	40			0.000
R1-P2-P2												
SdE-16	0–5	2.829	22.46	63.55	79.21		1.58			0.178	0.013	0.165
SdE-17	5–10	1.43	27.15	38.82	52.91		1.06			0.186	0.038	0.147
SdE-18	10–15	0.588	33.31	19.59	24.99		2.08			0.197	0.034	0.163
SdE-19	15–20	0.425	28.12	11.95	15.73		2.40			0.171	0.042	0.129
SdE-20	20–25	0.329	30.46	10.02	13.49	144	2.67	186	37			0.000
S1-P1-P1												
SdE-21	0–5	1.704	23.84	40.62	50.27		1.01			0.176	0.013	0.163
SdE-22	5–10	1.201	32.29	38.78	40.23		1.81			0.170	0.002	0.168
SdE-23	10–15	0.787	29.49	23.21	25.58		2.32			0.185	0.014	0.171
SdE-24	15–20	0.461	30.00	13.83	14.75		2.62			0.196	0.053	0.143
SdE-25	20–25	0.119	29.14	3.47	3.75	120	2.69	135	27	0.191	0.031	0.160
S1-P1-P2												
SdE-26	0–5	1.278	37.74	48.24	46.65		0.93			0.167	0.025	0.142
SdE-27	5–10	0.461	29.08	13.41	14.52		1.22			0.194	0.011	0.183
SdE-28	10–15	0.225	29.49	6.64	6.75		1.36			0.197	0.016	0.181
SdE-29	15–20	0.098	32.70	3.20	3.28		1.42					
SdE-30	20–25	0.042	36.47	1.53	1.66	73	1.46	73	15			
S1-P2-P1												
SdE-31	0–5	0.742	6.98	5.18	6.68		0.13			0.207	0.037	0.169
SdE-32	5–10	0.445	22.06	9.81	13.35		0.40			0.179	0.018	0.161
SdE-33	10–15	0.098	22.82	2.24	3.72		0.48					
SdE-34	15–20	0	29.08	0.00	0.00		0.48					
SdE-35	20–25	0	35.30	0.00	0.00	17	0.48	24	5			
S1-P2-P2												
SdE-36	0–5	1.565	13.80	21.60	19.56		0.39			0.155	0.001	0.153
SdE-37	5–10	0.512	29.44	15.07	18.18		0.75			0.166	0.017	0.149
SdE-38	10–15	0.122	28.37	3.46	4.45		0.84			0.167	0.049	0.118
SdE-39	15–20	0.102	38.71	3.95	4.03		0.92			0.187	0.010	0.176
SdE-40	20–25	0.106	21.80	2.31	3.45	46	0.99	50	10	0.184	0.007	0.177
S2-P1-P1												
SdE-41	0–5	2.171	41.21	89.46	104.21		2.08			0.177	0.018	0.159
SdE-42	5–10	0.425	30.71	13.05	21.04		0.42			0.221	0.025	0.196
SdE-43	10–15	0.24	32.80	7.87	10.08		0.20			0.211	0.014	0.196
SdE-44	15–20	0	39.73	0.00	0.00		0.00					
SdE-45	20–25	0	38.41	0.00	0.00	110	0.00	135	27			
S2-P1-P2												
SdE-46	0–5	1.753	36.98	64.83	78.89		1.58			0.165	0.004	0.161
SdE-47	5–10	0.186	34.94	6.50	9.49		0.19			0.207	0.025	0.182
SdE-48	10–15	0.091	24.86	2.26	4.05		0.08			0.180	0.042	0.138
SdE-49	15–20	0	32.19	0.00	0.00		0.00					
SdE-50	20–25	0.042	33.11	1.39	2.14	75	0.04	95	19			
S2-P2-P1												
SdE-51	0–5	0.961	25.82	24.82	39.88		0.80			0.176	0.002	0.174
SdE-52	5–10	0.691	15.69	10.84	33.17		0.66			0.169	0.005	0.164
SdE-53	10–15	0.07	19.81	1.39	2.98		0.06			0.167	0.017	0.150
SdE-54	15–20	0.033	26.08	0.86	1.68		0.03					
SdE-55	20–25	0	18.24	0.00	0.00	38	0.00	78	16			
S2-P2-P2												
SdE-56	0–5	0.736	20.32	14.96	33.49		0.67			0.185	0.011	0.173
SdE-57	5–10	0.255	18.18	4.64	12.37		0.25			0.189	0.008	0.181
SdE-58	10–15	0	22.87	0.00	0.00		0.00					
SdE-59	15–20	0.036	20.78	0.75	1.75		0.03					
SdE-60	20–25	0	22.92	0.00	0.00	20	0.00	48	10			

Table 26; Plutonium results of the investigated sites at Location 2

Site	Depth [cm]	Pu inventory [Bqkg^{-1}]	Section Mass [Bqm^{-2}]	Section Activity - FE [Bqm^{-2}]	Section Activity - SD [Bqm^{-2}]	Pu-Inv. Sum. [Bqm^{-2}]	Incre.Sum. [Bqm^{-2}]	Activity Sum. [Bqm^{-2}]	Std. Dev. [Bqm^{-2}]	$^{239+240}$Pu 240/239	$^{239+240}$Pu sd 240239	$^{239+240}$Pu Average
Location 2 (glaciated)												
R2-P1-P1												
SdE-61	0–5	1.333	33.67	44.88	35.32		0.71			0.172	0.012	0.160
SdE-62	5–10	0.596	34.69	20.67	19.07		0.38			0.176	0.010	0.166
SdE-63	10–15	0.195	41.26	8.05	6.83		0.14					
SdE-64	15–20	0.16	39.02	6.24	5.92		0.12					
SdE-65	20–25	0	39.83	0.00	0.00		0.00					
SdE-66	30-35	0	22.97	0.00	0.00	80	0.00	67	11			
R2-P1-P2												
SdE-67	0–5	0.751	41.56	31.21	25.53		0.51			0.187	0.014	0.174
SdE-68	5–10	0.595	35.09	20.88	18.45		0.37			0.196	0.003	0.193
SdE-69	10–15	0.162	36.57	5.92	5.43		0.11			0.152	0.058	0.093
SdE-70	15–20	0	34.18	0.00	0.00		0.00					
SdE-71	20–25	0	30.82	0.00	0.00		0.00					
SdE-72	30-35		25.42	0.00	0.00	58	0.00	49	8			
R2-P2-P1												
SdE-73	0–5	2.187	38.86	85.00	75.45		1.51			0.179	0.006	0.174
SdE-74	5–10	0.965	37.74	36.42	37.15		0.74			0.167	0.004	0.163
SdE-75	10–15	0.61	35.20	21.47	19.83		0.40			0.192	0.002	0.190
SdE-76	15–20	0.084	35.50	2.98	2.98		0.06					
SdE-77	20–25	0	28.27	0.00	0.00	146	0.00	135	27			
R2-P2-P2												
SdE-78	0–5	2.159	30.97	66.86	64.77		1.30			0.181	0.006	0.176
SdE-79	5–10	0.584	35.55	20.76	20.73		0.41			0.193	0.017	0.176
SdE-80	10–15	0.78	38.05	29.68	28.08		0.56			0.172	0.017	0.155
SdE-81	15–20	0	37.69	0.00	0.00		0.00					
SdE-82	20–25	0.108	35.96	3.88	3.83	121	0.08	117	23			
S3-P1-P1												
SdE-83	0–5	0.97	28.88	28.01	33.47		0.67			0.172	0.011	0.161
SdE-84	5–10	0.381	29.90	11.39	15.24		0.97			0.201	0.009	0.192
SdE-85	10–15	0.461	36.83	16.98	18.44		1.34			0.184	0.020	0.164
SdE-86	15–20	0.055	36.72	2.02	2.15		1.39					
SdE-87	20–25	0	30.61	0.00	0.00	58	1.39	69	14			
S3-P1-P2												
SdE-88	0–5	2.254	35.09	79.10	71.00		1.42			0.181	0.011	0.170
SdE-89	5–10	1.137	33.16	37.70	38.66		2.19			0.188	0.002	0.186
SdE-90	10–15	0.617	38.25	23.60	24.06		2.67			0.190	0.023	0.167
SdE-91	15–20	0.449	37.44	16.81	18.86		3.05			0.185	0.031	0.154
SdE-92	20–25	0.06	29.44	1.77	2.16	159	3.09	155	31			
S3-P2-P1												
SdE-93	0–5	1.802	33.57	60.49	55.86		1.12			0.193	0.005	0.188
SdE-94	5–10	1.119	22.62	25.31	42.52		1.97			0.190	0.008	0.182
SdE-95	10–15	0.362	23.07	8.35	12.49		2.22			0.191	0.023	0.168
SdE-96	15–20	0.246	21.90	5.39	9.47		2.41			0.172	0.029	0.143
SdE-97	20–25	0.213	20.58	4.38	8.73	104	2.58	129	26			
S3-P2-P2												
SdE-98	0–5	2.681	32.50	87.12	80.43		1.61			0.169	0.005	0.164
SdE-99	5–10	1.261	30.41	38.35	49.81		2.60			0.188	0.000	0.188
SdE-100	10–15	0.719	29.64	21.31	25.88		3.12			0.166	0.012	0.154
SdE-101	15–20	0.252	19.25	4.85	10.58		3.33					
SdE-102	20–25	0.17	20.02	3.40	7.23	155	3.48	174	35	0.173	0.018	0.155
S4-P1-P1												
SdE-103	0–5	2.679	34.84	93.34	77.69		1.55			0.180	0.004	0.176
SdE-104	5–10	2.335	37.54	87.66	82.89		1.66			0.183	0.009	0.174
SdE-105	10–15	0.615	31.43	19.33	23.37		0.47			0.187	0.008	0.180
SdE-106	15–20	0.197	30.61	6.03	7.98		0.16					
SdE-107	20–25	0	33.31	0.00	0.00		0.00					
SdE-108	30-35	0	28.58	0.00	0.00	206	0.00	192	32			
S4-P1-P2												
SdE-109	0–5	2.717	40.60	110.30	95.10		1.90			0.177	0.008	0.169
SdE-110	5–10	1.663	37.79	62.85	64.03		3.18			0.178	0.007	0.171
SdE-111	10–15	0.486	39.32	19.11	20.17		3.59			0.188	0.003	0.184
SdE-112	15–20	0.398	34.89	13.89	14.93		3.88			0.202	0.004	0.199
SdE-113	20–25	0	37.90	0.00	0.00	206	3.88	194	39			
S4-P2-P1												
SdE-114	0–5	2.7	35.09	94.76	76.95		1.54			0.180	0.007	0.173
SdE-115	5–10	1.246	37.85	47.16	40.50		2.35			0.198	0.019	0.180
SdE-116	10–15	0.628	32.75	20.57	18.21		2.71			0.178	0.011	0.167
SdE-117	15–20	0.236	35.40	8.35	8.61		2.89					
SdE-118	20–25	0.072	36.83	2.65	2.74	173	2.94	147	29			
S4-P2-P2												
SdE-119	0–5	2.212	29.70	65.69	54.19		1.08			0.192	0.004	0.188
SdE-120	5–10	0.826	33.36	27.56	26.02		1.60			0.189	0.038	0.151
SdE-121	10–15	0.769	32.65	25.11	26.15		2.13			0.187	0.003	0.184
SdE-122	15–20	0.349	36.83	12.85	12.39		2.37					
SdE-123	20–25	0	32.45	0.00	0.00	131	2.37	119	24			

Table 27; Average, standard deviation, and standard error for Bulk density. n=4, except from R2 30-35 (n=2) and S4 30-35cm (n=1). These data are shown in Figure 11.

Depth [cm]	Ref 1	Slope 1	Slope 2	Ref 2	Slope 3	Slope 4
Average [gcm^{-3}]						
0–5	0.58	0.44	0.90	0.63	0.69	0.59
5–10	0.70	0.65	0.99	0.69	0.71	0.69
10–15	0.76	0.68	0.87	0.69	0.77	0.71
15–20	0.71	0.71	0.92	0.73	0.78	0.75
20–25	0.73	0.73	0.93	0.81	0.77	0.74
30–35				1.02		0.76
Standard deviation						
0–5	0.02	0.26	0.06	0.08	0.09	0.09
5–10	0.08	0.05	0.02	0.07	0.09	0.07
10–15	0.08	0.07	0.03	0.03	0.05	0.11
15–20	0.07	0.07	0.10	0.06	0.05	0.05
20–25	0.16	0.11	0.07	0.13	0.08	0.06
30–35				0.07		
Standard error						
0–5	0.01	0.13	0.03	0.04	0.05	0.04
5–10	0.04	0.02	0.01	0.03	0.04	0.03
10–15	0.04	0.04	0.02	0.02	0.02	0.05
15–20	0.04	0.04	0.05	0.03	0.02	0.02
20–25	0.08	0.05	0.04	0.07	0.04	0.03
30–35				0.03		

Table 28; Average, standard deviation, and standard error for pH($CaCl_2$). n=8, except from R2 30-35 (n=4) and S4 30-35cm (n=2). These data are shown in Figure 12.

Depth [cm]	Ref 1	Slope 1	Slope 2	Ref 2	Slope 3	Slope 4
Average						
0–5	3.35	3.59	4.22	3.86	3.76	3.75
5–10	3.44	3.76	4.25	3.85	3.78	3.74
10–15	3.53	3.85	4.25	3.86	3.81	3.75
15–20	3.63	3.87	4.28	3.91	3.90	3.81
20–25	3.72	3.90	4.28	3.94	3.96	3.86
30–35				4.12		4.05
Standard deviation						
0–5	0.02	0.07	0.04	0.07	0.06	0.05
5–10	0.06	0.04	0.06	0.04	0.06	0.06
10–15	0.07	0.08	0.08	0.03	0.03	0.04
15–20	0.08	0.07	0.10	0.03	0.03	0.05
20–25	0.10	0.05	0.10	0.02	0.03	0.05
30–35				0.01		
Standard error						
0–5	0.01	0.03	0.02	0.04	0.03	0.02
5–10	0.03	0.02	0.03	0.02	0.03	0.03
10–15	0.04	0.04	0.04	0.02	0.02	0.02
15–20	0.04	0.03	0.05	0.01	0.02	0.03
20–25	0.05	0.03	0.05	0.01	0.02	0.02
30–35				0.00		

Table 29; Average, standard deviation, and standard error for LOI. n=4, except from R2 30-35 (n=2) and S4 30-35cm (n=1). These data are shown in Figure 14.

Depth [cm]	Ref 1	Slope 1	Slope 2	Ref 2	Slope 3	Slope 4
Average [%]						
0–5	24.45	32.50	9.91	13.28	14.90	12.61
5–10	21.25	12.63	8.96	14.21	13.66	12.07
10–15	17.16	11.91	11.11	14.53	14.24	12.16
15–20	15.48	11.02	9.11	14.82	14.09	12.87
20–25	14.97	11.03	7.70	13.87	14.79	11.90
30–35				14.91		11.02
Standard deviation						
0–5	2.36	21.57	0.63	0.91	1.19	1.24
5–10	3.44	0.97	3.23	0.92	0.75	1.24
10–15	2.42	1.57	5.23	0.88	0.72	0.51
15–20	2.24	1.01	5.28	0.83	0.95	1.17
20–25	2.94	2.14	2.73	0.70	1.38	1.01
30–35				0.32		0.00
Standard error						
0–5	1.18	10.78	0.32	0.46	0.60	0.62
5–10	1.72	0.48	1.61	0.46	0.37	0.62
10–15	1.21	0.79	2.62	0.44	0.36	0.25
15–20	1.12	0.51	2.64	0.41	0.47	0.59
20–25	1.47	1.07	1.36	0.35	0.69	0.51
30–35				0.16		

Table 30; Average, standard deviation, and standard error for total Carbon. n=8, except from R2 30-35 (n=4) and S4 30-35cm (n=2). These data are shown in Figure 15.

Depth [cm]	Ref 1	Slope 1	Slope 2	Ref 2	Slope 3	Slope 4
Average [gkg^{-1}]						
0–5	11.93	15.45	4.07	6.52	7.04	5.98
5–10	10.32	5.64	3.28	6.66	6.10	5.75
10–15	8.36	5.32	3.86	6.89	6.65	5.72
15–20	7.47	5.20	2.57	7.03	6.40	6.20
20–25	7.48	5.40	2.01	6.30	6.62	5.73
30–35				6.73		4.64
Standard deviation						
0–5	1.09	9.37	0.58	0.42	0.51	0.64
5–10	1.30	0.79	1.38	0.46	0.52	0.71
10–15	1.04	0.56	2.24	0.38	0.53	0.30
15–20	1.01	0.37	1.70	0.39	0.48	0.68
20–25	1.22	1.05	1.09	0.39	0.63	0.68
30–35				0.49		0.08
Standard error						
0–5	0.55	4.69	0.29	0.21	0.26	0.32
5–10	0.65	0.40	0.69	0.23	0.26	0.35
10–15	0.52	0.28	1.12	0.19	0.26	0.15
15–20	0.50	0.19	0.85	0.20	0.24	0.34
20–25	0.61	0.52	0.54	0.19	0.32	0.34
30–35				0.24		0.04

Table 31; Average, standard deviation, and standard error for total Nitrogen. n=8, except from R2 30-35 (n=4) and S4 30-35cm (n=2). These data are shown in Figure 15.

Depth [cm]	Ref 1	Slope 1	Slope 2	Ref 2	Slope 3	Slope 4
Average [gkg^{-1}]						
0–5	0.83	0.83	0.28	0.49	0.53	0.45
5–10	0.76	0.40	0.22	0.51	0.52	0.44
10–15	0.63	0.36	0.24	0.53	0.53	0.45
15–20	0.54	0.34	0.16	0.55	0.51	0.48
20–25	0.51	0.34	0.13	0.49	0.52	0.44
30–35				0.54		0.37
Standard deviation						
0–5	0.06	0.35	0.04	0.03	0.05	0.06
5–10	0.09	0.06	0.09	0.04	0.07	0.06
10–15	0.08	0.04	0.13	0.03	0.04	0.02
15–20	0.09	0.03	0.11	0.03	0.04	0.05
20–25	0.07	0.05	0.08	0.03	0.06	0.05
30–35				0.04		0.00
Standard error						
0–5	0.03	0.18	0.02	0.01	0.03	0.03
5–10	0.05	0.03	0.05	0.02	0.03	0.03
10–15	0.04	0.02	0.07	0.01	0.02	0.01
15–20	0.04	0.02	0.05	0.02	0.02	0.03
20–25	0.03	0.02	0.04	0.01	0.03	0.03
30–35				0.02		0.00

Table 32; Average, standard deviation, and standard error for C/N. n=8, except from R2 30-35 (n=4) and S4 30-35cm (n=2). These data are shown in Figure 15.

Depth [cm]	Ref 1	Slope 1	Slope 2	Ref 2	Slope 3	Slope 4
Average						
0–5	14.37	17.43	14.81	13.20	12.50	13.23
5–10	13.57	14.08	14.71	13.01	12.38	12.94
10–15	13.27	14.82	15.64	12.91	12.35	12.82
15–20	13.94	15.12	15.66	12.86	12.47	12.91
20–25	14.55	15.72	15.81	12.79	12.46	12.93
30–35				12.56		12.39
Standard deviation						
0–5	0.52	4.43	0.50	0.56	0.32	0.34
5–10	0.53	0.37	0.39	0.24	0.35	0.20
10–15	0.22	0.81	1.64	0.30	0.22	0.10
15–20	0.61	0.82	0.90	0.44	0.22	0.12
20–25	0.54	1.97	1.01	0.32	0.24	0.12
30–35				0.28		0.07
Standard error						
0–5	0.26	2.22	0.25	0.28	0.16	0.17
5–10	0.26	0.18	0.19	0.12	0.17	0.10
10–15	0.11	0.41	0.82	0.15	0.11	0.05
15–20	0.30	0.41	0.45	0.22	0.11	0.06
20–25	0.27	0.99	0.51	0.16	0.12	0.06
30–35				0.14		0.03

Table 33; Average, standard deviation, and standard error for $\delta^{13}C$. n=4, except from R2 30-35 (n=2) and S4 30-35cm (n=1). These data are shown in Figure 16.

Depth [cm]	Ref 1	Slope 1	Slope 2	Ref 2	Slope 3	Slope 4
Average [‰]						
0–5	-28.24	-28.40	-28.19	-28.55	-28.51	-29.03
5–10	-27.89	-28.35	-27.81	-28.22	-28.53	-28.57
10–15	-27.77	-27.85	-27.39	-27.92	-28.16	-28.17
15–20	-27.61	-27.62	-27.78	-27.64	-28.02	-27.94
20–25	-27.32	-27.63	-27.54	-27.59	-27.90	-27.81
30–35				-27.32		-27.71
Standard deviation						
0–5	0.16	0.30	0.20	0.28	0.55	0.36
5–10	0.44	0.29	0.52	0.09	0.39	0.36
10–15	0.29	0.09	0.59	0.26	0.28	0.21
15–20	0.50	0.15	0.86	0.18	0.27	0.32
20–25	0.26	0.23	0.45	0.19	0.15	0.29
30–35				0.03		0.00
Standard error						
0–5	0.08	0.15	0.10	0.14	0.27	0.18
5–10	0.22	0.14	0.26	0.05	0.20	0.18
10–15	0.15	0.04	0.30	0.13	0.14	0.10
15–20	0.25	0.07	0.43	0.09	0.13	0.16
20–25	0.13	0.11	0.23	0.10	0.07	0.14
30–35				0.02		

Table 34; Average, standard deviation, and standard error for SiO_2. n=4, except from R2 30-35 (n=2) and S4 30-35cm (n=1). These data are shown in Figure 19.

Depth [cm]	Ref 1	Slope 1	Slope 2	Ref 2	Slope 3	Slope 4
Average [gkg^{-1}]						
0–5	38.91	35.28	41.79	48.29	47.20	52.82
5–10	39.56	43.10	41.38	47.26	49.68	51.53
10–15	40.87	42.98	39.38	46.66	47.33	50.52
15–20	40.76	43.84	40.65	45.65	47.18	49.11
20–25	40.09	42.89	42.43	45.66	45.77	49.49
30–35				42.54		45.27
Standard deviation						
0–5	1.67	9.59	0.97	0.90	3.73	2.20
5–10	1.80	0.42	3.43	0.72	1.64	2.37
10–15	0.67	0.95	3.57	0.50	0.91	1.65
15–20	1.23	0.94	4.22	0.33	1.53	2.43
20–25	2.20	1.85	2.15	0.62	2.77	2.84
30–35				0.58		0.00
Standard error						
0–5	0.84	4.80	0.49	0.45	1.86	1.10
5–10	0.90	0.21	1.71	0.36	0.82	1.18
10–15	0.34	0.47	1.78	0.25	0.46	0.83
15–20	0.61	0.47	2.11	0.17	0.77	1.22
20–25	1.10	0.93	1.07	0.31	1.38	1.42
30–35				0.29		

Table 35; Average, standard deviation, and standard error for TiO_2. n=4, except from R2 30-35 (n=2) and S4 30-35cm (n=1). These data are shown in Figure 19.

Depth [cm]	Ref 1	Slope 1	Slope 2	Ref 2	Slope 3	Slope 4
Average [gkg^{-1}]						
0–5	0.43	0.40	0.48	0.45	0.38	0.35
5–10	0.47	0.47	0.40	0.44	0.37	0.38
10–15	0.50	0.50	0.27	0.44	0.41	0.39
15–20	0.52	0.52	0.27	0.45	0.39	0.40
20–25	0.56	0.50	0.26	0.45	0.40	0.39
30–35				0.44		0.44
Standard deviation						
0–5	0.03	0.11	0.07	0.03	0.05	0.04
5–10	0.04	0.04	0.06	0.01	0.02	0.04
10–15	0.04	0.02	0.08	0.02	0.01	0.04
15–20	0.02	0.03	0.04	0.01	0.02	0.04
20–25	0.02	0.03	0.06	0.02	0.04	0.05
30–35				0.01		0.00
Standard error						
0–5	0.02	0.05	0.04	0.02	0.02	0.02
5–10	0.02	0.02	0.03	0.01	0.01	0.02
10–15	0.02	0.01	0.04	0.01	0.00	0.02
15–20	0.01	0.01	0.02	0.01	0.01	0.02
20–25	0.01	0.01	0.03	0.01	0.02	0.03
30–35				0.00		

Table 36; Average, standard deviation, and standard error for Al_2O_3 n=4, except from R2 30-35 (n=2) and S4 30-35cm (n=1). These data are shown in Figure 19.

Depth [cm]	Ref 1	Slope 1	Slope 2	Ref 2	Slope 3	Slope 4
Average [gkg^{-1}]						
0–5	21.69	20.59	31.95	22.71	22.34	19.86
5–10	23.31	27.41	34.71	22.80	21.95	20.99
10–15	25.49	28.25	37.55	23.00	22.67	21.68
15–20	26.46	28.62	37.82	23.60	23.01	22.26
20–25	27.10	29.15	37.36	24.19	23.64	22.76
30–35				26.27		26.40
Standard deviation						
0–5	0.84	6.53	1.76	0.65	1.79	1.26
5–10	1.65	1.00	1.46	0.33	1.47	1.23
10–15	0.98	1.00	1.87	0.12	0.87	1.05
15–20	0.82	0.60	1.90	0.36	1.34	1.36
20–25	0.32	2.39	0.37	0.31	1.49	1.56
30–35				0.24		0.00
Standard error						
0–5	0.42	3.26	0.88	0.32	0.90	0.63
5–10	0.82	0.50	0.73	0.17	0.73	0.61
10–15	0.49	0.50	0.93	0.06	0.43	0.52
15–20	0.41	0.30	0.95	0.18	0.67	0.68
20–25	0.16	1.19	0.19	0.16	0.75	0.78
30–35				0.12		

Table 37; Average, standard deviation, and standard error for K_2O n=4, except from R2 30-35 (n=2) and S4 30-35cm (n=1). These data are shown in Figure 19.

Depth [cm]	Ref 1	Slope 1	Slope 2	Ref 2	Slope 3	Slope 4
Average [gkg^{-1}]						
0–5	5.02	5.12	6.13	7.44	7.31	7.79
5–10	5.26	6.39	5.62	7.34	7.37	7.85
10–15	5.39	6.28	5.39	7.32	7.35	7.85
15–20	5.53	6.52	5.16	7.14	7.35	7.69
20–25	5.56	6.54	5.52	7.23	7.21	7.79
30–35				6.93		7.72
Standard deviation						
0–5	0.28	1.65	0.34	0.09	0.33	0.35
5–10	0.26	0.09	0.26	0.14	0.32	0.33
10–15	0.26	0.11	0.74	0.24	0.08	0.10
15–20	0.18	0.33	0.69	0.20	0.17	0.16
20–25	0.46	0.30	0.47	0.14	0.29	0.13
30–35				0.02		0.00
Standard error						
0–5	0.14	0.82	0.17	0.05	0.17	0.17
5–10	0.13	0.05	0.13	0.07	0.16	0.16
10–15	0.13	0.05	0.37	0.12	0.04	0.05
15–20	0.09	0.16	0.34	0.10	0.09	0.08
20–25	0.23	0.15	0.24	0.07	0.14	0.07
30–35				0.01		

Table 38; Average, standard deviation, and standard error for (Ca+K)/1, n=4, except from R2 30-35 (n=2) and S4 30-35cm (n=1). These data are shown in Figure 20.

Depth [cm]	Ref 1	Slope 1	Slope 2	Ref 2	Slope 3	Slope 4
Average						
0–5	12.05	13.81	13.09	14.98	17.11	19.96
5–10	11.72	13.54	14.90	14.64	17.80	18.32
10–15	11.21	12.55	20.76	14.58	15.97	17.72
15–20	10.94	12.58	20.63	14.07	16.69	17.22
20–25	10.21	13.01	22.84	14.06	16.27	17.64
30–35				14.07		15.37
Standard deviation						
0–5	1.17	1.39	1.68	1.37	2.74	3.10
5–10	1.13	1.18	2.88	0.52	1.79	2.20
10–15	0.89	0.68	5.04	0.91	0.43	1.67
15–20	0.64	0.89	5.47	0.49	1.15	2.35
20–25	0.95	0.19	6.22	0.73	2.11	2.73
30–35				0.12		0.00
Standard error						
0–5	0.59	0.70	0.84	0.69	1.37	1.55
5–10	0.57	0.59	1.44	0.26	0.89	1.10
10–15	0.45	0.34	2.52	0.45	0.22	0.84
15–20	0.32	0.45	2.74	0.24	0.57	1.17
20–25	0.48	0.10	3.11	0.37	1.05	1.36
30–35				0.06		

Table 39; Average, standard deviation, and standard error for WIP, n=4, except from R2 30-35 (n=2) and S4 30-35cm (n=1). These data are shown in Figure 20.

Depth [cm]	Ref 1	Slope 1	Slope 2	Ref 2	Slope 3	Slope 4
Average						
0–5	85.04	83.69	91.45	98.33	97.46	99.89
5–10	87.53	96.31	84.61	96.99	96.48	100.93
10–15	89.48	95.21	76.18	97.74	98.01	100.99
15–20	90.85	90.80	75.69	95.83	97.28	100.63
20–25	89.91	96.10	77.99	97.21	96.52	100.02
30–35				96.27		103.16
Standard deviation						
0–5	3.86	16.66	3.11	2.55	1.88	4.06
5–10	3.30	2.58	4.57	1.84	5.56	2.40
10–15	3.40	1.24	9.18	1.43	1.06	1.66
15–20	2.33	14.40	11.30	2.76	1.78	1.70
20–25	5.36	4.38	5.05	2.14	1.48	1.28
30–35				1.44		0.00
Standard error						
0–5	1.93	8.33	1.55	1.27	0.94	2.03
5–10	1.65	1.29	2.29	0.92	2.78	1.20
10–15	1.70	0.62	4.59	0.71	0.53	0.83
15–20	1.16	7.20	5.65	1.38	0.89	0.85
20–25	2.68	2.19	2.53	1.07	0.74	0.64
30–35				0.72		

Table 40; Average, standard deviation, and standard error for B-Index, n=4, except from R2 30-35 (n=2) and S4 30-35cm (n=1). These data are shown in Figure 20.

Depth [cm]	Ref 1	Slope 1	Slope 2	Ref 2	Slope 3	Slope 4
Average						
0–5	0.38	0.40	0.31	0.39	0.39	0.42
5–10	0.37	0.35	0.28	0.38	0.39	0.41
10–15	0.36	0.34	0.23	0.38	0.39	0.40
15–20	0.35	0.33	0.24	0.37	0.38	0.40
20–25	0.34	0.34	0.24	0.37	0.37	0.39
30–35				0.35		0.36
Standard deviation						
0–5	0.01	0.05	0.01	0.01	0.02	0.02
5–10	0.01	0.01	0.02	0.00	0.03	0.02
10–15	0.00	0.01	0.03	0.00	0.01	0.01
15–20	0.00	0.04	0.04	0.01	0.01	0.02
20–25	0.01	0.03	0.02	0.01	0.01	0.01
30–35				0.00		0.00
Standard error						
0–5	0.01	0.02	0.01	0.01	0.01	0.01
5–10	0.00	0.01	0.01	0.00	0.02	0.01
10–15	0.00	0.00	0.02	0.00	0.00	0.01
15–20	0.00	0.02	0.02	0.00	0.01	0.01
20–25	0.01	0.01	0.01	0.00	0.01	0.01
30–35				0.00		

Table 41; Average, standard deviation, and standard error for CIA n=4, except from R2 30-35 (n=2) and S4 30-35cm (n=1). These data are shown in Figure 20.

Depth [cm]	Ref 1	Slope 1	Slope 2	Ref 2	Slope 3	Slope 4
Average						
0–5	61.65	59.87	69.33	61.44	61.18	57.92
5–10	62.73	64.78	72.44	61.91	61.12	59.06
10–15	64.37	65.70	76.54	61.90	61.48	59.84
15–20	64.93	67.47	76.16	62.95	62.02	60.50
20–25	65.79	66.30	75.71	63.22	62.80	61.27
30–35				65.17		63.91
Standard deviation						
0–5	1.35	4.94	1.13	1.46	2.30	1.91
5–10	0.91	1.48	2.26	0.45	3.02	1.54
10–15	0.09	0.88	3.08	0.27	0.83	1.12
15–20	0.46	4.41	4.47	0.50	1.43	1.70
20–25	1.34	2.75	2.22	0.73	1.47	1.42
30–35				0.23		0.00
Standard error						
0–5	0.67	2.47	0.56	0.73	1.15	0.95
5–10	0.45	0.74	1.13	0.22	1.51	0.77
10–15	0.04	0.44	1.54	0.13	0.41	0.56
15–20	0.23	2.20	2.24	0.25	0.72	0.85
20–25	0.67	1.37	1.11	0.37	0.74	0.71
30–35				0.11		

Table 42; Average, standard deviation, and standard error for SA, n=4, except from R2 30-35 (n=2) and S4 30-35cm (n=1). These data are shown in Figure 20.

Depth [cm]	Ref 1	Slope 1	Slope 2	Ref 2	Slope 3	Slope 4
Average						
0–5	3.05	2.95	2.23	3.61	3.62	4.54
5–10	2.89	2.67	2.03	3.52	3.86	4.18
10–15	2.72	2.58	1.79	3.44	3.55	3.97
15–20	2.61	2.60	1.83	3.28	3.49	3.76
20–25	2.51	2.51	1.93	3.20	3.30	3.71
30–35				2.75		2.91
Standard deviation						
0–5	0.14	0.20	0.17	0.15	0.55	0.48
5–10	0.18	0.12	0.23	0.09	0.34	0.41
10–15	0.06	0.07	0.21	0.03	0.16	0.32
15–20	0.00	0.11	0.26	0.07	0.30	0.43
20–25	0.14	0.27	0.08	0.08	0.39	0.48
30–35				0.06		0.00
Standard error						
0–5	0.07	0.10	0.08	0.08	0.27	0.24
5–10	0.09	0.06	0.11	0.05	0.17	0.20
10–15	0.03	0.04	0.10	0.01	0.08	0.16
15–20	0.00	0.05	0.13	0.03	0.15	0.21
20–25	0.07	0.14	0.04	0.04	0.20	0.24
30–35				0.03		

Appendix

Table 43; Average (summed up to 100%), standard deviation, and standard error for Grain size distribution. These data are shown in Figure 12.

Depth [cm]	Sand				Silt				Clay			
	Ref 1	n	Ref 2	n	Ref 1	n	Ref 2	n	Ref 1	n	Ref 2	n
Average [%]												
0–5			32.13	4			25.80	4			42.07	4
5–10	32.00	1	25.58	4	31.20	1	35.35	4	36.80	1	39.07	4
10–15	31.31	3	23.18	4	33.84	3	35.22	4	34.85	3	41.60	4
15–20	38.80	1	27.44	4	26.00	1	32.26	4	35.20	1	40.30	4
20–25	36.02	2	27.64	4	31.39	2	28.32	4	32.60	2	44.04	4
30–35												
Standard deviation												
0–5			9.07	4			4.59	4			6.88	4
5–10			8.07	4			3.77	4			5.40	4
10–15	6.85	3	8.78	4	3.52	3	11.88	4	4.30	3	4.58	4
15–20			5.40	4			5.14	4			5.14	4
20–25	3.68	2	7.56	4	5.09	2	10.04	4	9.62	2	5.63	4
30–35												
Standard error												
0–5			4.53	4			2.29	4			3.44	4
5–10			4.03	4			1.89	4			2.70	4
10–15	3.43	3	4.39	4	1.76	3	5.94	4	2.15	3	2.29	4
15–20			2.70	4			2.57	4			2.57	4
20–25	1.84	2	3.78	4	2.55	2	5.02	4	4.81	2	2.82	4
30–35												

Table 44; Average, standard deviation, and standard error for oxalate. These data are shown in Figure 18.

Depth [cm]	Al_o [gkg^{-1}]				Si_o [mgkg^{-1}]				Fe_o [gkg^{-1}]				Mn_o [mgkg^{-1}]			
	Ref 1	n	Ref 2	n	Ref 1	n	Ref 2	n	Ref 1	n	Ref 2	n	Ref 1	n	Ref 2	n
Average																
0–5	1.59	4	1.10	4	80.37	4	47.92	4	4.77	7	4.14	8	15.05	5	6.99	6
5–10	1.94	5	1.19	5	77.66	4	56.59	4	6.55	5	4.61	7	14.52	5	4.36	4
10–15	2.17	6	1.46	4	109.85	4	81.55	4	8.10	5	5.03	7	9.41	5	3.53	4
15–20	2.03	5	1.75	5	114.42	4	74.09	4	7.37	4	6.34	6	9.63	4	3.60	6
20–25	2.50	7	2.19	3	109.18	4	67.60	4	7.64	5	4.74	8	7.35	4	3.36	5
30–35			3.25	3			277.45	2			4.30	2			8.78	2
Standard deviation																
0–5	0.07	4	0.14	4	25.18	4	32.62	4	2.62	7	1.67	8	8.20	5	6.70	6
5–10	0.22	5	0.16	5	18.65	4	20.88	4	2.21	5	1.73	7	13.18	5	1.12	4
10–15	0.33	6	0.34	4	39.26	4	34.44	4	3.83	5	2.13	7	6.50	5	1.43	4
15–20	0.44	5	0.27	5	28.78	4	30.25	4	2.93	4	3.14	6	2.03	4	1.33	6
20–25	1.17	7	0.15	3	28.84	4	22.72	4	3.89	5	0.35	8	2.58	4	2.43	5
30–35			0.10	3			113.91	2			0.96	2			0.40	2
Standard error																
0–5	0.04	4	0.07	4	12.59	4	16.31	4	1.31	7	0.84	8	4.10	5	3.35	6
5–10	0.11	5	0.08	5	9.32	4	10.44	4	1.11	5	0.86	7	6.59	5	0.56	4
10–15	0.17	6	0.17	4	19.63	4	17.22	4	1.92	5	1.06	7	3.25	5	0.72	4
15–20	0.22	5	0.14	5	14.39	4	15.12	4	1.46	4	1.57	6	1.01	4	0.67	6
20–25	0.58	7	0.08	3	14.42	4	11.36	4	1.95	5	0.17	8	1.29	4	1.21	5
30–35			0.05	3			56.96	2			0.48	2			0.20	2

Table 45; Average, standard deviation, and standard error for dithionite and crystalline. These data are shown in Figure 18.

Depth [cm]	Al_d [gkg^{-1}] Ref 1	n	Ref 2	n	Si_d [mgkg^{-1}] Ref 1	n	Ref 2	n	Fe_d [gkg^{-1}] Ref 1	n	Ref 2	n	Fe_{cry} [gkg^{-1}] Ref 1	n	Ref 2	n
Average																
0–5	2.26	4	2.32	4	923.78	4	492.30	4	4.12	4	5.78	4	-0.66	-	1.64	-
5–10	3.49	5	2.76	4	822.63	4	396.15	4	4.33	4	6.50	4	-2.22	-	1.89	-
10–15	3.79	5	3.50	5	711.28	4	409.90	5	4.20	4	6.93	5	-3.89	-	1.90	-
15–20	4.32	4	4.41	5	529.23	4	284.08	6	4.17	5	7.80	5	-3.20	-	1.46	-
20–25	6.31	6	4.36	4	429.05	6	239.50	5	6.04	4	7.17	4	-1.60	-	2.43	-
30–35			5.70	2			342.60	2			6.34	2			2.04	-
Standard deviation																
0–5	0.46	4	0.58	4	93.35	4	62.69	4	0.34	4	1.55	4	-2.27	-	-0.12	-
5–10	0.24	5	0.54	4	158.77	4	121.69	4	0.33	4	1.15	4	-1.89	-	-0.57	-
10–15	0.71	5	0.37	5	304.50	4	56.44	5	0.85	4	0.51	5	-2.99	-	-1.62	-
15–20	0.64	4	0.67	5	223.90	4	30.72	6	1.57	5	1.27	5	-1.36	-	-1.87	-
20–25	2.17	6	0.59	4	69.58	6	52.05	5	1.69	4	0.53	4	-2.20	-	0.18	-
30–35			0.45	2			83.44	2			1.08	2			0.12	-
Standard error																
0–5	0.23	4	0.29	4	46.68	4	31.35	4	0.17	4	0.78	4	-1.14	-	-0.06	-
5–10	0.12	5	0.27	4	79.38	4	60.85	4	0.16	4	0.58	4	-0.94	-	-0.29	-
10–15	0.35	5	0.19	5	152.25	4	28.22	5	0.42	4	0.26	5	-1.49	-	-0.81	-
15–20	0.32	4	0.34	5	111.95	4	15.36	6	0.79	5	0.63	5	-0.68	-	-0.93	-
20–25	1.08	6	0.30	4	34.79	6	26.02	5	0.84	4	0.26	4	-1.10	-	0.09	-
30–35			0.23	2			41.72	2			0.54	2			0.06	-

Table 46; Correlation between meteoric ^{10}Be and Fe_o at Reference 2 including standard deviation and standard error. These data are shown in Figure 22

Site	Depth [cm]	Feo [gkg^{-1}]	n	Standard deviation	Standard error	Be [atoms g^{-1} x 10^8]	Standard error
Location 2							
R2-P1-P1							
SdE-61	0–5	3.27	1			28	0.81
SdE-62	5–10	4.69	2	0.03	0.01	35	1.07
SdE-63	10–15	4.72	1			37	1.07
SdE-64	15–20	5.47	1			42	1.28
SdE-65	20–25	2.58	1			34	1.04
SdE-66	30-35	3.62	1			29	0.98
R2-P1-P2							
SdE-67	0–5	4.34	2	1.96	0.98	32	0.93
SdE-68	5–10	4.11	2	3.05	1.52	31	0.91
SdE-69	10–15	5.90	2	0.14	0.07	36	1.06
SdE-70	15–20	4.85	2	0.70	0.35	36	1.04
SdE-71	20–25	4.40	2	1.58	0.79	32	0.93
SdE-72	30-35	4.98	1			31	0.91

Table 47; Correlation between meteoric ^{10}Be and Fe_o at Reference 1 including standard deviation and standard error. These data are shown in Figure 23

Site	Depth [cm]	Feo [gkg^{-1}]	n	Standard deviation	Standard error	Be [atoms g^{-1} x 10^8]
Location 1						Be = Fe_o x 6.1222 + 6.6542
average from all profiles						
	0–5	4.77	7	2.62	1.31	35.87
	5–10	6.55	5	2.21	1.11	46.77
	10–15	8.10	5	3.83	1.92	56.22
	15–20	7.37	4	2.93	1.46	51.79
	20–25	7.64	5	3.89	1.95	53.45
estimation	*30-35*	*7.00*				*49.51*

Personal declaration

"*I hereby declare that the submitted Thesis is the result of my own, independent work. All external sources are explicitly acknowledged in the Thesis*."

Signature

Uster ZH / 28.02.2021

Place / Date